

THE UNIVERSITY OF CALGARY

Simulated Secants and Overlapping Ovoids

by

Halsey J. Boyd

A THESIS

**SUBMITTED TO THE FACULTY OF GRADUATE STUDIES
IN PARTIAL FULFILLMENT OF THE REQUIREMENTS FOR THE
DEGREE OF MASTER OF SCIENCE**

DEPARTMENT OF MATHEMATICS AND STATISTICS

CALGARY, ALBERTA

July, 1993

© Halsey J. Boyd 1993



National Library
of Canada

Acquisitions and
Bibliographic Services Branch

395 Wellington Street
Ottawa, Ontario
K1A 0N4

Bibliothèque nationale
du Canada

Direction des acquisitions et
des services bibliographiques

395, rue Wellington
Ottawa (Ontario)
K1A 0N4

Your file *Votre référence*

Our file *Notre référence*

The author has granted an irrevocable non-exclusive licence allowing the National Library of Canada to reproduce, loan, distribute or sell copies of his/her thesis by any means and in any form or format, making this thesis available to interested persons.

L'auteur a accordé une licence irrévocable et non exclusive permettant à la Bibliothèque nationale du Canada de reproduire, prêter, distribuer ou vendre des copies de sa thèse de quelque manière et sous quelque forme que ce soit pour mettre des exemplaires de cette thèse à la disposition des personnes intéressées.

The author retains ownership of the copyright in his/her thesis. Neither the thesis nor substantial extracts from it may be printed or otherwise reproduced without his/her permission.

L'auteur conserve la propriété du droit d'auteur qui protège sa thèse. Ni la thèse ni des extraits substantiels de celle-ci ne doivent être imprimés ou autrement reproduits sans son autorisation.

ISBN 0-315-88484-3

Canada

Name Halsey Boyd

Dissertation Abstracts International is arranged by broad, general subject categories. Please select the one subject which most nearly describes the content of your dissertation. Enter the corresponding four-digit code in the spaces provided.

Statistics

0463

U·M·I

SUBJECT TERM

SUBJECT CODE

Subject Categories

THE HUMANITIES AND SOCIAL SCIENCES

COMMUNICATIONS AND THE ARTS
 Architecture 0729
 Art History 0377
 Cinema 0900
 Dance 0378
 Fine Arts 0357
 Information Science 0723
 Journalism 0391
 Library Science 0399
 Mass Communications 0708
 Music 0413
 Speech Communication 0459
 Theater 0465

EDUCATION
 General 0515
 Administration 0514
 Adult and Continuing 0516
 Agricultural 0517
 Art 0273
 Bilingual and Multicultural 0282
 Business 0688
 Community College 0275
 Curriculum and Instruction 0727
 Early Childhood 0518
 Elementary 0524
 Finance 0277
 Guidance and Counseling 0519
 Health 0680
 Higher 0745
 History of 0520
 Home Economics 0278
 Industrial 0521
 Language and Literature 0279
 Mathematics 0280
 Music 0522
 Philosophy of 0998
 Physical 0523

Psychology 0525
 Reading 0535
 Religious 0527
 Sciences 0714
 Secondary 0533
 Social Sciences 0534
 Sociology of 0340
 Special 0529
 Teacher Training 0530
 Technology 0710
 Tests and Measurements 0288
 Vocational 0747

LANGUAGE, LITERATURE AND LINGUISTICS
 Language
 General 0679
 Ancient 0289
 Linguistics 0290
 Modern 0291
 Literature
 General 0401
 Classical 0294
 Comparative 0295
 Medieval 0297
 Modern 0298
 African 0316
 American 0591
 Asian 0305
 Canadian (English) 0352
 Canadian (French) 0355
 English 0593
 Germanic 0311
 Latin American 0312
 Middle Eastern 0315
 Romance 0313
 Slavic and East European 0314

PHILOSOPHY, RELIGION AND THEOLOGY
 Philosophy 0422
 Religion
 General 0318
 Biblical Studies 0321
 Clergy 0319
 History of 0320
 Philosophy of 0322
 Theology 0469

SOCIAL SCIENCES
 American Studies 0323
 Anthropology
 Archaeology 0324
 Cultural 0326
 Physical 0327
 Business Administration
 General 0310
 Accounting 0272
 Banking 0770
 Management 0454
 Marketing 0338
 Canadian Studies 0385
 Economics
 General 0501
 Agricultural 0503
 Commerce-Business 0505
 Finance 0508
 History 0509
 Labor 0510
 Theory 0511
 Folklore 0358
 Geography 0366
 Gerontology 0351
 History
 General 0578

Ancient 0579
 Medieval 0581
 Modern 0582
 Black 0328
 African 0331
 Asia, Australia and Oceania 0332
 Canadian 0334
 European 0335
 Latin American 0336
 Middle Eastern 0333
 United States 0337
 History of Science 0585
 Law 0398
 Political Science
 General 0615
 International Law and Relations 0616
 Public Administration 0617
 Recreation 0814
 Social Work 0452
 Sociology
 General 0626
 Criminology and Penology 0627
 Demography 0938
 Ethnic and Racial Studies 0631
 Individual and Family Studies 0628
 Industrial and Labor Relations 0629
 Public and Social Welfare 0630
 Social Structure and Development 0700
 Theory and Methods 0344
 Transportation 0709
 Urban and Regional Planning 0999
 Women's Studies 0453

THE SCIENCES AND ENGINEERING

BIOLOGICAL SCIENCES
 Agriculture
 General 0473
 Agronomy 0285
 Animal Culture and Nutrition 0475
 Animal Pathology 0476
 Food Science and Technology 0359
 Forestry and Wildlife 0478
 Plant Culture 0479
 Plant Pathology 0480
 Plant Physiology 0817
 Range Management 0777
 Wood Technology 0746

Biology
 General 0306
 Anatomy 0287
 Biostatistics 0308
 Botany 0309
 Cell 0379
 Ecology 0329
 Entomology 0353
 Genetics 0369
 Limnology 0793
 Microbiology 0410
 Molecular 0307
 Neuroscience 0317
 Oceanography 0416
 Physiology 0433
 Radiation 0821
 Veterinary Science 0778
 Zoology 0472
 Biophysics
 General 0786
 Medical 0760

EARTH SCIENCES
 Biogeochemistry 0425
 Geochemistry 0996

Geodesy 0370
 Geology 0372
 Geophysics 0373
 Hydrology 0388
 Mineralogy 0411
 Paleobotany 0345
 Paleocology 0426
 Paleontology 0418
 Paleozoology 0985
 Palynology 0427
 Physical Geography 0368
 Physical Oceanography 0415

HEALTH AND ENVIRONMENTAL SCIENCES
 Environmental Sciences 0768
 Health Sciences
 General 0566
 Audiology 0300
 Chemotherapy 0992
 Dentistry 0567
 Education 0350
 Hospital Management 0769
 Human Development 0758
 Immunology 0982
 Medicine and Surgery 0564
 Mental Health 0347
 Nursing 0569
 Nutrition 0570
 Obstetrics and Gynecology 0380
 Occupational Health and Therapy 0354
 Ophthalmology 0381
 Pathology 0571
 Pharmacology 0419
 Pharmacy 0572
 Physical Therapy 0382
 Public Health 0573
 Radiology 0574
 Recreation 0575

Speech Pathology 0460
 Toxicology 0383
 Home Economics 0386

PHYSICAL SCIENCES
 Pure Sciences
 Chemistry
 General 0485
 Agricultural 0749
 Analytical 0486
 Biochemistry 0487
 Inorganic 0488
 Nuclear 0738
 Organic 0490
 Pharmaceutical 0491
 Physical 0494
 Polymer 0495
 Radiation 0754
 Mathematics 0405
 Physics
 General 0605
 Acoustics 0986
 Astronomy and Astrophysics 0606
 Atmospheric Science 0608
 Atomic 0748
 Electronics and Electricity 0607
 Elementary Particles and High Energy 0798
 Fluid and Plasma 0759
 Molecular 0609
 Nuclear 0610
 Optics 0752
 Radiation 0756
 Solid State 0611
 Statistics 0463
 Applied Sciences
 Applied Mechanics 0346
 Computer Science 0984

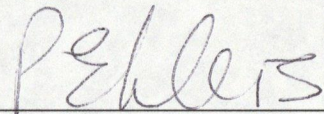
Engineering
 General 0537
 Aerospace 0538
 Agricultural 0539
 Automotive 0540
 Biomedical 0541
 Chemical 0542
 Civil 0543
 Electronics and Electrical 0544
 Heat and Thermodynamics 0348
 Hydraulic 0545
 Industrial 0546
 Marine 0547
 Materials Science 0794
 Mechanical 0548
 Metallurgy 0743
 Mining 0551
 Nuclear 0552
 Packaging 0549
 Petroleum 0765
 Sanitary and Municipal 0554
 System Science 0790
 Geotechnology 0428
 Operations Research 0796
 Plastics Technology 0795
 Textile Technology 0994

PSYCHOLOGY
 General 0621
 Behavioral 0384
 Clinical 0622
 Developmental 0620
 Experimental 0623
 Industrial 0624
 Personality 0625
 Physiological 0989
 Psychobiology 0349
 Psychometrics 0632
 Social 0451

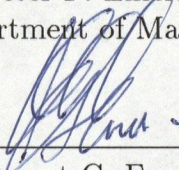


THE UNIVERSITY OF CALGARY
FACULTY OF GRADUATE STUDIES

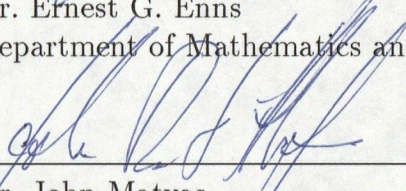
The undersigned certify that they have read, and recommend to the Faculty of Graduate Studies for acceptance, a thesis entitled, "Simulated Secants and Overlapping Ovoids," submitted by Halsey J. Boyd in partial fulfillment of the requirements for the degree of Master of Science.



Dr. Peter F. Ehlers
Department of Mathematics and Statistics



Dr. Ernest G. Enns
Department of Mathematics and Statistics



Dr. John Matyas
Postdoctoral Research Fellow
Department of Medicine
University of Calgary

Date 93-08-06

Abstract

The determination of chord-length distributions for various measures of randomness (including $\lambda, \nu, \mu, \gamma, \beta, \alpha$) through arbitrary ovoids K is important in many scientific disciplines, particularly stereology. Traditional methods of generating chord-length distributions for egg-shaped ovoids and non-symmetric polygons for which analytical results are difficult to obtain have previously involved direct simulation.

However, relationships exist between an overlap function Ω and chord, ray and segment distributions for various randomness measures that allow generation by two new approaches — the $f_{T;\lambda}$ and Ω methods.

In this thesis, the feasibility of the $f_{T;\lambda}$ and Ω methods will be examined for various two-dimensional ovoids, including circles, ellipses and arbitrary polygons. In three dimensions, only the $f_{T;\lambda}$ method will be studied for the ovoids ellipsoids, spheres, cubes, cylinders and hemispheres. Comparisons are made between the new approaches and the traditional simulation approach. Future directions and recommendations will also be discussed.

Acknowledgements

I would like to thank Dr. Peter F. Ehlers for his support, friendship and encouragement throughout my stay at the University of Calgary. Dr. Ehlers introduced me to the interesting world of stereology, and for that I shall forever be grateful. Dr. Ehlers has also provided me with financial support, whether it be to travel to California or Edmonton or photocopy irrelevant articles. His generosity was greatly appreciated. It was a pleasure being his teaching and research assistant.

Dr. E.G. Enns also provided me with funds for my trip to Nova Scotia and in my summer research duties, which can gladly start with the end of this thesis. His humour has enlightened me and has provided me with the stamina to go forward.

Tom Morrison has been a friend and colleague since our fateful meeting in September, 1991. I thank him for showing me how to appreciate life to the fullest, and relive my lost youth. Passing on his consulting knowledge and expertise was also a greatly appreciated sacrifice.

My family kept me well-fed, in-transit and sleepless, and I thank Taggart, Darby, Chad, Peggy and Mom and Dad for their support. Without them I would have been even later for my meetings with my supervisor. Mr. and Mrs. Santosh Dey offered continuous support and encouragement since Grade 10, plus a relaxing environment in Salmon Arm.

Finally, four friends at the University of Calgary have helped tremendously — Indy Lagu, Bonaventure Anthonio, Kelly Candy and Peter Gibson.

Contents

Approval Page	ii
Abstract	iii
Acknowledgements	iv
1 Introduction	1
1.1 Some Practical Applications of Stochastic Geometry	1
1.1.1 Geology	2
1.1.2 Radiology	2
1.1.3 Nuclear Physics	3
1.1.4 Metallurgy	4
1.1.5 Biology	5
1.1.6 Acoustics	5
1.1.7 Computer Science	6
1.1.8 Oceanography	6
1.2 Types of Randomness	7
1.3 The Direct Simulation Method	12
1.4 The $f_{T,\lambda}$ or Segment Method	14
1.5 The Overlap or Ω Method	15
1.6 The New Approaches	16
1.7 Comparisons To Be Made	18
1.8 Overview	20
2 Review of Theory	22
2.1 Introduction and Notation	22
2.2 The Randomness Measure μ	26
2.3 The Randomness Measure ν	28
2.4 The Randomness Measure λ	34
2.5 The Randomness Measure γ	38
2.6 The Randomness Measure α	40
2.7 The Randomness Measure β	43
2.8 Inequalities and Moment Relations	45
2.9 Summary of Fundamental Relationships	47

3	Ovoids in Two Dimensions	51
3.1	The $f_{T;\lambda}$ Method	52
3.1.1	Orthogonal Series Estimators	53
3.1.2	Kernel Smoothers	54
3.2	The Ω Method	57
3.3	Methods of Comparison	59
3.4	Polygons	60
3.4.1	The $f_{T;\lambda}$ Program	60
3.4.2	The Ω or Polygon Program	62
3.4.3	Results For The Triangle	65
3.4.4	Results For The Rectangle $a \times b$	75
3.5	The n -Sphere — Special Case: Circular Ovoid	82
3.5.1	Theory	82
3.5.2	Results for $n = 2$ — Circle	84
3.6	Results For The Ellipse	93
4	Ovoids in Three Dimensions	101
4.1	Results For The Box (Cube)	101
4.2	Results For The Ellipsoid	116
4.2.1	The Prolate Spheroid	116
4.3	Results For The Sphere	120
4.4	Results For The Hemisphere	133
4.5	Results For The Cylinder	135
4.6	$\Omega(l)$ versus $f_{T;\lambda}$ — A Brief Summary	138
5	Future Directions	140
5.1	Polyhedra	140
5.2	Bivariate Rays	142
5.3	Non-uniform Directions	144
5.4	Exotic and Embedded Bodies	144
	Bibliography	150
	Appendix A Computer Code for Polygon Program	158

List of Tables

1.1	Types of randomness	10
1.2	References for computer simulations of chords through selected ovoids	12
1.3	References for computer simulations of chords through selected ovoids	13
1.4	Summary of simulations performed — 2-dimensions	19
1.5	Summary of simulations performed — 3-dimensions	19
2.1	Notation	22
2.2	Notation	23
2.3	Notation	24
2.4	Moment relations between densities depending only on $V(K)$ and $S(K)$	46
2.5	Moment relations between densities	47
2.6	Relationships of pdfs to $\Omega(l)$	48
2.7	Relationships to $\hat{f}_{T;\lambda}(l)$	50
3.1	Types of kernels used	56
3.2	Actual distributions for the unit circle	83

List of Figures

1.1	Types of randomness	11
1.2	Illustration of the $f_{T;\lambda}$ method	14
1.3	Overlap volume of 2 semicircles	15
2.1	Conical subsets $\Pi(l, P)$ that fall partially outside K (shaded)	24
2.2	Surface overlap function (ω) for the rectangle	25
2.3	Demonstration of μ -random secants	26
2.4	Illustration of ν -random chords and rays	28
2.5	Relation of ν -random ray length distribution to Ω	29
2.6	Solid angles subtended at a random point	33
2.7	Illustration of λ -random chords and rays	34
2.8	Sample chord under γ -randomness	38
2.9	Illustration of α -random chords and rays	40
2.10	Representative chords under α -randomness	42
2.11	Illustration of β -random chords and rays	44
3.1	Testing for interior points for a polygon	61
3.2	Classifying points for the polygon program	63
3.3	Polygonal area	64
3.4	Surface Randomness for the Triangle	66
3.5	$f_{L,\gamma}$ for the equilateral triangle — several kernel fits to demonstrate surface-randomness	68
3.6	$f_{T,\lambda}$ for various triangles from Ω program	69
3.7	$\Omega(l)$ for various triangles from Ω program	70
3.8	$f_{R,\nu}$ for the equilateral triangle — estimate via Ω method versus $f_{T,\lambda}$ method	71
3.9	$f_{R,\lambda}$ for the equilateral triangle — actual curve versus Ω method versus $f_{T,\lambda}$ method [actual curve and Ω method are indistinguishable]	72
3.10	$f_{L,\nu}$ for the equilateral triangle — actual curve versus Ω method versus $f_{T,\lambda}$ method	73
3.11	$f_{L,\lambda}$ for the equilateral triangle — actual curve versus Ω method versus $f_{T,\lambda}$ method	74
3.12	$f_{T,\lambda}$ for the rectangle ($a = 1.0$) — fitted kernel smoother versus polygon program [actual curve and Ω method are indistinguishable]	77
3.13	$f_{T,\lambda}$ for the rectangle ($a = 0.4$) — fitted kernel smoother versus polygon program [actual curve and Ω method are indistinguishable]	78
3.14	$f_{R,\lambda}$ for the rectangle ($a = 0.5$) — estimate via Ω versus estimate via $f_{T,\lambda}$	79

3.15	$f_{L,\lambda}$ for the rectangle ($a = 1.0$) — estimate via Ω versus estimate via $f_{T,\lambda}$	80
3.16	$f_{L,\nu}$ for the rectangle ($a = 0.2$) — estimate via Ω versus estimate via $f_{T,\lambda}$	81
3.17	Convergence of $f_{T,\lambda}$ using Ω for inscribed polygons	86
3.18	$f_{T,\lambda}$ for the unit circle — estimate via Ω versus estimate via direct simulation (best kernel fit) [actual curve and Ω method are indistinguishable]	87
3.19	Convergence of $f_{T,\lambda}$ using Ω for equal-area polygons	88
3.20	$f_{R,\lambda}$ for the unit circle — estimate via Ω versus estimate via $f_{T,\lambda}$	89
3.21	$f_{R,\nu}$ for the unit circle — estimate via Ω versus estimate via $f_{T,\lambda}$	90
3.22	$f_{L,\nu}$ for the unit circle — estimate via Ω	91
3.23	$f_{L,\mu}$ for the unit circle — estimate via Ω	92
3.24	Ellipse Surface Randomness	94
3.25	$f_{L,\gamma}$ for the ellipse ($a = 2, b = 1$) — several kernel fits	96
3.26	$f_{L,\beta}$ for the ellipse ($a = 2, b = 1$) — several kernel fits	97
3.27	$f_{R,\alpha}$ for the ellipse ($a = 2, b = 1$) — several kernel fits	98
3.28	$f_{L,\alpha}$ for the ellipse ($a = 2, b = 1$) — several kernel fits	99
3.29	$f_{T,\lambda}$ for the ellipse ($a = 2, b = 1$) — direct simulation versus estimate via Ω method	100
4.1	$f_{T,\lambda}(l)$ for the cube — several kernel fits	105
4.2	$f_{R,\lambda}(l)$ for the cube — several kernel fits	106
4.3	$f_{R,\lambda}$ for the cube — estimates via the $f_{T,\lambda}$ method	107
4.4	$f_{R,\nu}(l)$ for the cube — several kernel fits	108
4.5	$f_{R,\nu}$ for the Cube — estimates via $f_{T,\lambda}$ method	109
4.6	$f_{L,\nu}(l)$ for the cube — several kernel fits	110
4.7	$f_{L,\nu}$ for the Cube — estimates via $f_{T,\lambda}$ method	111
4.8	$f_{L,\lambda}(l)$ for the cube — several kernel fits	112
4.9	$f_{L,\lambda}$ for the cube — estimates via $f_{T,\lambda}$ method	113
4.10	$f_{L,\mu}(l)$ for the cube — several kernel fits	114
4.11	$f_{L,\mu}$ for the cube — estimates via $f_{T,\lambda}$ method	115
4.12	$f_{R,\lambda}(l)$ for the ellipsoid ($a = 3, b = 2, c = 1$) — kernel fit versus estimate via $f_{T,\lambda}$ method	118
4.13	$f_{L,\mu}(l)$ for some ellipsoids	119
4.14	$f_{L,\mu}(l)$ for the sphere — several kernel fits	122
4.15	$f_{L,\gamma}(l)$ for the sphere — several kernel fits	123
4.16	$f_{R,\alpha}(l)$ for the sphere — several kernel fits	124
4.17	$f_{L,\alpha}(l)$ for the sphere — several kernel fits	125
4.18	$f_{R,\nu}(l)$ for the sphere — several kernel fits	126

4.19	$f_{L,\nu}(l)$ for the sphere — several kernel fits	127
4.20	$f_{L,\lambda}(l)$ for the sphere — several kernel fits	128
4.21	$f_{T,\lambda}(l)$ for the sphere — several kernel fits	129
4.22	$f_{R,\lambda}(l)$ for the sphere — several kernel fits	130
4.23	$f_{R,\nu}$ for the sphere — estimates via $f_{T,\lambda}$ method	131
4.24	$f_{R,\lambda}$ for the sphere — estimates via $f_{T,\lambda}$ method	132
4.25	$f_{L,\nu}(l)$ for the hemisphere — several Gaussian kernel fits for different window widths	134
4.26	$f_{T,\lambda}$ for the cylinder — several Gaussian kernel fits for different window widths	136
4.27	$f_{R,\lambda}$ for the cylinder — estimates via $f_{T,\lambda}$ method from Gaussian parent kernel	137
5.1	Bivariate overlap function	143
5.2	Embedded body — generation of T	145
5.3	Embedded body — generation from within K	146
5.4	Rays in G generated by two points in K and G	148

Chapter 1

Introduction

Stochastic geometry (synonymous with geometric probability) deals with random geometric objects. For an excellent introduction to this growing field see Kendall and Moran [50] or Solomon [91].

Stereology, a branch of applied stochastic geometry, is primarily concerned with the problem of recovering, from available planar or linear sections, information on a three-dimensional structure. An important objective of stereology is to determine particle size/shape distributions from planar or linear cuts through the particle, such cuts usually at a microscopic level. Linear cuts through a specimen yield secant length distributions, a secant being a chord through two points on the boundary of the particle, i.e. the intersection of a straight line with the particle. Relationships between particle size/shape distributions and linear intercept distributions can be found in Kok [53], Weibel [103], Russ [82] or Stoyan *et al.* [95]. Determining secant length distributions for various particle shapes is therefore important in stereology, and indeed in many other scientific disciplines.

1.1 Some Practical Applications of Stochastic Geometry

In this section, applications that require the calculation of intercept length distributions will be discussed. Many problems arising in geology, radiology, nuclear physics, metallurgy, biology, acoustics, computer science and oceanography, among others,

involve determining the length distribution of some type of ray through a body K .

1.1.1 Geology

In geology, Hanson [38] verifies through computer simulation the relationship of grain density of minerals to the average intercept length of a test line with the grain surface. Riss and Durand [78] simulate areal sectioning applied to identification of particle shape for cubes and various polyhedra for a geological application. In this paper they are interested in typical mosaic patterns seen on thin or polished sections of crystalline aggregates. Warren [98] conducted an experimental study where a microstructure was simulated of uniformly sized steel cubes dispersed in a matrix of a lead-tin alloy. This application verified Itoh's [44] result.

1.1.2 Radiology

Radiology connotes the use of ionizing radiation as a diagnostic tool. Applications in radiology are therefore those that analyze the diagnostic devices. For example, Birkhoff *et al.* [4] note that pulse height spectra observed from energy-proportional devices, such as a cylindrical gas proportion counter, depend partly on the track length distributions of charged particles in the sensitive volume of the device. Birkhoff simulates chord length distributions in right circular cylinders of finite length, and reviews results for infinite slabs, spheres and infinite cylinders. Wilson and Emery [107] are also interested in this problem, and present a calculation of path length distributions for cylinders in an isotropic distribution of straight tracks.

1.1.3 Nuclear Physics

Applications of linear-intercept distributions to nuclear physics are basically confined to analysis of paths of radioactive rays through some sensitive area. Primak [77] estimates the gamma-ray dosage in samples undergoing irradiation in nuclear reactors through path length of such a ray to a reactor wall. Goudsmit [33] solves a problem asked of him by Niels Bohr. In cloud chamber experiments errors could occur in interpretation because tracks might seem to originate from the same point. In response to this Goudsmit studied the probability of several independent tracks intersecting at almost the same point. Dirac *et al.* [20] used chord length distributions in relation to the shape of radioactive material in the atomic bomb, since the critical mass of the bomb depends on the shape of uranium. Also, bombardment by cosmic rays and the corresponding threat of spontaneous ignition were contributing factors to their research. Caswell [10] considers neutrons in spheres, and Rossi [80] evaluates pulse height spectra obtained with proportional counters.

Langworthy and Bendel recently extended the study of path lengths through some sensitive area to space electronics. In space electronics, one is often interested in predicting single event “upsets”. Such upsets include events that produce sufficient ionization, such as alpha emission by some radioactive impurity in the materials, highly ionized cosmic ray tracks and interactions with high energy protons. Langworthy [61], [63] and Bendel [3] apply linear-intercept distributions, and note that upsets occur when the rate of ionization along a path multiplied by the path length of a ray through a sensitive area exceeds the critical charge.

Kellerer [47] gives other references for acoustics, reactor design, microscopy, ra-

diation physics, microdosimetry and general dosimetry. He calculates the μ -random chord distribution for the cylinder and considers surface radiator (γ) randomness in the context of radiation physics.

1.1.4 Metallurgy

In metallurgical science it is often of interest to estimate the distribution of sizes of particles embedded in an opaque material such as an alloy. For an example, see Fullman [28]. Hilliard [41], [42] hints at another application — the analysis of semi-transparent materials by reflected light, where the depth of light penetration corresponds to the section's thickness. Hilliard shows the relationship between moments of the size distribution and the distribution of intercept lengths on particle profiles. Gurland [36] and Butler [9] analyze WC-Co alloy strengths (WC is simply a cement). They note that above a critical mean path length of intercepts the strength of the alloy is proportional to the volume fraction of WC, and is inversely proportional to the WC particle size. Thus they relate the material behaviour with the structure of this alloy.

Using an alternative approach, Sepulveda *et al.* [88] use a computer simulation to determine volumetric abundance of certain valuable minerals from linear intercepts through the volume. Goldsmith [32] uses particle size distributions, obtained from measurements of particle sizes in a thin section, applied to delustrant and pigment particle sizes seen in a micrograph of a slice of polymer chip or extruded fibre.

1.1.5 Biology

In biology Melhuish and Lang [57], [58] use planar cuts of plant roots to estimate lengths and diameters. They do so by relating the probable total length of root to the number of intersections made with a plane of unit area cut through the soil. McIntyre [67] uses linear intercepts to estimate the percentage ground cover by different species in a stand. McIntyre considers different sampling quadrats and determines that established perennials in open shrub or grassland communities having plants of fairly regular shape and cover have densities which can be estimated from transect chords. Hammersley [37] measured the damage caused to plants by the presence of radioactive tracers in the fertilizers (which could also be considered a radiology application).

In biology and in medicine in the organs of the body (animal or human) a number of small, fairly regular shaped particles are embedded in the tissue. These particles vary greatly in size and number between and within organs, and between individuals. For example, Wicksell [105], [106] used areas of spleen contours to express the distribution of sizes of embedded particles, and uses linear intercepts of these contours to calculate a distribution function of particle diameters.

Gundersen *et al.* [35] study needle biopsies of the kidneys of four humans and wedge biopsies of the kidneys of two animals (a rat and a bull) by intercepts to determine membrane thickness.

1.1.6 Acoustics

In acoustics Kingman [52] considers a convex room with perfectly reflecting walls having a particle projected from a point inside. The particle bounces around, its

trajectory after many reflections being many segments whose average length is the mean free path. For certain room shapes, then, the mean free path depends on the point of initial trajectory and the direction of projection. Bate and Pillow [2] calculate this mean path of sound in an auditorium. Kosten [54] uses the mean free path of an enclosure, which is of practical use in diffuse sound fields, and develops stereological relationships dealing with reverberation time in proportion to path length of reflected sound rays.

1.1.7 Computer Science

In computer science applications You *et al.* [108] use chord length distributions in pattern recognition. Such distributions can help discriminate between planar closed shapes. In this article a Kolmogorov-Smirnov goodness-of-fit test is used to distinguish between shapes, and a simulation is done using countries as shapes. In a related article Heckbert [40] uses ray-surface intersections as a means or algorithm to synthesize general images, in this case Jell-O[®].

1.1.8 Oceanography

In oceanography, Rothrock and Thorndike [81] measure the distribution of ice floe sizes by sampling lengths of line segments on floes. Another application of stereological methods to Arctic oceanography is the determination of the probability of an object colliding with a ridge in an old (multi-year) ice floe. The structure has to dissipate the kinetic energy of the ice floe. The greatest loads occur when the structure is interacting with a ridge, ridges being the thicker portions of the floe. Knowledge of the probability of an interaction between a structure and a ridge can

be used in risk analyses and design load calculations. In one study the distance from the edge of a floe to a ridge, the spacing between ridges, and the angle between the centreline of a ridge and a structure were determined by drawing random lines across aerial photographs of floes (see Morrison [70]).

Marcellus and Morrison [65] also consider the size distribution of ice floes. They relate structure design for locations in the Beaufort Sea with the distribution of sizes of old, multi-year ice floes. From publicly available records of upward-looking profiles of the under-ice canopy of the Arctic Ocean obtained from American nuclear submarine transects, they determine the distributions of chord lengths of floes. See also Wadhams *et al.* [97] and McLaren *et al.* [56].

1.2 Types of Randomness

Clearly, linear intercept distributions are important. These distributions can be generated by segments T , rays R or chords L . A *segment* connects two points in the interior of some body K , a *ray* connects a point in the interior of K with a point on the boundary of K , and a *chord* connects two boundary points of K . Both segments and rays can obviously be extended to the boundary of K to form chords.

Various types of randomness define different segment, ray or chord distributions. These measures arise when different processes are used to generate the linear element (segment, chord or ray). For K we consider only *ovoids* (compact convex subsets of \mathcal{R}^n with nonempty interior). For example, ν -random rays are generated as follows: choose a point P randomly inside K . Then choose, independently of P , some random direction θ . The resulting ν -random ray extends from P to the surface of

K in direction θ . Other types of randomness consist of choosing independently and uniformly random (IUR) combinations of points (both surface and interior points of K) and directions.

In a series of papers, Enns and Ehlers [22], [23], [24], [25], [26] have discussed the theory of random linear probes in convex bodies. Their focus has been on six types of randomness. These random measures fall naturally into three sets. The so-called β -measure involves two surface-random points. The measures labelled α and γ involve one point selected in the surface of the body. Finally, measures μ , ν and λ do not employ any surface-random points.

Kingman [51], [52] has shown that the chord-length distributions for the three measures μ , ν and λ are simply related. Enns and Ehlers provide further relations involving ray-length and segment-length distributions. They also derive (Enns and Ehlers [24]) a relation between α - and γ -random chord-length distributions.

Analytical results are extremely complicated for any but the simplest shapes of convex bodies. Simulation of probability density functions for chord- and ray-length is therefore important. Such simulations have been reported by Itoh [44] and Warren and Naumovich [101]. All of the reported simulations have employed what in this thesis will be called the *direct simulation method*. For example, Itoh directly simulates μ -random chords in a cube and compares the resulting density function of chord length with the analytical density function. Warren simulates μ -random chords through cubes and ellipsoids.

The principal aim of this thesis is the investigation of the feasibility of two alternative methods for the simulation of chord- and ray-length density function of type in $\{\mu, \nu, \lambda\}$. One of these methods ($f_{T,\lambda}$ or *segment method*) is based on the fact that

all such density functions are related to the probability density function for segment length under λ -randomness, which is relatively easy to generate. The second new method (*overlap* or Ω *method*) results from the relation of chord-, ray- and segment-length density functions to the *overlap function* for the convex body, as defined by Enns and Ehlers [23]. This overlap-function method is inherently appealing since it is deterministic, that is, it does not involve any random-number generation.

The various types of randomness are defined in Table 1.1 and Figure 1.1. Note in particular that different types of randomness generate multiple distributions of path lengths. Under λ -randomness, in particular, three different distributions exist: one for segments, one for rays and one for chords. Table 1.1 includes references to Figures in Chapter 2 where theory is presented.

Table 1.1: Types of randomness

Randomness		<i>Description</i>
W, ν	Interior radiator randomness Weighted invariant randomness.	A point $P \in K$ and a direction θ are chosen independently and uniformly random. See Figures 2.4, 2.5.
μ	Invariant uniform randomness Isotropic uniform randomness Mean-free path randomness.	From a beam of parallel rays with a uniformly random orientation that hit the body, the secant is uniformly random. See Figure 2.3.
λ	—	Points P and Q in K are chosen independently and uniformly random. See Figure 2.7.
α	—	A point P in K and a point Q on the surface of K are chosen independently and uniformly random. See Figures 2.9, 2.10.
β	—	Both points P and Q are chosen independently and uniformly random from the surface of K . See Figure 2.11.
S, γ	Surface radiator randomness	A point P on the surface of K and a direction θ are chosen independently and uniformly random. See Figure 2.8.

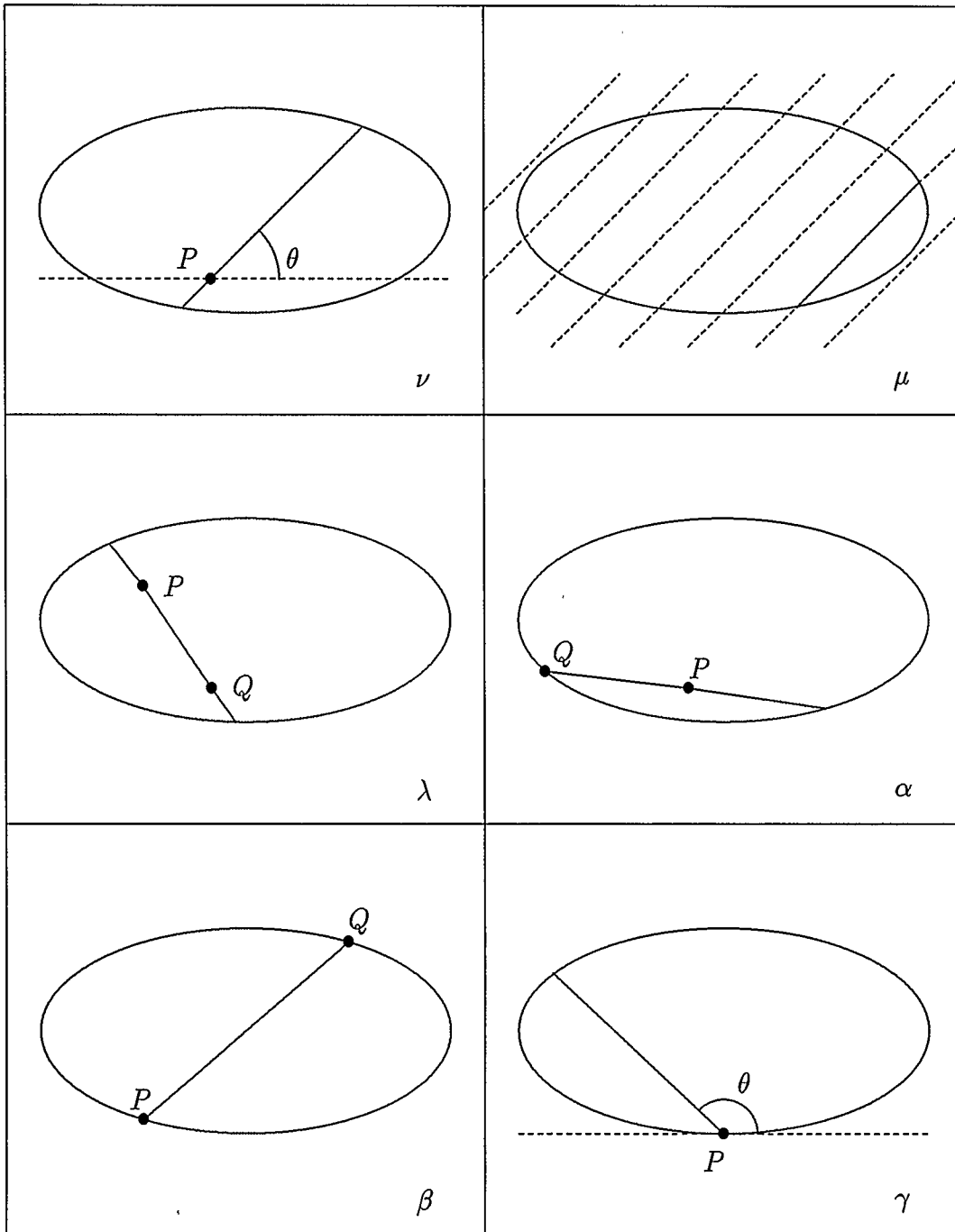


Figure 1.1: Types of randomness

1.3 The Direct Simulation Method

For simple ovoids K , calculation of the analytical distributions for various randomnesses is possible. In Chapters 3 and 4, results and article references are given for various ovoids. However, for non-simple ovoids, such as non-symmetric polygons or egg-shaped ovoids, the calculation of actual intercept length distributions is difficult. Direct simulation was the only method available for determining within some accuracy an estimate of a distribution.

Traditionally, Warren and Naumovich [101] and Itoh [44] were the first to simulate chord distributions under μ -randomness. Tables 1.2 and 1.3 give several articles where simulations were performed through various convex bodies. Results given in these articles will provide a useful check on simulation results for Chapters 3 and 4.

Table 1.2: References for computer simulations of chords through selected ovoids

Reference	Description
Barbery [1]	Analysis by test lines for the measures γ , β , λ , α and μ for right cylinders, ellipsoids and boxes.
Itoh [44]	Derives analytical expressions of distribution of μ -random chord length of a randomly oriented cube, and confirms with a computer simulation.
Riss <i>et al.</i> [79]	Simulates μ -random chord distribution for various polyhedra.

Table 1.3: References for computer simulations of chords through selected ovoids

Reference	Description
Naumovich and Kriskovets [72]	A computer simulation of the random intersecting process used to derive relative frequency distribution of random intercepts through deformed cubes and pentagonal and hexagonal prisms of different heights.
Naumovich and Warren [73]	Simulation of μ -random chords to determine relative influence of particle size and particle shape distribution on intercept length distribution observed on a section. Ovoids considered included the sphere, ellipsoids, cube-spheres, cube, rectangular prisms and triangular prisms.
Naumovich <i>et al.</i> [71]	Uses a Monte-Carlo simulation of μ -random chords through a cube as a check for programs simulating μ -random chords through various polyhedra.
Warren and Naumovich [101]	Computer simulation of μ -random chords through ellipsoids, rounded cubes, orthogonally-faceted spheres, rectangular prisms and triangular prisms in a method similar to Itoh [44].
Warren and Durand [100]	Explores stereological relationships between such parameters as mean number of features per volume and the number per unit area of section by computer simulation μ -random chords through cubic particles, plates, polyhedra and ellipsoids.
Wasén and Warren [102]	A comprehensive look at chord distributions for various polyhedra.

1.4 The $f_{T;\lambda}$ or Segment Method

The segment method first involves direct simulation of the segment λ -random distribution. This simulation is relatively easy to generate, since it involves choosing two points inside some convex body K (see Figure 1.2). This is done by choosing two random interior points in the rectangle $[a, b] \times [c, d]$ and classifying them as interior/exterior.

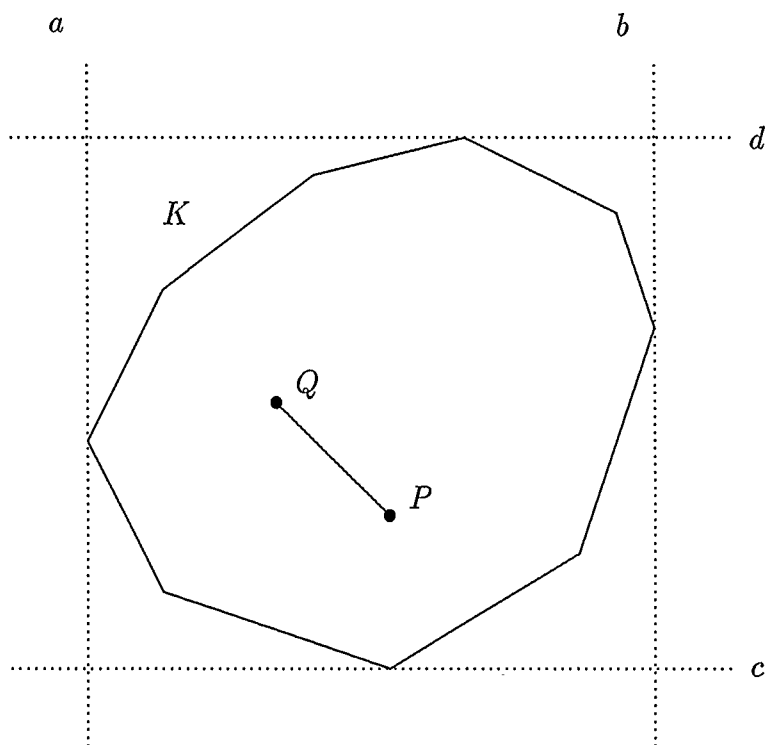


Figure 1.2: Illustration of the $f_{T;\lambda}$ method

The segment method involves repeated selection of interior points to generate a number of random segments whose lengths are then grouped to form a histogram. Relationships between several densities and the segment λ -random density are developed in Chapter 2. Several of these relations require the use of derivatives of

the estimated segment density. Calculation of derivatives requires the use of non-parametric density estimates, other than the histogram, that smooth the density and provide differentiable estimates. These nonparametric density smoothers will be explained in Chapter 3.

1.5 The Overlap or Ω Method

The overlap function can be explained by first translating some body K a distance l in direction θ to form $K(l, \theta)$ (see Figure 1.3).

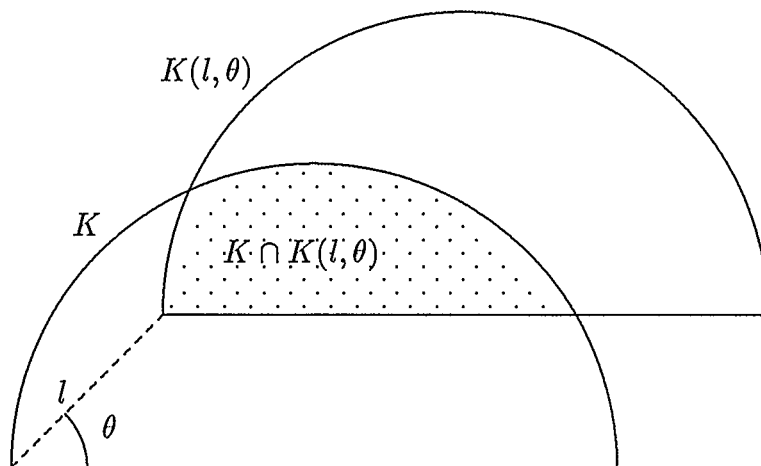


Figure 1.3: Overlap volume of 2 semicircles

The volume of the intersection of K with its translate, when averaged over θ , yields $\Omega(l)$. The overlap function is important because it is related to the λ -, ν - and μ -random length distributions. These relationships will be discussed in Chapter 2.

1.6 The New Approaches

A new approach, proposed in this thesis, is to exploit the relationships that exist between the segment length distribution, the overlap function, and the λ -, μ - and ν -random length distributions to determine the relevant ray, chord or segment distributions. Relevant in this sense means ν - and λ -random ray and chord and μ -random chord densities, integrally related to the overlap function and to the segment density. We wish to determine the feasibility of the Ω method or the $f_{T;\lambda}$ method as generators of the related distributions. The following comparisons will be made:

Estimate via direct simulation

versus

Estimate via Ω method (new)

versus

Estimate via $f_{T;\lambda}$ method (new).

Both proposed new methods obtain chord- and ray-length probability density functions by differentiating a simulated function. Such derived functions are strongly dependent on the accuracy of the original, simulated function. The principal value of these methods lies in their simplicity. Direct simulation for arbitrarily shaped convex bodies is very awkward to implement. From a programming point of view, existing code for one shape requires significant modification for other shapes. The ‘segment’ method, on the other hand, involves only the generation of two random

interior points. Shape dependence is then confined to the problem of classifying random points as exterior/interior.

In the Ω or ‘overlap’ method one must determine the content of the intersection of the convex body with a translate of itself. While this is not quite as simple as the ‘segment’ method, it is nonetheless much simpler than the direct simulation approach. This is particularly true for arbitrary polygonal regions in \mathcal{R}^2 .

This thesis reports results of applying the ‘segment’ method to both two- and three-dimensional bodies. The chief difficulty is the problem of fitting the segment-length density curve sufficiently well to obtain good estimates for the first two derivatives of this curve which are required for the chord- and ray-length density functions. Unfortunately, the results are not encouraging.

The Ω method was applied only to polygons in \mathcal{R}^2 . Comparison of polygonal approximations with analytical results for the circle indicates that polygonal approximations with relatively few vertices should work well for non-polygonal shapes. We expect that in \mathcal{R}^3 polyhedral approximations will work as well. The decision to restrict this method to \mathcal{R}^2 was made because there exists a very efficient procedure for computing the area of a polygon in terms of its vertices. Thus we are able to avoid computing the overlap by pixel-counting. We are not aware of a similar efficient procedure in \mathcal{R}^3 . Three-dimensional problems would therefore have to employ voxel-counting, which we consider to be too inefficient for determining the overlap. (It may be possible to use image analysis software to determine the overlap function. This possibility was not investigated.)

Objects in reality do not appear as perfect circles and ellipses, and it is the purpose of this thesis to try to determine a methodology for dealing with non-trivial shapes,

such as non-symmetric polygons and egg-shaped ovoids. “Simulated Secants and Overlapping Ovoids”¹ is a step in this direction.

1.7 Comparisons To Be Made

In two dimensions, comparisons will be made only for the following two-dimensional ovoids: arbitrary ellipses and polygons (including the circle, square, equilateral triangle). In three dimensions, comparisons will be made between direct simulation and the segment density approaches for the following ovoids: hemispheres, spheres, cubes, ellipsoids, cylinders. A summary of the work completed for this thesis is given in Tables 1.4 and 1.5. In the two-dimensional table, there are three columns. Direct denotes direct simulation of the density, $f_{T;\lambda}$ denotes generation of that density through the segment length distribution, and Ω denotes generation through the overlap function. In three dimensions, of course, only the direct simulation and the segment length density approaches are possible. A “√” denotes completed work and an “F” signifies that more work is required. Chapter 5 considers possible directions in extending the comparisons to include those entries marked with an “F”.

¹This title basically refers to the comparison of simulated intercepts through a body and the corresponding overlap function.

Table 1.4: Summary of simulations performed — 2-dimensions

Measure		Ellipse (Circle)			Rectangle			Triangle			Polygons		
		Direct	$f_{T;\lambda}$	$\Omega(l)$	Direct	$f_{T;\lambda}$	$\Omega(l)$	Direct	$f_{T;\lambda}$	$\Omega(l)$	Direct	$f_{T;\lambda}$	$\Omega(l)$
λ	R	✓	✓	✓	✓	✓	✓	✓	✓	✓	✓	✓	✓
λ	L	✓	✓	✓	✓	✓	✓	✓	✓	✓	✓	✓	✓
ν	R	✓	✓	✓	✓	✓	✓	✓	✓	✓	✓	✓	✓
ν	L	✓	✓	✓	✓	✓	✓	✓	✓	✓	✓	✓	✓
μ	L	✓	✓	✓	✓	✓	✓	✓	✓	✓	✓	✓	✓
α	R	✓			✓			✓			✓		
α	L	✓			✓			✓			✓		
γ	L	✓			✓			✓			✓		
β	L	✓			✓			✓			✓		

✓ — Completed F — Future

Table 1.5: Summary of simulations performed — 3-dimensions

Measure		Sphere		Ellipsoid		Box		Hemisphere		Cylinder		Polyhedra	
		Direct	$f_{T;\lambda}$	Direct	$f_{T;\lambda}$	Direct	$f_{T;\lambda}$	Direct	$f_{T;\lambda}$	Direct	$f_{T;\lambda}$	Direct	$f_{T;\lambda}$
λ	R	✓	✓	✓	✓	✓	✓	✓	✓	✓	✓	F	F
λ	L	✓	✓	✓	✓	✓	✓	✓	✓	✓	✓	F	F
ν	R	✓	✓	✓	✓	✓	✓	✓	✓	✓	✓	F	F
ν	L	✓	✓	✓	✓	✓	✓	✓	✓	✓	✓	F	F
μ	L	✓	✓	✓	✓	✓	✓	✓	✓	✓	✓	F	F
α	R	✓		F		✓		✓		✓		F	
α	L	✓		F		✓		✓		✓		F	
γ	L	✓		F		✓		✓		✓		F	
β	L	✓		F		✓		✓		✓		F	

✓ — Completed F — Future

Comparisons were made only visually. Recall that the purpose of this thesis is to study the feasibility of using the alternative methods to generate distributions. Quantitative comparisons between the methods, although important, were not incorporated into the analysis. Note also that some α , β and γ results are presented, although they do not fit into the comparison category since they are not related to either the overlap function or the segment density.

1.8 Overview

Chapter 2 contains the theory and its development that relates the segment length distribution, the overlap function and the λ , ν and μ densities. Chapter 2 also derives relationships between the β , γ and α densities.

Chapter 3 presents results for two-dimensional ovoids. In this chapter, some of the techniques used to generate λ - and ν -random ray and λ -, ν - and μ -random chord densities from either the segment length distribution or the overlap function are given. These techniques include the use of splines and the use of nonparametric density smoothers. Chapter 3 also contains the driving algorithm behind the polygon program. References for theoretical results for each ovoid — circles, ellipses, rectangles, triangles — are given, as well as special techniques that may have been required in direct simulations, including some new results for ellipse surface-randomness.

Chapter 4 extends the analysis to three dimensions (but no overlap method) by presenting results for the sphere, cube, cylinder, hemisphere and ellipsoid. Again, techniques for direct simulation and references where appropriate or available are given.

Chapter 5 points to possible future directions, such as extending the polygon program to three dimensions.

Chapter 2

Review of Theory

2.1 Introduction and Notation

Six different random measures for generating chords, rays and segments are discussed in this thesis. A number of relations exist between the corresponding probability density functions. This chapter provides definitions of the measures and reviews relations between them.

The notation that will be used is provided in Tables 2.1, 2.2 and 2.3. Figures 2.1 and 2.2 illustrate some of the terms used.

Table 2.1: Notation

<i>Notation</i>	<i>Description</i>
IUR	Independently and uniformly random. Refers to the choice of combinations of points and directions which define r -randomness, $r \in [\nu, \mu, \lambda, \gamma, \beta, \alpha]$.
K	Arbitrary convex bodies in n -dimensional Euclidean space.
L	Chord length, the distance between two points on the boundary of K .
R	Ray length.
T	Segment length.
$K(l, \theta)$	The body K translated a distance l in direction θ .

Table 2.2: Notation

<i>Notation</i>	<i>Description</i>
$V(\cdot)$	Volume of (\cdot) .
$S(\cdot)$	Surface content of (\cdot) .
$\text{Var}_r(\cdot)$	Variance of (\cdot) under r -randomness.
$E_r(\cdot)$	Expectation of (\cdot) under r -randomness.
$E_D(\cdot)$	Expected value of (\cdot) when averaged over D . For example for D being point P , the average is taken over the point P . When D is some angle θ , the average is taken over the angle θ .
$\Omega(l, \theta)$	$= V(K \cap K(l, \theta))/V(K)$ = the (normalized) overlap of K with its translated self $K(l, \theta)$. See Figure 1.3.
$\Omega(l)$	$= E_\theta(\Omega(l, \theta))$ = the expected value of the normalized overlap volume when averaged over θ distributed uniformly over all possible directions.
$\omega(l)$	$= E_\theta[S(K \cap K(l, \theta))/S(K)]$ = the expected value of the normalized surface content when averaged over all possible θ .
$\Pi(l, P)$	The conical subsets of $B(l, P)$ that fall partially outside K . See Figure 2.1.
$\phi(l, P)$	The total angle subtended at P by components of $\Pi(l, P)$.
$F_r(l)$	$= P\{L \leq l r\text{-randomness}\}, r \in [\nu, \mu, \lambda]$
$\bar{F}_r(l)$	$= 1 - F_r(l)$
$f_r(l)$	Probability density function of chord length under r -randomness.
$f_{X;r}(l)$	Probability density function of X -length obtained through r -randomness where $X \in [L, R, T]$ and $r \in [\mu, \nu, \lambda, \gamma, \alpha, \beta]$.
$B(l, P)$	The n -ball of radius l centered at P .
C_n	$= 2\pi^{n/2}/[n\Gamma(n/2)]$, the volume or content of the unit n -ball.

Table 2.3: Notation

<i>Notation</i>	<i>Description</i>
$\Omega_{K,G}(l)$	$= V[K(l, \theta) \cap G]/V(K)$ = overlap function for embedded bodies. See Chapter 5.
∂K	Surface of K . (Note that $\partial B(l, P)$ means the surface of $B(l, P)$.)

Figure 2.1 illustrates the conical subsets $\Pi(l, P)$ (shaded). In figure 2.2 $\omega(l)$ for the rectangle is shown.

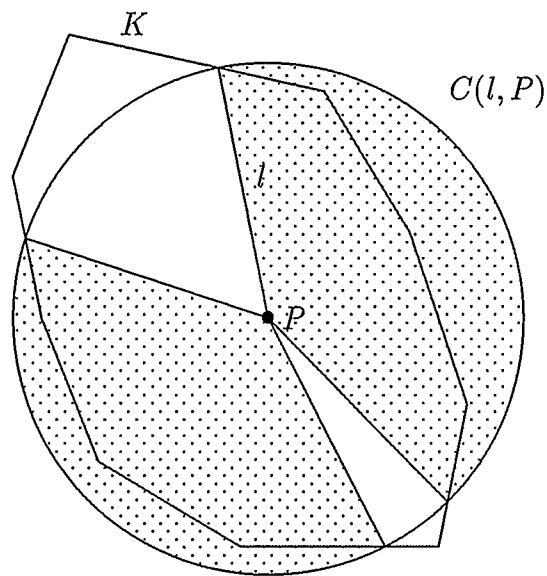


Figure 2.1: Conical subsets $\Pi(l, P)$ that fall partially outside K (shaded)

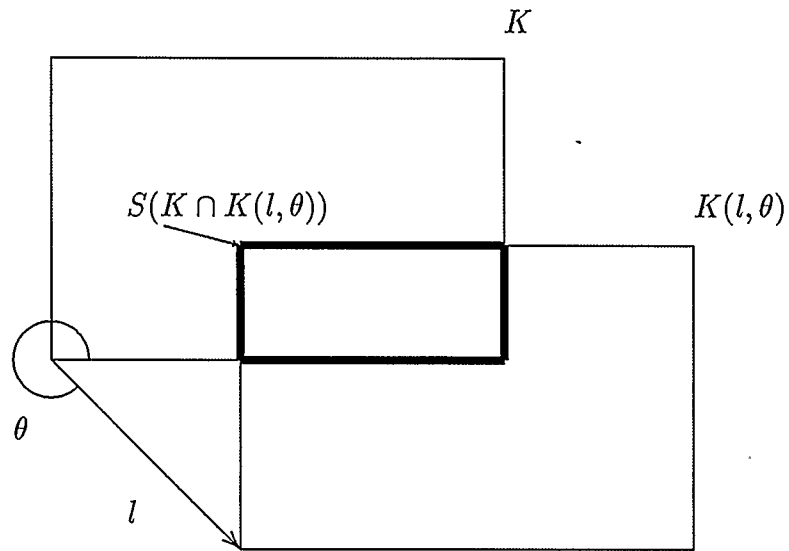


Figure 2.2: Surface overlap function (ω) for the rectangle

This review will focus on presenting density functions in terms of the overlap functions $\Omega(l)$ and $\omega(l)$ which are defined in Table 2.2. Part of this review requires a result of Kingman [51], [52] who has shown that

$$f_{\mu}(l) \propto l^{-1} f_{\nu}(l) \propto l^{-(n+1)} f_{\lambda}(l).$$

2.2 The Randomness Measure μ

Consider a randomly-directed (uniform angular distribution) beam of parallel lines intersecting a convex body K . Choose (uniformly random) one of the lines hitting K and a μ -random chord has been generated (see Figure 2.3). Much of the theoretical work for μ -random measure was done by Kingman [52], [51] and Coleman ([12]).

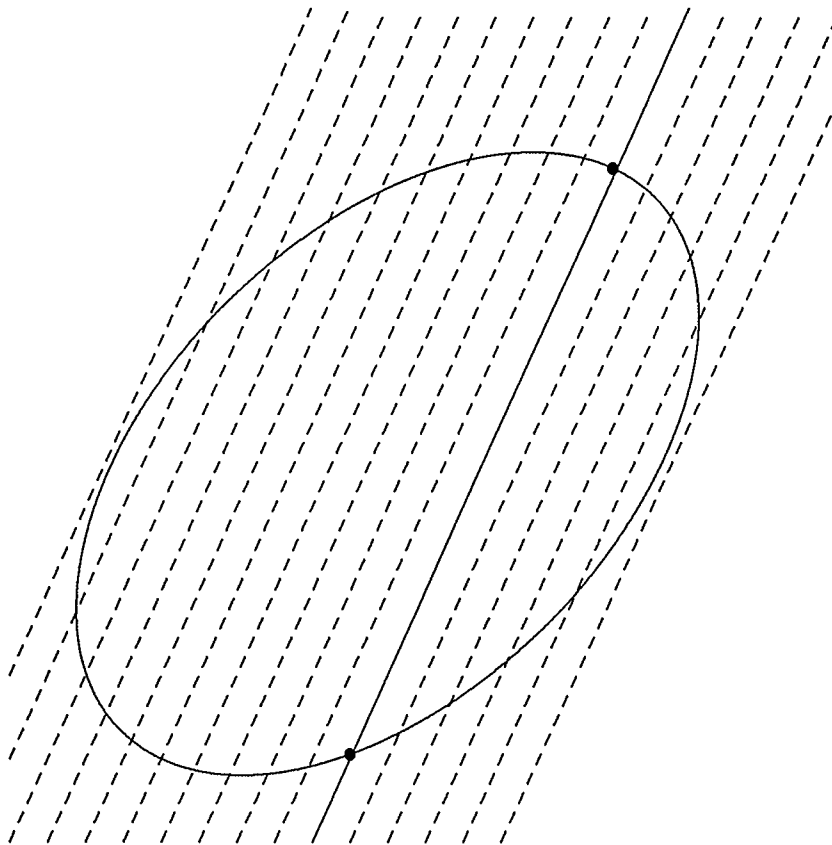


Figure 2.3: Demonstration of μ -random secants

Enns and Ehlers [23] show (implicitly) that the probability density function of chord length may be written in terms of the overlap function Ω as follows:

$$f_{\mu}(l) = -\frac{\Omega''(l)}{\Omega'(0)} \quad (2.1)$$

where primes denote differentiation with respect to l .

Coleman [12] proves an interesting theorem according to which μ -random chords may be generated in a convex body K by embedding K in a large sphere K' and generating γ -random chords (see Section 2.5) for the sphere. The intercepts of the γ -random chords of K' with K form (approximately) μ -random chords of K .

Theorem 2.1 *Secants of a convex body K are μ -random if when extended they are the γ -random chords of a sphere K' of very large radius $r \rightarrow \infty$ having K near its centre.*

This theorem is of practical importance because it is a very interesting way of relating γ -random chords with μ -random chords.

2.3 The Randomness Measure ν

ν -random rays are generated by selecting a uniformly random point in K and then forming the connecting line segment to ∂K in a uniformly random direction. ν -random chords consist of the union of a ν -random ray with the ray in the opposite direction (the “forward” and “backward” rays; see Figure 2.4).

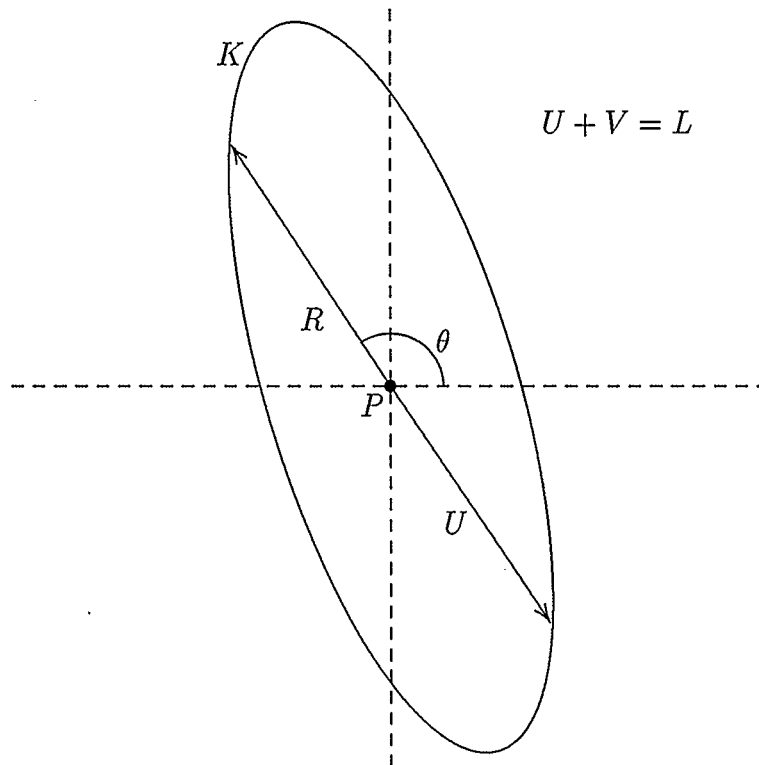


Figure 2.4: Illustration of ν -random chords and rays

Enns and Ehlers [24] show that the ray length density is given by

$$f_{R,\nu}(r) = -\Omega'(r). \quad (2.2)$$

This result is easily established. In a convex body K , let a point P and a direction θ be chosen independently and uniformly random. Let R denote the length of the

ray from P to the boundary of ∂K in direction θ . Then (see Figure 2.5)

$$P(R \geq r | \theta) = \frac{V[K \cap K(r, \theta)]}{V(K)} \quad (2.3)$$

$$= \Omega(r, \theta). \quad (2.4)$$

Averaging over direction yields

$$P(R \geq r) = \Omega(r) \quad (2.5)$$

which is equivalent to Equation (2.2).

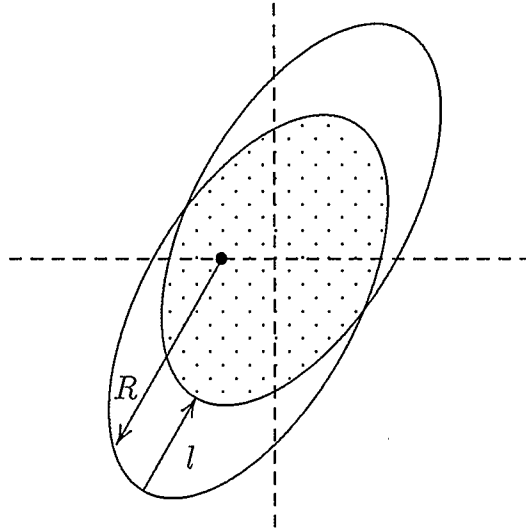


Figure 2.5: Relation of ν -random ray length distribution to Ω

The chord length density may be derived from the joint distribution of “forward” and “backward” ray lengths R and U :

$$\begin{aligned} P(R \geq r, U \geq s | \theta) &= \frac{V(K(r, \theta) \cap K \cap K(-s, \theta))}{V(K)} \\ &= \frac{V(K(r, \theta) \cap K(-s, \theta))}{V(K)} \end{aligned}$$

$$\begin{aligned}
&= \frac{V(K \cap K(r+s, \theta))}{V(K)} \\
&= \Omega(r+s, \theta).
\end{aligned}$$

Integration over θ yields the unconditional joint distribution

$$P(R \geq r, U \geq s) = \Omega(r+s). \quad (2.6)$$

Since $L = R + U$, a change of variable results in

$$f_\nu(l) = l\Omega''(l). \quad (2.7)$$

The moments of ν -random chords and rays are given by

$$E_\nu(L^k) = \int_0^\infty l^k dF_\nu(l) = k(k+1) \int_0^\infty l^{k-1} \Omega(l) dl = (k+1)E_\nu(R^k). \quad (2.8)$$

Special cases are:

$$E_\nu(L) = 2 \cdot \int_0^\infty \Omega(l) dl, \quad (2.9)$$

$$E_\nu(L^n) = \frac{(n+1)V}{C_n}, \quad (2.10)$$

and

$$E_\nu(R^n) = \frac{V(K)}{C_n}. \quad (2.11)$$

The latter two moments are clearly independent of the shape of K . Their derivation follows most easily from normalization in Equations (2.23) and (2.24) [see the next section]. It also follows from Equations (2.1) and (2.7) that $E_\nu(L^k) = E_\mu(L^{k+1})/E_\mu(L)$. Since $\text{Var}_\mu(L) > 0$ this shows that $E_\nu(L) > E_\mu(L)$.

Next consider the expectation of L^{-1} . From Equation (2.7)

$$E_\nu(L^{-1}) = \int_0^\infty \frac{d^2\Omega(l)}{dl^2} dl = -\left. \frac{d\Omega(l)}{dl} \right|_{l=0}. \quad (2.12)$$

This expectation becomes (Enns and Ehlers [23])

$$E_\nu(L^{-1}) = \frac{C_{n-1}}{nC_n} \left(\frac{S}{V} \right). \quad (2.13)$$

If attention is restricted to the n -ball of radius r , this expectation simplifies to

$$E_\nu(L^{-1}) = C_{n-1}/(rC_n). \quad (2.14)$$

Equation (2.13) implies that $E_\mu(L) = [E_\nu(L^{-1})]^{-1}$ is maximized for the n -sphere. The following two theorems were originally conjectured by Enns and Ehlers [23]. A reference is given for the subsequent proof, but that proof is omitted here.

Theorem 2.2 *Over all bodies of unit volume, $E_\nu(L)$ is maximum for the n -sphere.*

Proof. For a proof, see Schneider [86], Davy [17] or Santalo [84]. ■

Enns and Ehlers [23] concluded that the theorem would be true if for any convex K , the graphs of $\Omega(l)$ for K and B , the unit n -sphere, cross only once (see Equation (2.9)).

Theorem 2.3 *$\text{Var}_\nu(L)$ is minimum for the disc when compared with any other body K of equal volume.*

Proof. This follows from Equation (2.10) and Theorem 2.2. ■

Note that Theorem 2.3 refers to arbitrary dimensionality but Theorem 2.2 is restricted to the two-dimensional case. Therefore, for $n \geq 3$, the Enns and Ehlers [23] conjecture remains unproved.

This section ends with a note on averaging, which will be of use in the next section on λ -measure. The equation $P(R \geq r) = \Omega(r)$ was obtained above as an average

over θ of $\Omega(r, \theta)$. But since the generation of a ν -random ray requires two random variables (a point P and a direction θ), there are in fact two averages involved in deriving $P(R \geq r)$, one over θ and one over P . [Above, the average over P is implicit in the use of $V[K \cap K(l, \theta)]$]. Switching the order of these averages results in a useful relation for $\Omega(r)$.

Let $I(x)$ denote the indicator function for which $I(x) = 1$ if $x \geq 0$ and $I(x) = 0$ if $x < 0$. Let $d(\theta, P)$ denote the distance from P to ∂K in direction θ . Then

$$P(R \geq r | \theta, P) = I[d(\theta, P) - r]. \quad (2.15)$$

Averaging first over P , then over θ :

$$P(R \geq r) = E_\theta E_P I[d(\theta, P) - r] \quad (2.16)$$

$$= E_\theta \Omega(r, \theta) \quad (2.17)$$

$$= \Omega(r). \quad (2.18)$$

Averaging first over θ requires $E_\theta I[d(\theta, P) - r]$. To evaluate this in the two-dimensional case, surround P with $C(r, P)$, a circle of radius r . The intersection of the circle with K defines angles Φ_1, Φ_2, \dots , subtended at P (see Figure 2.6), for which $I[d(\theta, P) - r] = 1$. Let $\Phi(r, P) = \Phi_1 + \Phi_2 + \dots$. Then

$$E_\theta I[d(\theta, P) - r] = \frac{\Phi(r, P)}{2\pi} \quad (2.19)$$

For the n -dimensional case, let Φ denote solid angle. The corresponding result is

$$P(R \geq r | P) = \frac{\Phi(r, P)}{nC_n}. \quad (2.20)$$

Therefore

$$P(R \geq r) = E_{P \in K} \left[\frac{\Phi(r, P)}{nC_n} \right]. \quad (2.21)$$

This may be used to relate Ω and Φ :

$$E_{P \in K}[\Phi(r, P)] = n C_n \Omega(r). \quad (2.22)$$

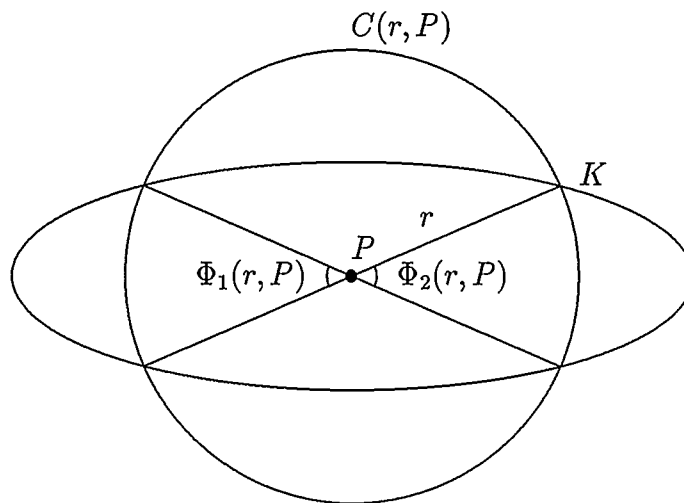


Figure 2.6: Solid angles subtended at a random point

2.4 The Randomness Measure λ

Recall that the measure λ arises whenever two points are selected at random from within K . Hence a chord of length L , a ray of length R and a segment of length T are defined. This is demonstrated in Figure 2.7.

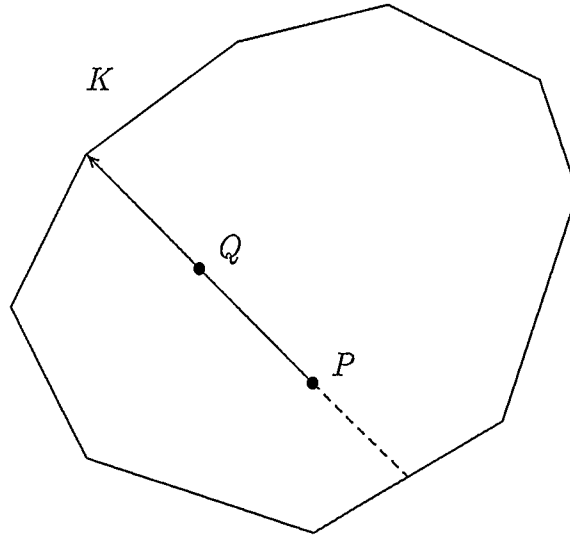


Figure 2.7: Illustration of λ -random chords and rays

Using the fact that $f_\lambda(l) \propto l^n f_\nu(l)$ (Kingman [52]), the distribution of chord length under λ -randomness is

$$f_\lambda(l) = \frac{C_n}{(n+1)V} l^{(n+1)} \frac{d^2 \Omega(l)}{dl^2}, \quad (2.23)$$

where the normalization coefficient follows from $E_\nu(L^n)$.

The distribution of segment lengths under λ -randomness was considered for the n -sphere by Kendall and Moran (1963), and for general convex K by Kingman [52]. Enns and Ehlers [25] show that, for arbitrary (that is, not necessarily convex) regions K , the probability density function of segment length can be written in terms of the overlap function $\Omega(\cdot)$ as

$$f_{T;\lambda}(l) = \frac{nC_n}{V(K)} l^{n-1} \Omega(l). \quad (2.24)$$

The distribution of ray length under λ -randomness can be derived from the distribution of segment length. This distribution can be written (see Figure 2.1)

$$P(T < l) = \frac{E_{P_K}[V\{C(l, P) \cap K\}]}{V(K)}. \quad (2.25)$$

The distribution of ray length R is

$$P(R_\lambda < l) = \frac{E_{P_K}[V\{\Pi(l, P) \cap K\}]}{V(K)}. \quad (2.26)$$

It is clear that

$$V(\Pi(l, P)) - V(\Pi(l, P) \cap K) = V(C(l, P)) - V(C(l, P) \cap K),$$

which implies that

$$P(R_\lambda < l) = \frac{E_{P_K}[V(\Pi(l, P)) - V(C(l, P)) + V(C(l, P) \cap K)]}{V(K)}.$$

Substituting the obvious relations $V(C(l, P)) = C_n l^n$ and $V(\Pi(l, P)) = l^n \Phi(l, P)/n$, and (Equations 2.5, 2.20)

$$E_{P_K}\{\Phi(l, P)\} = nC_n P(R_\nu < l) = nC_n(1 - \Omega(l)) \quad (2.27)$$

leaves

$$P(R_\lambda < l) = P(T < l) - \frac{l^n C_n \Omega(l)}{V(K)}.$$

The density function through differentiation is then

$$f_{R;\lambda}(l) = \frac{d}{dl}P(R_\lambda < l) = \frac{-C_n l^n}{V(K)}\Omega'(l). \quad (2.28)$$

Equations (2.2) and (2.28) show that

$$f_{R;\lambda}(l) \propto l^n f_{R;\nu}(l). \quad (2.29)$$

With the distribution for ray lengths under λ -randomness, it is an easy task to calculate moments. For example,

$$E(R_\lambda^k) = \frac{(n+k)C_n}{V(K)} \int_0^\infty l^{n+k-1}\Omega(l)dl.$$

In particular, when k is zero,

$$\int_0^\infty l^{n-1}\Omega(l)dl = \frac{V(K)}{nC_n}.$$

Moments for λ -random chords can also be related to moments of segment lengths.

Such a relationship is given by the equation

$$E_\lambda(L^k) = \frac{(n+k)(n+k+1)}{n(n+1)}E(T^k). \quad (2.30)$$

The following theorem demonstrates that λ -random rays have greater mean than ν -random rays. This fact will provide a useful check on simulation results when actual distributions are not available for comparisons.

Theorem 2.4 $E(R_\lambda) > E(R_\nu)$.

Proof. Using the inequality

$$E(X^{n+1}) \geq E(X^n)E(X)$$

and Equation (2.29), it is possible to write

$$E(R_\lambda) = \frac{E(R_\nu^{n+1})}{E(R_\nu^n)} \quad (2.31)$$

$$\geq E(R_\nu) \quad (2.32)$$

where equality holds only when K is just a single point. For any K of interest, therefore, this theorem holds. ■

Similarly, the relation $f_\lambda(l) \propto l^n f_\nu(l) \propto l^{n+1} f_\mu(l)$ implies

$$E_\mu(L) \leq E_\nu(L) \leq E_\lambda(L). \quad (2.33)$$

2.5 The Randomness Measure γ

γ -random chords of K are defined as follows. Choose a uniformly random point P in the boundary ∂K and a uniformly random direction θ . The intersection of the line through P in direction θ is then a γ -random chord of K (see Figure 2.8).

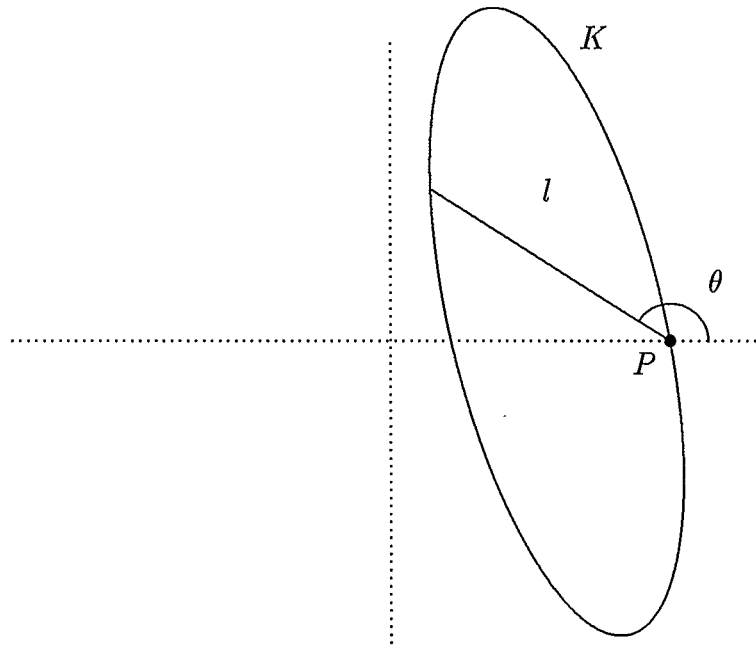


Figure 2.8: Sample chord under γ -randomness

Paralleling the derivation of the distribution of ν -random rays, the θ -conditional distribution of γ -random chords satisfies

$$P_\gamma(L > l|\theta) = \frac{S(K(l, \theta) \cap K)}{S(K)}, \quad (2.34)$$

where $S(\cdot)$ is the surface content of (\cdot) and $K(l, \theta)$ is the l -translate of K in direction θ . The unconditional distribution is then

$$P_\gamma(L > l) = \frac{E_\theta[S(K(l, \theta) \cap K)]}{S(K)} \equiv \omega(l), \quad (2.35)$$

which shall be defined as the surface overlap function of K (see Figure 2.2). The probability density function of γ -random chord length is thus

$$f_\gamma(l) = -\omega'(l). \quad (2.36)$$

As was the case for ν -measure, the averages over P and θ may be done in either order which results in the relation

$$E_{P \in \partial K} \{\Phi(l, P)\} = \frac{nC_n}{2} \omega(l), \quad (2.37)$$

or, equivalently,

$$P_\gamma(L > l) = \frac{2}{nC_n} E_{P \in \partial K} \{\Phi(l, P)\}. \quad (2.38)$$

Moments of chord length are easily shown to be given by

$$E_\gamma(L^k) = k \cdot \int_0^\infty l^{k-1} \omega(l) dl. \quad (2.39)$$

Since it can be shown (see Equation (2.45)) that

$$\int_0^\infty l^{n-1} \omega(l) dl = \frac{2V(K)}{nC_n}, \quad (2.40)$$

the following shape-independent relation holds:

$$E_\gamma(L^n) = \frac{2}{C_n} V(K). \quad (2.41)$$

2.6 The Randomness Measure α

Recall that under α -randomness, both rays and chords can be generated by choosing points P and Q independently and uniformly random in K and ∂K , respectively. The corresponding ray can be extended through P to form a chord. Figure 2.9 demonstrates rays and chords under α -randomness.

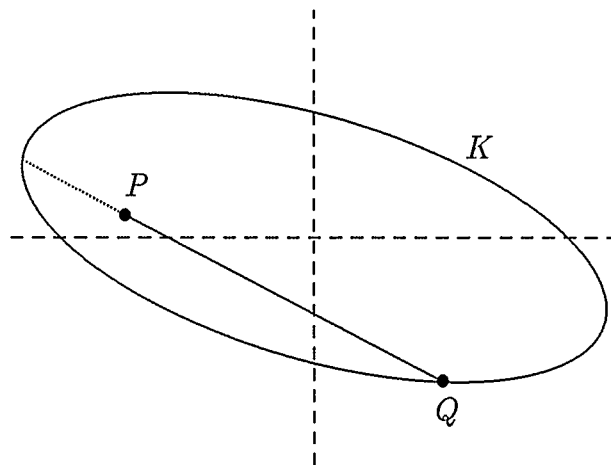


Figure 2.9: Illustration of α -random chords and rays

The distribution of α -random rays can also be written in terms of the surface overlap function $\omega(l)$. Enns and Ehlers [24] show that

$$P(R_\alpha < l) = \frac{nC_n}{2V(K)} \int_0^l r^{n-1} \omega(r) dr, \quad (2.42)$$

and the ray length density is therefore

$$f_{R;\alpha}(l) = \frac{nC_n}{2V(K)} l^{n-1} \omega(l). \quad (2.43)$$

Now moments of R_α can be derived as

$$E(R_\alpha^k) = \frac{nC_n}{2V(K)} \int_0^\infty l^{n+k-1} \omega(l) dl \quad (2.44)$$

for which a value of $k = 0$ gives the relation

$$\int_0^\infty l^{n-1} \omega(l) dl = \frac{2V(K)}{nC_n}. \quad (2.45)$$

This establishes Equation (2.40).

Chords under α -randomness are formed by the line through $P \in K$ and $Q \in \partial K$. The conditional distribution of $P_\alpha(L \leq l|Q)$ may be derived as follows. Consider the intersection of the ball $B(l, Q)$ with K . See Figure 2.10 where $\Phi_1(l, Q) + \Phi_2(l, Q) + \dots = \Phi(l, Q)$ is the total angle subtended at Q as shown. Then

$$V[B(l, Q) \cap K] = V[\Pi(l, Q) \cap K] + \frac{l^n \Phi(l, Q)}{n} \quad (2.46)$$

is a partition of the intersection volume of $B(l, Q)$ with K . Dividing by $V(K)$, the first two terms can be interpreted as probabilities:

$$P_\alpha(R \leq l|Q) = P_\alpha(L \leq l|Q) + \frac{l^n \Phi(l, Q)}{nV(K)}. \quad (2.47)$$

Averaging over $Q \in \partial K$ and using Equation (2.38) yields

$$P_\alpha(R \leq l) = P_\alpha(L \leq l) + \frac{C_n l^n}{2V(K)} P_\gamma(L > l), \quad (2.48)$$

from which the probability density function of α -random chord length is

$$f_\alpha(l) = -\frac{C_n l^n}{2V(K)} \omega'(l). \quad (2.49)$$

It is also noted that $f_\alpha(l) \propto l^n f_\gamma(l)$.

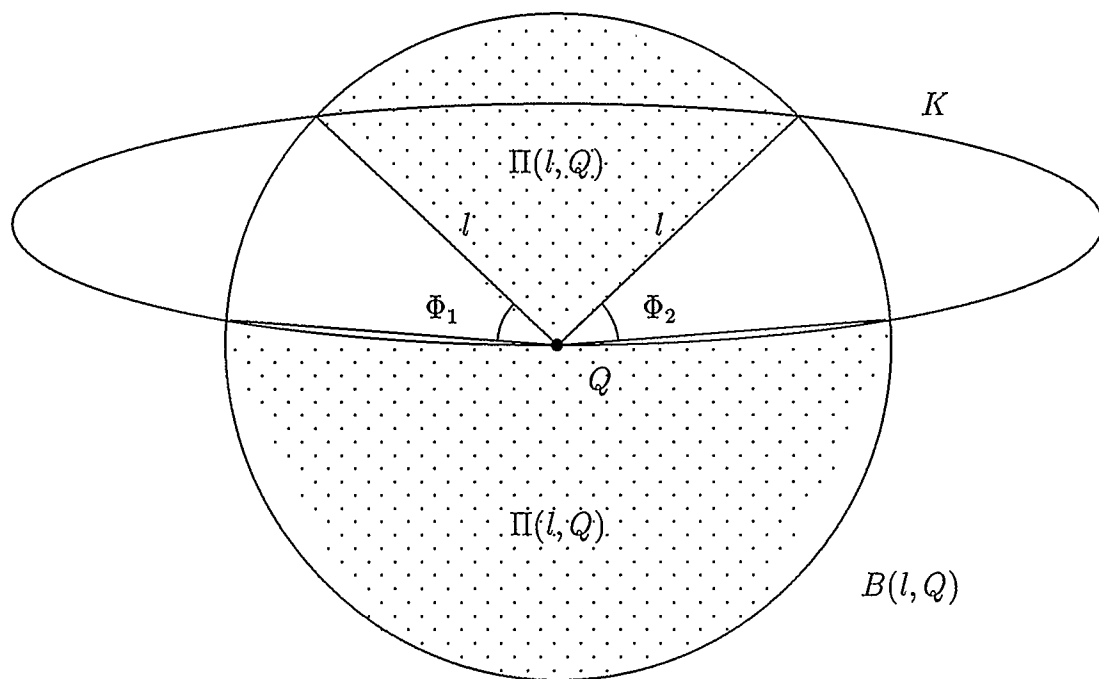


Figure 2.10: Representative chords under α -randomness

Moments of α -random ray and chord length and γ -random chord length are then related by

$$E_\alpha(L^k) = \frac{n+k}{n} E_\alpha(R^k) = \frac{C_n}{2V(K)} E_\gamma(L^{n+k}). \quad (2.50)$$

It follows (cf. Theorem 2.4) that

$$E_\alpha(L) > E_\gamma(L). \quad (2.51)$$

2.7 The Randomness Measure β

A β -random chord is defined as the line segment connecting two independent uniformly random points in ∂K . Figure 2.11 illustrates the creation of a β -random chord.

To derive the chord density under β -randomness, Ehlers and Enns [22] proceed by noting the density can be obtained as a limit of λ -random segments. Recall Equation (2.24) for the distribution of segment lengths under λ -randomness. Also recall that Enns and Ehlers [25] show that this holds for arbitrary (that is, not necessarily convex) regions K . Therefore, if K_1 is a shell of width Δx around K , then choosing two points in K_1 is equivalent to choosing two points in a non-convex region (see Figure 2.11).

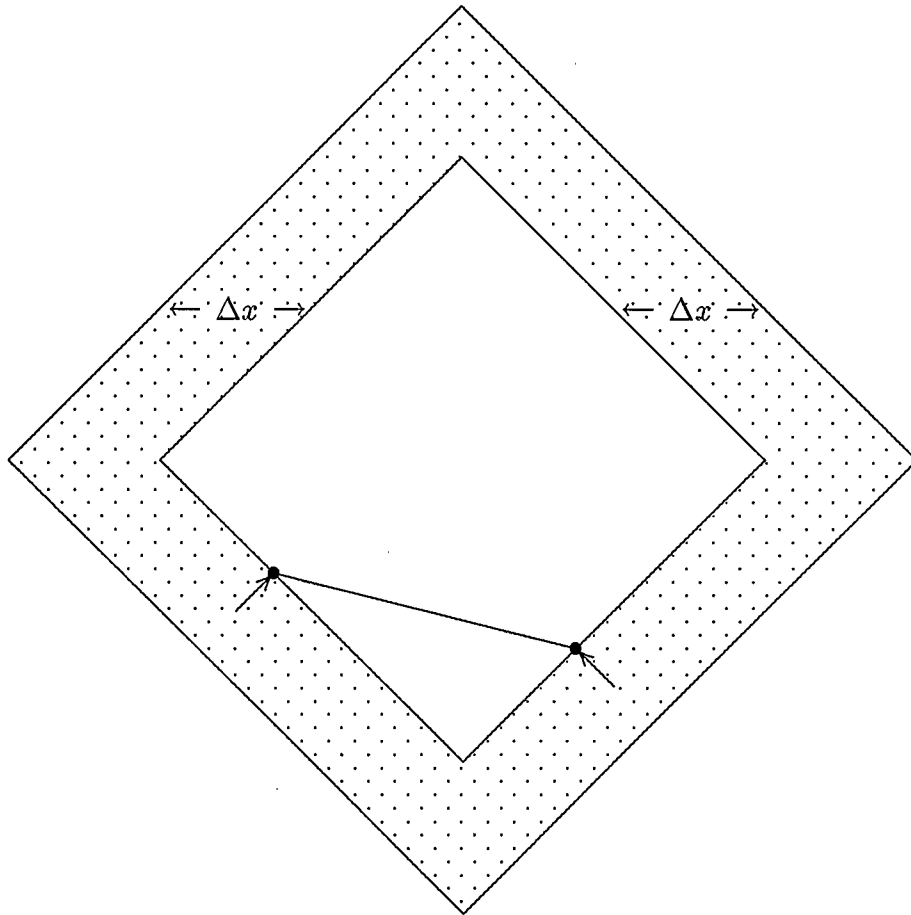


Figure 2.11: Illustration of β -random chords and rays

Therefore, denote the distance between two points P and Q chosen according to λ -randomness in K_1 as T , which clearly has as distribution Equation 2.24. As Δx approaches zero, T converges to the β -random secant length, L , that is

$$\lim_{\Delta x \rightarrow 0} P_\lambda(T \leq l) = P_\beta(L \leq l). \quad (2.52)$$

Since the distribution of T is known,

$$f_{L;\beta}(l) = \lim_{\Delta x \rightarrow 0} f_{T;\lambda}(l) \quad (2.53)$$

$$= nC_n l^{n-1} \lim_{\Delta x \rightarrow 0} \left(\frac{\Omega_{K_1}(l)}{V(K_1)} \right), \quad (2.54)$$

where $V(K_1) = S(K)\Delta x + O(\Delta x)^2$ implies that

$$f_{L;\beta}(l) = \frac{nC_n}{(S(K))^2} l^{n-1} \epsilon(l), \quad (2.55)$$

with $\epsilon(l)$ defined as

$$\epsilon(l) \equiv \lim_{\Delta x \rightarrow 0} \frac{E_\theta[V(K_1(l, \theta) \cap K_1)]}{(\Delta x)^2}. \quad (2.56)$$

Note that normalization of the chord density yields

$$\int_0^\infty l^{n-1} \epsilon(l) dl = \frac{(S(K))^2}{nC_n}. \quad (2.57)$$

For bodies whose boundary ∂K contains flat portions (e.g. polyhedra, hemispheres, cylinders), the above derivation permits chords which lie entirely within ∂K . For such bodies, it may be desirable to restrict points P and Q so as to form chords which contain interior points of K .

2.8 Inequalities and Moment Relations

For several distributions relationships exist between moments of the ray- and chord-length distributions. For example, moments may be related by some inequality as in

the following theorem and conjecture.

Theorem 2.5 $E(R_\nu) < E(R_\alpha)$ for any n and K .

For a proof, see Enns and Ehlers [24]. The following conjecture remains unproved.

Conjecture 2.1 $E(R_\alpha) < E(R_\lambda)$.

Moment relations involving equalities are given throughout the Enns and Ehlers papers. Enns and Ehlers [22] gives a summary of the moment relations, which is summarized here in Tables 2.4 and 2.5. Moment relations depending only on $S(K)$ and $V(K)$ are provided in Table 2.4.

Table 2.4: Moment relations between densities depending only on $V(K)$ and $S(K)$

Moment	Relations
$E_\nu(R^n)$	$= (E_\lambda(R^{-n}))^{-1} = V(K)/C_n$
$E_\nu(L^n)$	$= (E_\lambda(L^{-n}))^{-1} = (n+1)V(K)/C_n$
$E_\gamma(L^n)$	$= (E_\alpha(L^{-n}))^{-1} = 2V(K)/C_n$
$E_\mu(L)$	$= (E_\nu(L^{-1}))^{-1} = nC_nV(K)/(C_{n-1}S(K))$
$E_\mu(L^{n+1})$	$= (E_\lambda(L^{-n-1}))^{-1} = n(n+1)(V(K))^2/(C_{n-1}S(K))$

Table 2.5: Moment relations between densities

Moment	Relation
$E_\nu(R^{m+n})$	$= \frac{E_\nu(L^{m+n})}{m+n+1}$ $= \frac{E_\mu(L^{m+n+1})}{n(m+n+1)} \frac{C_{n-1}S(K)}{C_nV(K)}$ $= \frac{E_\lambda(R^m)V(K)}{C_n}$ $= \frac{E_\lambda(L^m)(n+1)V(K)}{C_n(n+m+1)}$ $= \frac{E_\lambda(T^m)(n+m)V(K)}{C_n n}$
$E_\gamma(L^{m+n})$	$= \frac{2(n+m)V(K)}{nC_n} E_\alpha(R^m)$ $= \frac{2V(K)}{C_n} E_\alpha(L^m).$

2.9 Summary of Fundamental Relationships

Table 2.6 summarizes the fundamental relationships of the ray, chord and segment densities with the overlap function. These relationships will be used for the two- and three-dimensional ovoids to be discussed in Chapters 3 and 4. Note that primes denote differentiation with respect to l .

Table 2.6: Relationships of pdfs to $\Omega(l)$

Density	Relation to $\Omega(l)$	Equation
$f_{R;\nu}(l)$	$= -\Omega'(l)$	(2.2)
$f_{L;\nu}(l)$	$= l\Omega''(l)$	(2.7)
$f_{L;\mu}(l)$	$= \frac{-\Omega''(l)}{\Omega'(0)} = nC_n V(K) \frac{\Omega''(l)}{C_{n-1} S(K)}$	(2.1)
$f_{R;\lambda}(l)$	$= -C_n l^n \frac{\Omega'(l)}{V(K)}$	(2.26)
$f_{L;\lambda}(l)$	$= C_n l^{n+1} \frac{\Omega''(l)}{(n+1)V(K)}$	(2.23)
$f_{T;\lambda}(l)$	$= nC_n l^{n-1} \frac{\Omega(l)}{V(K)}$	(2.24)
$f_{R;\alpha}(l)$	$= nC_n l^{n-1} \frac{\omega(l)}{2V(K)}$	(2.43)
$f_{L;\alpha}(l)$	$= -C_n l^n \frac{\omega'(l)}{2V(K)}$	(2.49)
$f_{L;\gamma}(l)$	$= -\omega'(l)$	(2.36)
$f_{L;\beta}(l)$	$= \frac{nC_n}{(S(K))^2} l^{n-1} \epsilon(l)$	(2.55)

Primes denote differentiation with respect to l

Given the direct proportionality between the overlap function Ω and the λ -random segment density $f_{T;\lambda}$ (Equation (2.24)), consider the overlap function in terms of the segment density:

$$\Omega(l) = \frac{V(K)}{nC_n l^{n-1}} f_{T;\lambda}(l). \quad (2.58)$$

An estimate of the overlap function is thus

$$\hat{\Omega}(l) = \frac{V(K)}{nC_n} \left\{ \frac{\hat{f}_{T;\lambda}(l)}{l^{n-1}} \right\}. \quad (2.59)$$

An estimate of the first derivative of $\Omega(l)$ is then

$$\hat{\Omega}'(l) = \frac{V(K)}{nC_n} \left\{ \frac{l\hat{f}'_{T;\lambda}(l) - (n-1)\hat{f}_{T;\lambda}(l)}{l^n} \right\}, \quad (2.60)$$

with the second derivative of $\Omega(l)$ having as estimate

$$\hat{\Omega}''(l) = \frac{V(K)}{nC_n} \left\{ \frac{l^2 \hat{f}''_{T;\lambda}(l) + (2-2n)l\hat{f}'_{T;\lambda}(l) + n(n-1)\hat{f}_{T;\lambda}(l)}{l^{n+1}} \right\}. \quad (2.61)$$

In Table 2.6, simply replace $\Omega(l)$ and its derivatives by the estimates above, and what remains are estimates of the densities in terms of the estimated segment density $\hat{f}_{T;\lambda}(l)$. These estimates are given in Table 2.7.

Tables 2.6 and 2.7 provide two important methods of generating densities for μ -, λ - and ν -measures. By exploiting the relation between Ω , $f_{T;\lambda}$ and $f_{X;r}$, for $X \in [L, R]$ and $r \in [\mu, \nu, \lambda]$, an estimate for either Ω or $f_{T;\lambda}$ can be transformed into an estimate for the other densities. This is exactly what is done in Chapters 3 and 4 for various two- and three-dimensional ovoids, respectively.

Note also the relation between $\omega(l)$ (Figure 2.2) and the α - and γ -random densities (see Table 2.6). An estimate of ω or $f_{R;\alpha}$, which is proportional to ω , gives estimates of f_α and f_γ .

Table 2.7: Relationships to $\hat{f}_{T;\lambda}(l)$

Density	Relation to $\hat{f}_{T;\lambda}(l)$
$\hat{f}_{R;\nu}(l)$	$\frac{V(K)}{nC_n} \left[\frac{(n-1)\hat{f}_T - l\hat{f}'_T}{l^n} \right]$
$\hat{f}_{L;\nu}(l)$	$\frac{V(K)}{nC_n} \left[\frac{l^2 \hat{f}''_T + (2-2n)l\hat{f}'_T + n(n-1)\hat{f}_T}{l^n} \right]$
$\hat{f}_{R;\lambda}(l)$	$\left[\frac{(n-1)\hat{f}_T - l\hat{f}'_T}{n} \right]$
$\hat{f}_{L;\lambda}(l)$	$\left[\frac{l^2 \hat{f}''_T + (2-2n)l\hat{f}'_T + n(n-1)\hat{f}_T}{n(n+1)} \right]$
$\hat{f}_{L;\mu}(l)$	$\frac{[V(K)]^2}{C_{n-1}S(K)} \left[\frac{l^2 \hat{f}''_T + (2-2n)l\hat{f}'_T + n(n-1)\hat{f}_T}{l^{n+1}} \right]$

Primes denote differentiation with respect to l

Chapter 3

Ovoids in Two Dimensions

Recall from Chapter 1 comparisons between the new methods Ω and $f_{T;\lambda}$ and the old approach of direct simulation:

Estimate via *direct simulation*

versus

Estimate via Ω *method*

versus

Estimate via $f_{T;\lambda}$ *method*.

In Chapter 2, theory was developed that provided us with the necessary relationships that allow generation of chord densities with measure in $[\mu, \lambda, \nu]$ and ray densities with measure in $[\lambda, \nu]$ from $f_{T;\lambda}$ and Ω (see Tables 2.6 and 2.7). Note that the direct relation between Ω and $f_{T;\lambda}$ (Equation (2.24)) allows us to use either Ω or $f_{T;\lambda}$ as an estimate of the other. Note also that ray densities (ν, λ) depend on first derivatives of Ω or $f_{T;\lambda}$, while chord densities (μ, ν, λ) depend on second derivatives.

Therefore, calculation of derivatives of either Ω or $f_{T;\lambda}$ is required. For $f_{T;\lambda}$ this requires the use of nonparametric density estimates; for Ω this requires the use of splines. Both splines and nonparametric density estimates are necessary because they provide differentiable estimates of the functions. Ovoids considered include arbitrary polygons, circles and ellipses.

3.1 The $f_{T;\lambda}$ Method

The $f_{T;\lambda}$ method employed the generation of 10,000 independently and uniformly random pairs of points P and Q in the ovoid K . From each of these pairs of points a segment length T was calculated (a histogram was then produced by dividing the observations into 40 bins of equal width). The form of density estimation most statisticians use as a quick and simple tool is the histogram where the frequency of observations over some particular interval with specified bin (or window) width is measured. However, a histogram is not differentiable. Therefore, several other methods have been developed that provide differentiable estimates of the function (in this case, $f_{T;\lambda}$, although these estimates can apply to finding smoothed estimates of any directly simulated density). All of these methods deal with using random observations, and include the following:

(1) Use splines as follows:

- Fitting a spline through the midpoints of the histogram bins.
- Forming the empirical distribution function and estimating with a spline (such a method is appealing because a spline should be ideally suited to a monotonically increasing distribution function).
- Averaging the histogram by shifting it some small positive amount. An estimate of the density at a point is then an average of the values of each of the shifted histograms at that point. Fit a spline through the corresponding averaged points.

Splines were not used for the $f_{T,\lambda}$ method in this thesis. They are mentioned because they are computationally appealing.

- (2) Use nonparametric density estimates (NDEs). Such estimates include kernel smoothers and orthogonal series estimators (to be defined below). [A good review article on different nonparametric density estimates is Izenman [45]. Other references include Buckland [7], [8] (includes code) and Breiman and Peters [6] (extensive comparison of four nonparametric density estimators).]
- (3) Use local regression smoothers (LRSs). These estimates fit low-order polynomials locally, and were first considered by Stone [93] and Cleveland [11]. A heated discussion occurs over the merits and pitfalls of NDEs and LRSs in Hastie and Loader [39]. LRSs have been largely ignored, including in this thesis, but are included here because we believe they may not be susceptible to the same problems as NDEs (to be discussed later).

NDEs used in this thesis can be split into two categories — orthogonal series estimators and kernel smoothers. Both of these methods use the actual observations (like LRSs) on T to obtain an estimate of the segment density at x_0 , $f_{T,\lambda}(x_0)$, by weighting observations closest to x_0 with the largest weights.

3.1.1 Orthogonal Series Estimators

In an orthogonal series estimate (see Schwarz [87]), f is estimated by the coefficients of its series expansion. Define $\Phi_\nu(x)$ to be these coefficients. Then a natural unbiased

estimator for $\Phi_\nu(x)$ is given by

$$\hat{f}_\nu = \frac{1}{n} \sum_{i=1}^n \Phi_\nu(X_i).$$

A density estimate is then

$$\hat{f}(x) = \sum_{\nu=1}^{\kappa} \hat{f}_\nu \Phi_\nu(x) \lambda_\nu, \quad (3.1)$$

where λ_ν are weights and κ is a cutoff that truncates the series. Both the λ_ν and κ determine the amount of smoothing. That is, as κ increases, the amount of smoothing decreases and the faster the weights λ_ν go to zero, the more smoothing. κ was chosen by trial and error, i.e. κ was changed to obtain an accurate estimate that visually was closest to the true distribution where that was known. A value of κ of 10 or 15 was in all cases acceptable.

The orthogonal polynomials are convenient because simple recurrences can be derived for their derivatives. In this thesis, the following normalized orthogonal polynomials were considered: Hermite, Fourier, Legendre, Chebychev (first and second kinds) and Laguerre. However, the normalized Hermite polynomials were better than their counterparts because they fit the segment density $f_{T,\lambda}$ much closer. However, they had two distinct disadvantages. First, when κ is even moderately large, estimates using the orthogonal polynomials require a large number of computations. Second, even the Hermite polynomials, the best of the orthogonal polynomials, were poor in comparison to the kernel smoothers.

3.1.2 Kernel Smoothers

The kernel estimator of a density function (see Silverman [90]) is defined as

$$\hat{f} = \frac{1}{nh} \sum_{i=1}^n K\left(\frac{x - X_i}{h}\right),$$

where K is the type of kernel used, h is a window or bin width, and n is the number of observations. The kernel K must satisfy $K(x) \geq 0$ and

$$\int_{\mathcal{X}} K(x)dx = 1.$$

Several kernels $K(x)$ and their relative benefits and shortcomings are given in Table 3.1 below. These are the kernels that were used in this thesis.

A slight modification to the kernel approach yields the adaptive kernel. An adaptive kernel is a two-stage process, where an initial kernel estimate is improved in a second kernel estimate. Calculating a typical adaptive kernel would involve

(1) Estimating the density via kernel method.

(2) Computing

$$\lambda_i = \left\{ \frac{\hat{f}(X_i)}{g} \right\}^{-\alpha},$$

where

$$\log g = \frac{1}{n} \sum_{i=1}^n \log \hat{f}(X_i)$$

and $\alpha \in (0, 1)$ is a sensitivity parameter.

(3) Calculating the adaptive kernel estimate as

$$\hat{f}^* = \frac{1}{n} \sum_{i=1}^n \frac{1}{h\lambda_i} K\left(\frac{t - X_i}{h\lambda_i}\right).$$

Adaptive Kernels seemed to do no better or worse than regular kernels, and their computational difficulty (they require fitting a kernel twice) left them undesirable.

Table 3.1: Types of kernels used

Kernel	$K(y)$	Notes
Gaussian	$\frac{e^{-y^2/2}}{\sqrt{2\pi}}$	Initial fits and derivatives were good.
Cauchy	$\frac{1}{\pi(1+y^2)}$	Initial fits poor.
Sine	$\frac{1}{2\pi} \left(\frac{\sin y/2}{y/2} \right)^2$	Initial fits poor.
Epanechnikov	$\frac{3}{4\sqrt{5}} \left(1 - \frac{y^2}{5} \right) I_{ y < \sqrt{5}}$	Initial fits and derivatives were good; however, the Epanechnikov kernel is similar in fit to the Gaussian kernel and its second derivative is a constant. The Gaussian kernel then becomes the kernel of choice.
Polynomial	$\kappa_{rs} (1 - y ^r)^s I_{ y \leq 1}$ $\kappa_{rs} = \frac{r}{2B(s+1, 1/r)} \quad r > 0, s \geq 0$	The biweight kernel ($r = s = 2$) fit the initial density well but its derivatives were poor.
Logistic	$\frac{e^{-x/\beta}}{\beta [1 + e^{-x/\beta}]^2}$	Initial fits poor.

Kernel smoothers or estimators had the advantage that derivatives were easy to calculate. However, kernel smoothers misbehaved in the tails of the distributions (i.e. bias was introduced), and when substantial curvature effects were present, this bias would also occur (see Hastie and Loader [39]). [LRSs are a proposed alternative to these kernel smoothers.]

3.2 The Ω Method

The overlap function or Ω method involved translating a polygon (not necessarily convex) for some length l and averaging over $\theta \in (0, 2\pi)$. In all cases, θ was incremented over 400 equal intervals, l over 40 intervals from zero to the maximum chord length attainable. Thus $40 \times 400 = 16,000$ calculations were required. To estimate circles and ellipses, therefore, the polygon program could only be used in an approximating sense. The nodes were thus those lengths l for which the overlap function was calculated. Through these nodes a spline was fit. Simple cubic splines were used.

The program that computes, deterministically, the overlap function for arbitrary polygons is described in detail in the next section. Splines are naturally suited to fitting Ω , since the Ω method generates observed overlaps at each of several nodes through which a natural cubic polynomial is easily fit. Splines are also easy to differentiate, since they are polynomials. Thus, once a spline has been fit to Ω , it is a simple task to obtain its derivatives.

Several types of splines were considered in this thesis. They include

1. Histospline — used exclusively for histogram data, these splines have the added

condition that areas from one node to the next must match the area in the corresponding bin of the histogram. Histosplines are considered in Späth [92]. Histosplines have potential application with $\Omega(l)$ only in that densities that depend on $\Omega(l)$ could be required, through conditions such as those imposed on histosplines, to have unit area when integrated over their respective supports. Currently, densities derived from $\Omega(l)$ and its derivatives are not required to be densities in the sense that they integrate to one.

2. Weighted spline — ideal in that they are best suited to fit functions which vary considerably. Since many of the chord densities have discontinuities, weighted splines are more likely to smooth less in areas where jumps occur. Weighted splines were developed by Salkauskas [83] and code was provided by Bos [5].
3. Natural cubic spline — fits a piecewise cubic polynomial through adjacent nodes such that the approximating polynomial is then twice differentiable. Reliable computer code for the natural cubic spline is given in Press *et al.* [76].

Of these types of splines, only the natural cubic spline was actually used for the graphs reproduced in Chapters 3 and 4. Code was modified from Press *et al.* [76] to produce derivatives.

Note that the approaches used to differentiate the curves produced in the $f_{T;\lambda}$ and the Ω methods differs greatly. However, this is easily explained since $f_{T;\lambda}$ involves random observations and $\Omega(l)$ does not. Comparisons between the two methods then becomes even more interesting.

3.3 Methods of Comparison

To compare the distributions generated by the three methods, $f_{T;\lambda}$ and Ω and ‘direct simulation’, we considered only qualitative measures. Such measures included visual closeness, computer time (roughly) and computational ease.

The easiest way to compare the above three approaches is graphically. Any differences between the three methods should be apparent on graphs of the density function. Therefore, graphs have been reproduced for the chord densities $f_{L;x}$, $x \in \{\mu, \nu, \lambda\}$ and the ray densities $f_{R;x}$, $x \in \{\nu, \lambda\}$, which show a histogram, an actual (analytical) curve where available, a curve based on the density as a function of Ω , and the best curve based on the density as a function of $f_{T;\lambda}$. Best in this case means that more than one kernel and more than one orthogonal series estimator were calculated, and the one that appeared (visually) to be closest to the actual curve was taken to be the best estimate. Note that in three or more dimensions, the curve based on the density as a function of Ω is not available, since no program for arbitrary approximating polyhedra is yet functional.

Other methods are possible to measure the relative success of the Ω , $f_{T;\lambda}$ or *direct simulation* methods as generators of a distribution. These include Kolmogorov goodness-of-fit tests using measurements at the nodes or mean absolute deviation. Recall, however, that this thesis proposes to test the *feasibility* of the Ω or the $f_{T;\lambda}$ methods in comparison with *direct simulation*. Quantitative measures should be incorporated into future work and are important; however, this thesis has not included them.

For the chord densities $f_{L;x}$, $x \in \{\alpha, \gamma, \beta\}$, and for $f_{R;\alpha}$ only results for direct

simulation and nonparametric fits based on direct simulation were performed. Note that not all graphs are reproduced in this thesis.

Actual computer code is reproduced in Appendix A for the polygon program. Other programs, including the ellipse surface-randomness programs, where original work was required, are available from the author upon request.

3.4 Polygons

Generating chord-length distributions for arbitrary polygons is important because analytical results for non-symmetric polygons are difficult to obtain. For this reason, we found it necessary to extend comparisons between the Ω , $f_{T;\lambda}$ and *direct simulation* methods to arbitrary polygons. For this thesis, this has required the development of programs that determine the overlap function (the polygon program) and the segment density for arbitrary polygons. Results are established for triangles and rectangles, polygons for which results are known, as a check on the software.

3.4.1 The $f_{T;\lambda}$ Program

Recall that λ -random segments are generated through two points chosen independently and uniformly random in the interior of the ovoid K . For arbitrary polygons, choosing two points inside requires choosing two points in a bounding box (see Figure 1.2) and then checking if these points are internal.

To ascertain whether a point is internal, Preparata and Shamos [75] (c. 2) provide the following algorithm. For a point $Q = (q_1, q_2)$ in a convex polygon K , the wedge in which it lies (see Figure 3.1) is between the rays given by P_i and P_{i+1} through

some known internal point Z if and only if

$$\begin{vmatrix} q_1 & q_2 & 1 \\ z_1 & z_2 & 1 \\ x_{i+1} & y_{i+1} & 1 \end{vmatrix} < 0 \quad \text{and} \quad \begin{vmatrix} q_1 & q_2 & 1 \\ z_1 & z_2 & 1 \\ x_i & y_i & 1 \end{vmatrix} > 0. \quad (3.2)$$

The point Q is then internal if and only if

$$\begin{vmatrix} x_i & y_i & 1 \\ x_{i+1} & y_{i+1} & 1 \\ q_1 & q_2 & 1 \end{vmatrix} > 0. \quad (3.3)$$

This algorithm is very useful, not only for the purpose of determining the segment length distribution for arbitrary polygons, but also for the polygon program. If we choose a point inside some polygon K , then by determinants we can determine whether or not it lies inside the body K .

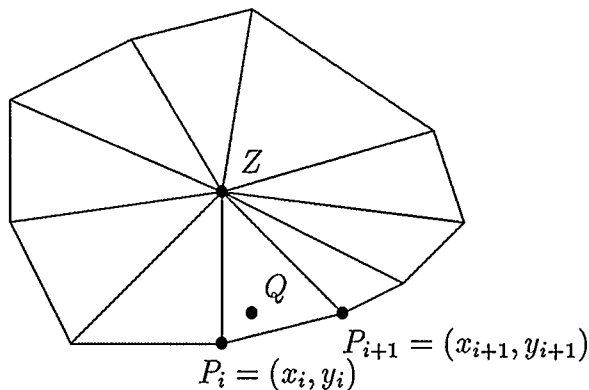


Figure 3.1: Testing for interior points for a polygon

3.4.2 The Ω or Polygon Program

For two-dimensional bodies with smooth boundaries, a program has been devised and developed that calculates the overlap function based on an approximating polygon. The following approach differs from one in which a computer science philosophy is applied by using pixels or voxels in two and three dimensions, respectively. A pixel or voxel approach was considered for calculating the overlap function, but not employed. The main difference between a computer science and the deterministic approach that we employ is that the computer science approach is at machine level (i.e. it involves approximating a body with pixels on a visual terminal) while the deterministic approach is much more user-guided (i.e. it involves solution of linear systems).

Instead, a program that takes an arbitrary polygon K , translates it to form $K(l, \theta)$, and then calculates the overlap volume from the coordinates of the convex polygon which forms the intersection of K and its translate was developed. This program calculates the overlap function for arbitrary polygons.

The algorithm employs the principle that for two overlapping convex polygons the region of overlap is also a convex polygon whose vertices can be of three types. First, a vertex can be a point of intersection of the two polygons. There will always be two points of intersection between two overlapping polygons. Second, a vertex may be a vertex of the original polygon that is interior to the translated polygon. Third, a vertex may be a vertex of the translated polygon which is interior to the original polygon (see Figure 3.2). Note that in this figure, the shift is somewhat special in that it happens to be parallel to two edges. Therefore, some cases exist

where there is conflict between identifying when a point is internal or when it is an intersection (Stone's algorithm, discussed below, can automatically remove the inconsistency).

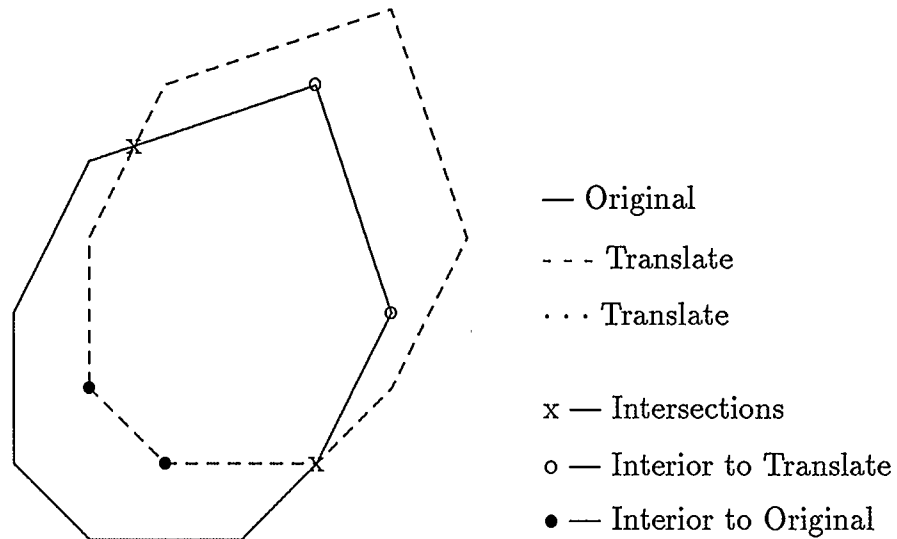


Figure 3.2: Classifying points for the polygon program

The polygon program's algorithm uses the fact that points are only of these three types and determines (see Figure 3.2):

- (1) the points of intersection of the polygon with its translate,
- (2) the points interior to the polygon which are vertices of the translate,
- (3) the points interior to the translate which are vertices of the original.

This set of points forms the vertices of the resulting overlapping polygon. Attention then moves to sorting the resulting set of vertices into counterclockwise order. Finally, the area of the overlapping polygon may be computed according to the the procedure of Stone [94].

Stone [94] writes an algorithm for the area of a polygon in terms of the coordinates of the vertices. This formula is

$$A = \frac{1}{2} \left\| \begin{array}{cccccc} x_1 & x_2 & \dots & x_{n-1} & x_n \\ y_1 & y_2 & \dots & y_{n-1} & y_n \end{array} \right\|$$

where $\|\dots\|$ is interpreted as the sum of positive products of downward-to-the-right diagonals ($x_1y_2 + \dots$) with negative products of upward-to-the-right diagonals ($-y_1x_2 + \dots$), including *wrap-around* for (x_n, y_n) . Figure 3.3 illustrates this for a polygon with four vertices (x_i, y_i) , $i = 1, 2, 3, 4$. This procedure, it should be noted, only works when the points are arranged in a counterclockwise (or clockwise) fashion.

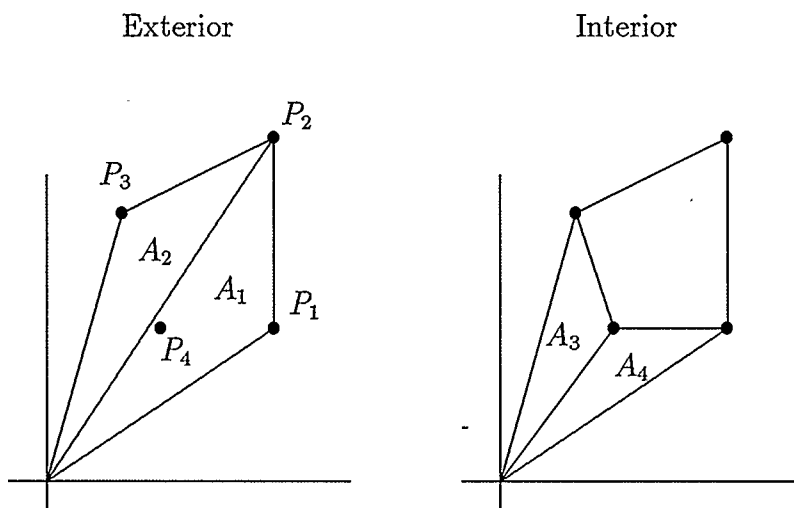


Figure 3.3: Polygonal area

In Figure 3.3,

$$\begin{aligned} A &= (A_1 + A_2) - (A_3 + A_4) \\ &= \frac{1}{2} \left\{ \begin{array}{c} \left| \begin{array}{cc} x_1 & x_2 \\ y_1 & y_2 \end{array} \right| + \dots + \left| \begin{array}{cc} x_4 & x_1 \\ y_4 & y_1 \end{array} \right| \end{array} \right\}. \end{aligned}$$

Recently, Strang [96] reaffirmed this result and added one based on boundaries with curvature. This may have some use for non-polygonal convex shapes. [Also interesting is Cowan's [16] suggestion to consider the distribution of intersection points of the polygons when the polygon K is translated randomly a distance l in direction θ . This is a simple modification of the polygon program which can be implemented in future work.]

3.4.3 Results For The Triangle

For the equilateral triangle, the overlap is difficult to calculate. Below, the overlap function will be given. But first, surface randomness for bodies with linear boundaries (polygons) can be described for the triangle and easily generalized for arbitrary polygons.

Take the perimeter of the triangle, p , and choose a random number in the interval $(0, p)$. Convert this number into a coordinate by going along the boundary until reaching the required distance. This has to be done by segment — that is, consider an equilateral triangle with sides each of length one and with starting point one of the vertices. If the random number chosen is 1.3, the point lies on the second side from some starting vertex, and the distance formula combined with a check on the coordinates in relation to the vertices returns a point on the surface (perimeter). See Figure 3.4 for an illustration. Points chosen for β -randomness were required to be on different segments, but this was not essential. Including chords that comprise only boundary points is possible, but changes the analysis slightly.

Figure 3.4 demonstrates surface-randomness. As a starting point take the vertex labelled \diamond . Proceed along the sides of the triangle so long as the perimeter travelled

does not exceed the random number chosen. In this figure, then, proceeding past \star to \bullet yields the random point on the surface. Actually, the distance along this side is known, so the distance to any of the nearest vertices is known, and two unique points exist at this distance from the reference vertex. A check that the point marked by \circ is not on the surface of this triangle gives \bullet as the only candidate. This algorithm is easily extended to arbitrary polygons. A distribution involving surface-randomness for the equilateral triangle is given in Figure 3.5.

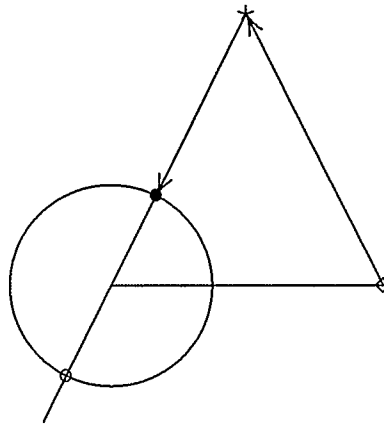


Figure 3.4: Surface Randomness for the Triangle

For the equilateral triangle, Enns, Ehlers and Stuhr [22] give $\Omega(l)$ as

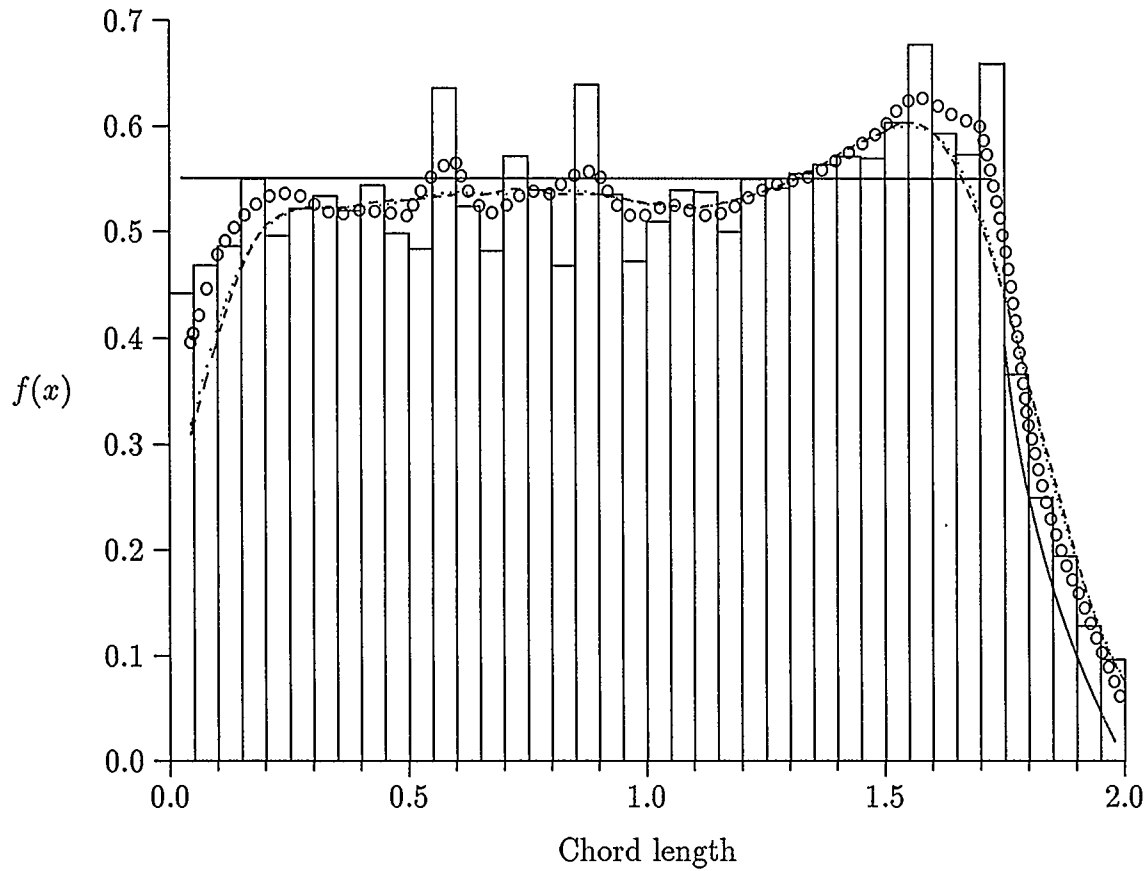
$$\begin{aligned}\frac{\pi}{3}\Omega(l) &= \frac{\pi}{3} - 2\rho + \left(\frac{\pi}{6} + \frac{\sqrt{3}}{4}\right)\rho^2 & 0 \leq \rho \leq 1 \\ &= \frac{\pi}{3} - 2\rho + \left(\frac{\pi}{6} + \frac{\sqrt{3}}{4}\right)\rho^2 \\ &\quad + 3\sqrt{\rho^2 - 1} - (2 + \rho^2)\sec^{-1}(\rho) & 1 \leq \rho \leq 2/\sqrt{3},\end{aligned}$$

and $\omega(l)$ as

$$\begin{aligned}\frac{\pi}{3}\omega(l) &= \frac{\pi}{3} - \rho & 0 \leq \rho \leq 1 \\ &= \frac{\pi}{3} - \rho + 2\sqrt{\rho^2 - 1} - 2\sec^{-1}(\rho) & 1 \leq \rho \leq 2/\sqrt{3},\end{aligned}$$

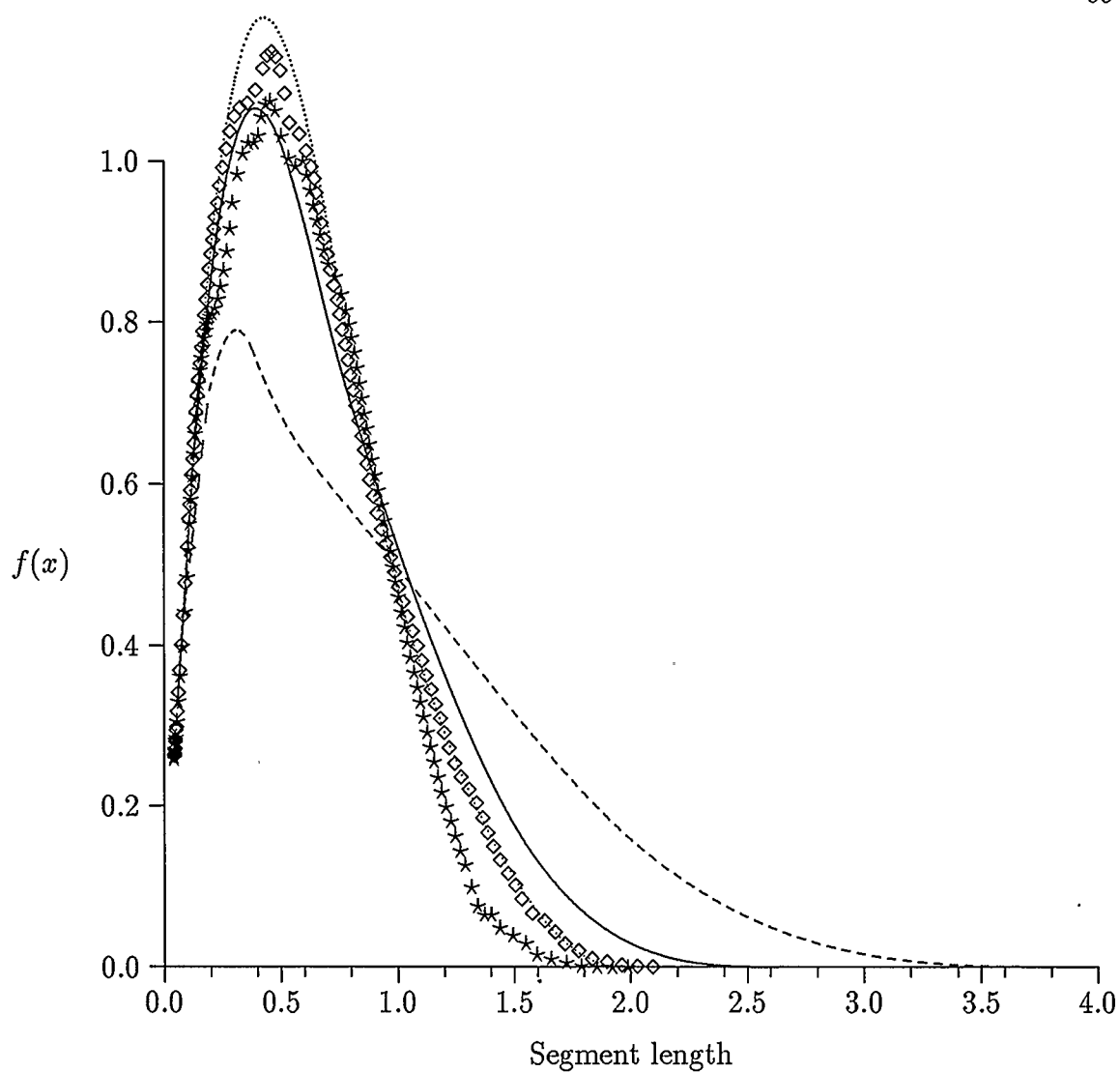
where $\rho = l/a$, a being the height of the triangle. These known results for the equilateral case will provide a useful check on arbitrary triangles. The following triangles were considered here: right triangles with angles $\pi/6$ and $\pi/4$, and isosceles triangles with common angles $\pi/6$, $5\pi/12$ and $\pi/12$. Each triangle is assumed to have unit area. A graph of the segment length density derived from Ω for these triangles is given in Figure 3.6, and a graph of the relative overlap functions Ω for the triangles is given in Figure 3.7.

Figures 3.8, 3.9, 3.10 and 3.11 demonstrate the accuracy of the Ω method once again. Using the polygon program, fits based on the derivatives of the overlap function are closer than fits based on the derivatives of the segment density. However, the segment density looks promising in each of the cases, and is a reasonable estimator.



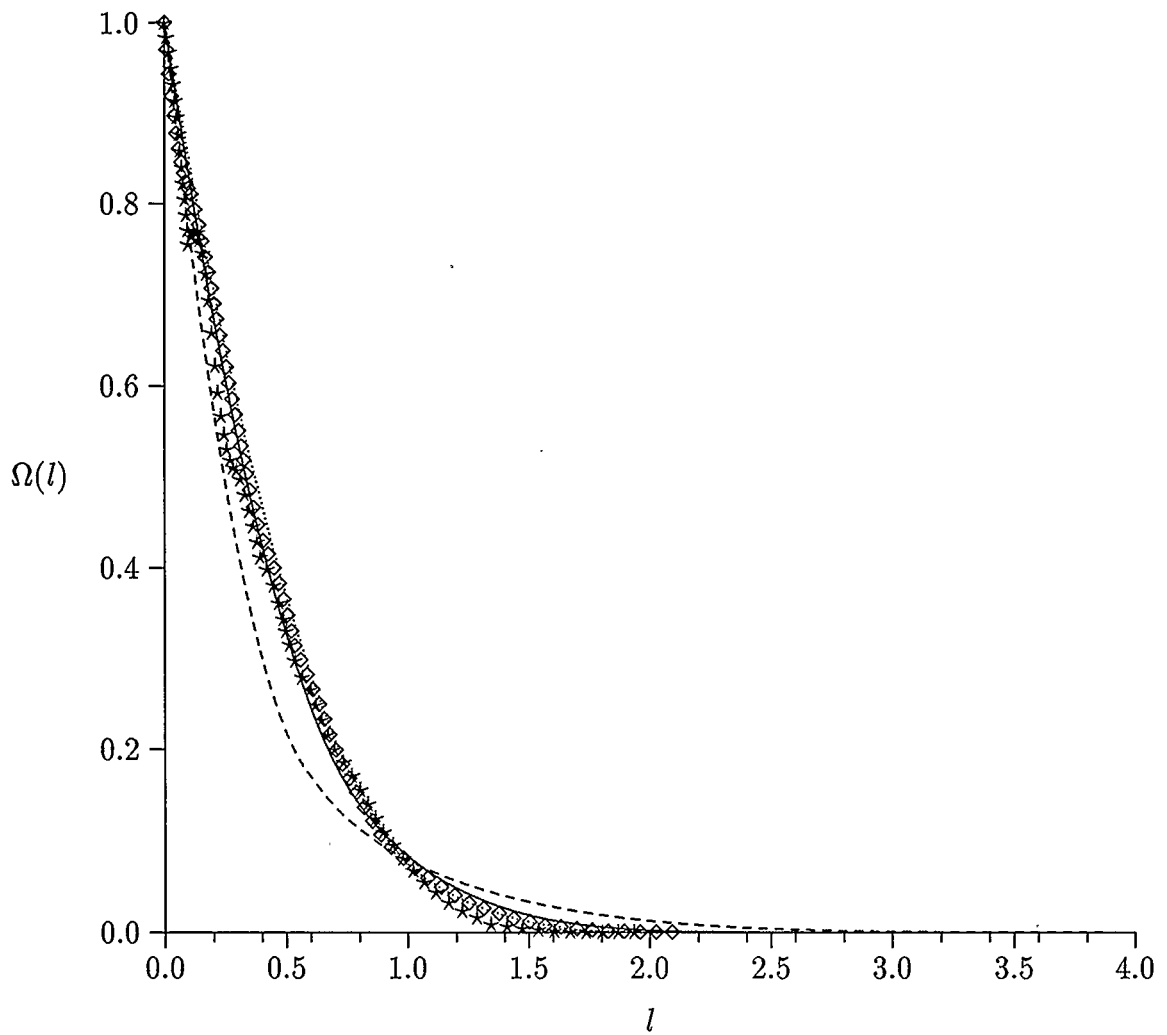
	Average	Variance		Symbol
Simulated	0.954220	0.286923	Gaussian	· ·
Analytical	0.908500	0.277200	Epanechnikov	- - -
		$h = 0.1$	Biweight	o o
			Actual	—

Figure 3.5: $f_{L,\gamma}$ for the equilateral triangle — several kernel fits to demonstrate surface-randomness



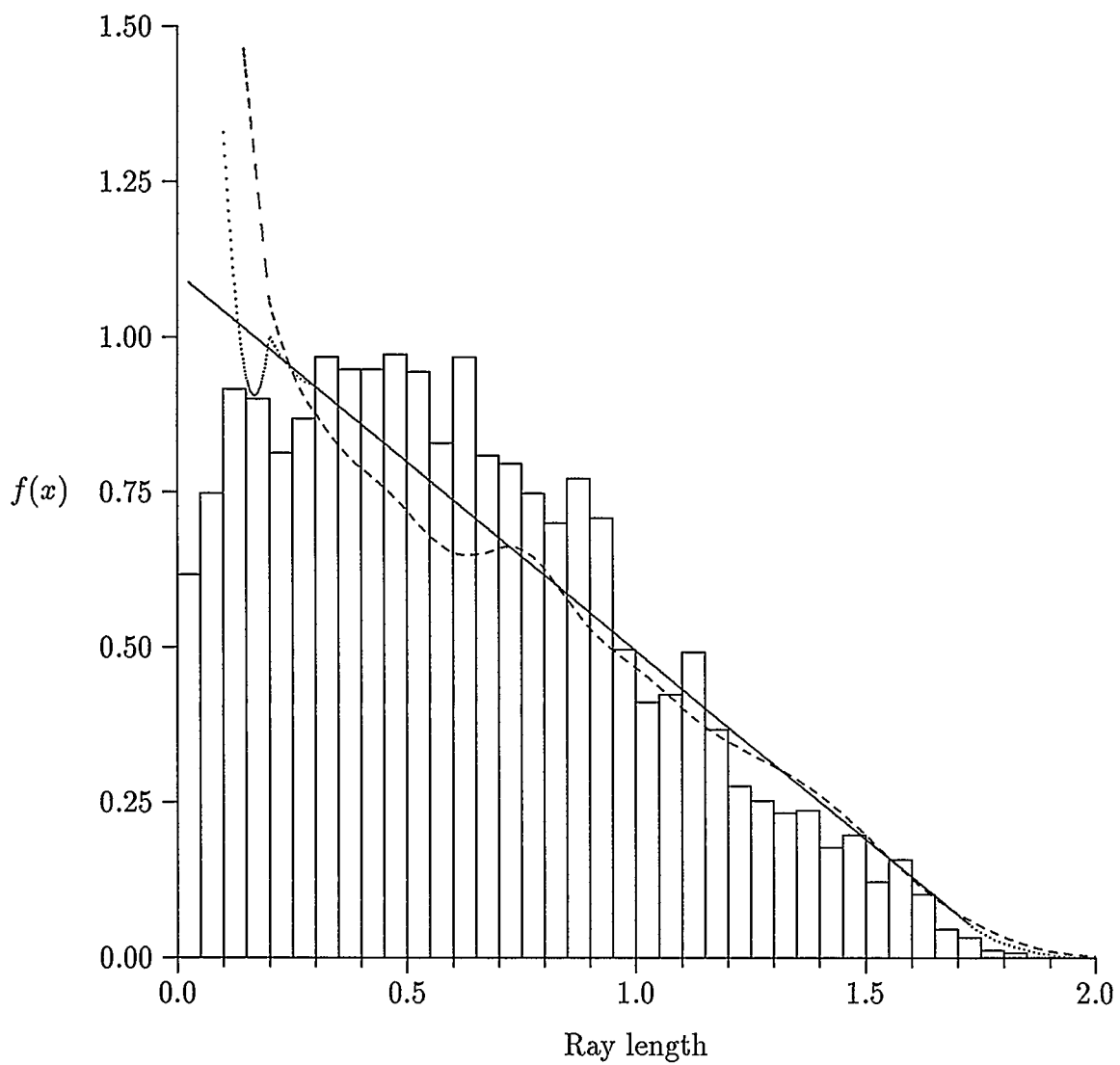
Type of Triangle	Symbol
Isosceles — 120, 30, 30	—
Isosceles — 30, 75, 75
Isosceles — 150, 15, 15	-----
Isosceles — 90, 45, 45	*****
Right — 90, 60, 30	◇◇◇◇

Figure 3.6: $f_{T,\lambda}$ for various triangles from Ω program



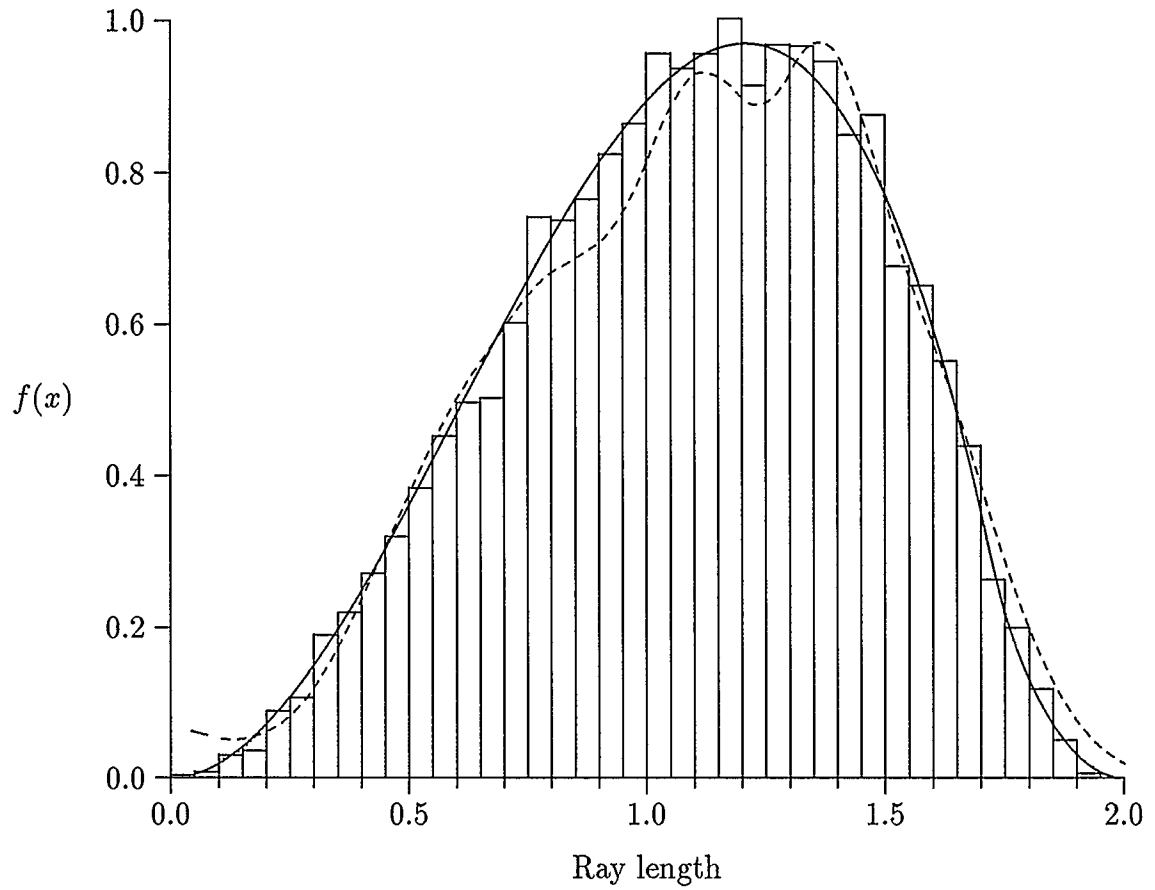
Type of Triangle	Symbol
Isosceles — 120, 30, 30	—
Isosceles — 30, 75, 75
Isosceles — 150, 15, 15	-----
Isosceles — 90, 45, 45	*****
Right — 90, 60, 30	◇◇◇◇

Figure 3.7: $\Omega(l)$ for various triangles from Ω program



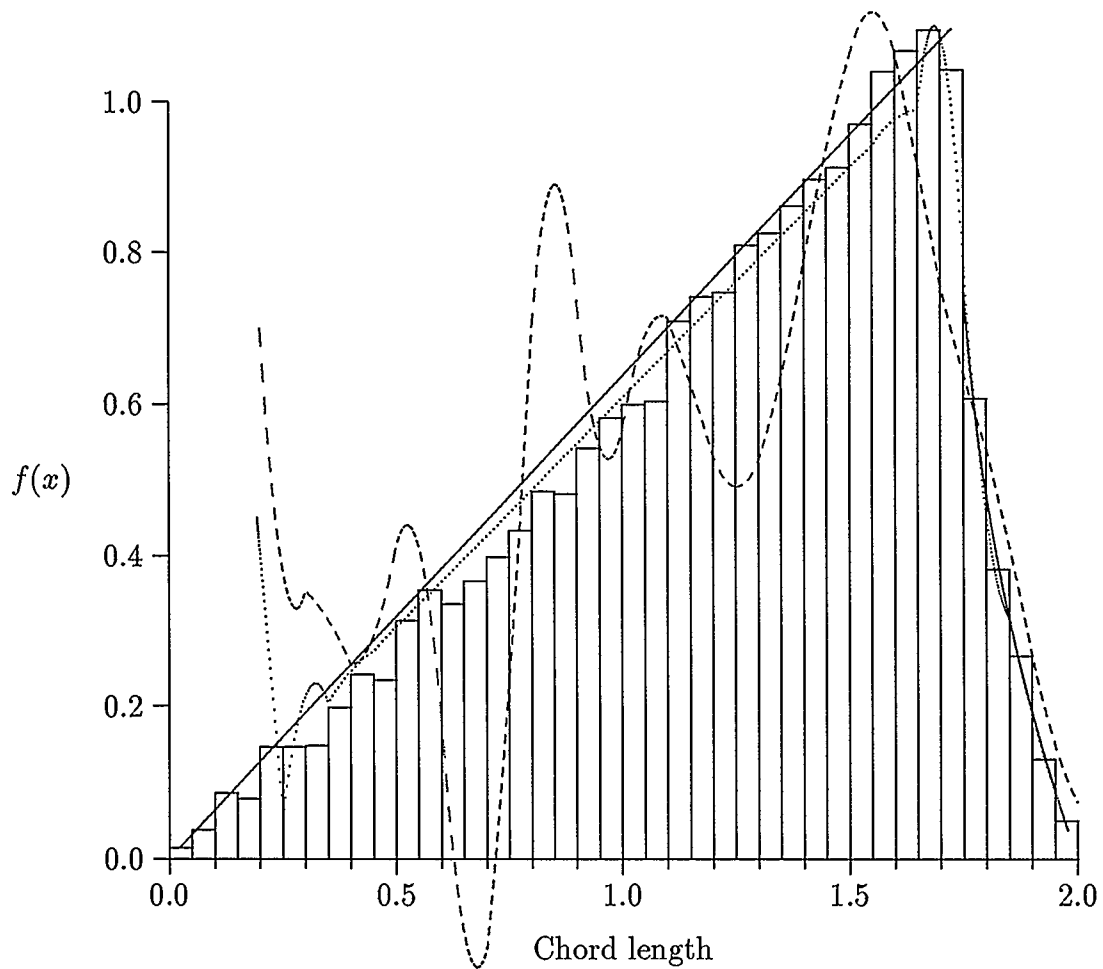
Symbol	
Actual	—
From $\Omega(l)$...
From $f_{T,\lambda}$	---

Figure 3.8: $f_{R,\nu}$ for the equilateral triangle — estimate via Ω method versus $f_{T,\lambda}$ method



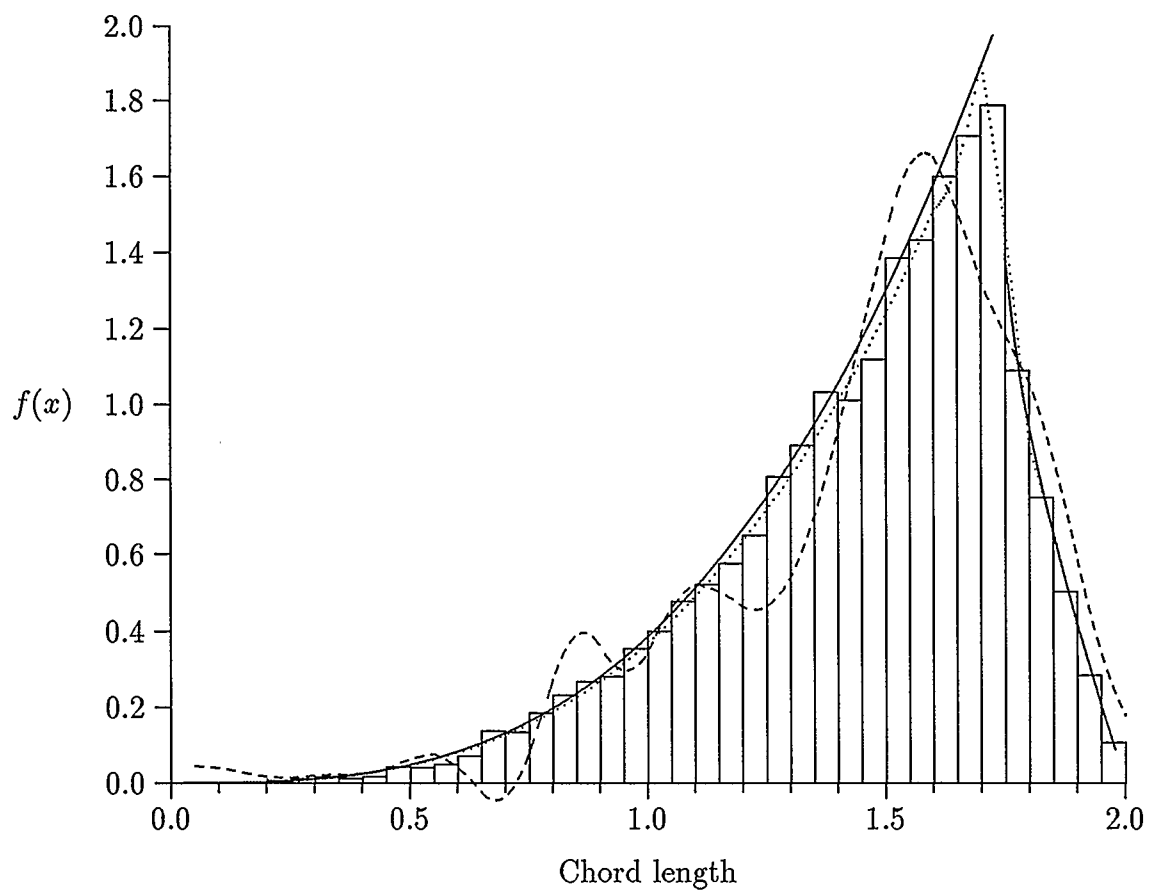
	Symbol
Actual	—
From $\Omega(l)$...
From $f_{T,\lambda}$	---

Figure 3.9: $f_{R,\lambda}$ for the equilateral triangle — actual curve versus Ω method versus $f_{T,\lambda}$ method [actual curve and Ω method are indistinguishable]



	Symbol
Actual	—
From $\Omega(l)$..
From $f_{T;\lambda}$	---

Figure 3.10: $f_{L,\nu}$ for the equilateral triangle — actual curve versus Ω method versus $f_{T;\lambda}$ method



	Symbol
Actual	—
From $\Omega(l)$...
From $f_{T,\lambda}$	- - -

Figure 3.11: $f_{L,\lambda}$ for the equilateral triangle — actual curve versus Ω method versus $f_{T,\lambda}$ method

3.4.4 Results For The Rectangle $a \times b$

The overlap function for the rectangle as given by Ehlers [21] is

$$\begin{aligned}
 \frac{\pi}{2}\Omega(l; a, b) &= \frac{\pi}{2} - \frac{l}{a} - \frac{l}{b} + \frac{l^2}{2ab} & 0 \leq l \leq a \\
 &= \frac{\pi}{2} - \cos^{-1}(a/l) - \frac{l}{a} + \frac{\sqrt{l^2 - a^2}}{a} - \frac{a}{2b} & a < l \leq b \\
 &= \sin^{-1}(b/l) - \cos^{-1}(a/l) + \frac{\sqrt{l^2 - a^2}}{a} \\
 &\quad + \frac{\sqrt{l^2 - b^2}}{b} - \frac{(a^2 + b^2 + l^2)}{2ab} & b < l \leq \sqrt{a^2 + b^2}.
 \end{aligned}$$

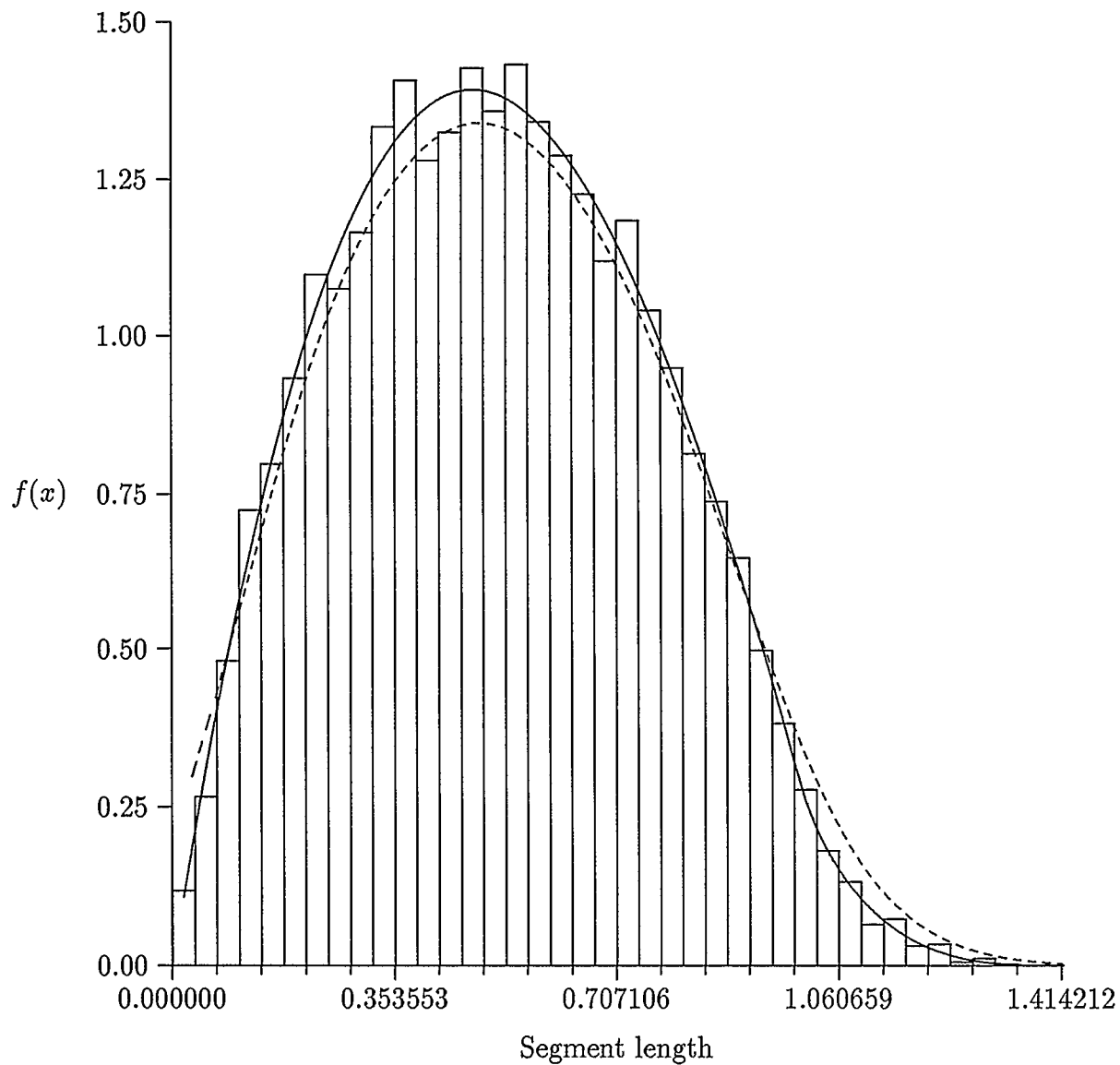
Horowitz [43] also calculates the γ -random chord distribution as

$$\begin{aligned}
 f_{L;\gamma}(l) &= \frac{4}{\pi(a+b)} & 0 \leq l \leq a \\
 &= \frac{4}{\pi(a+b)} \left[\frac{ab}{l\sqrt{l^2 - a^2}} - \frac{\sqrt{l^2 - a^2}}{l} + 1 \right] & a < l \leq b \\
 &= \frac{4}{\pi(a+b)} \left[\frac{ab}{l\sqrt{l^2 - a^2}} - \frac{l^2 - a^2}{l} \right] \\
 &\quad + \frac{2}{\pi(a+b)} \left[\frac{ab}{l\sqrt{l^2 - b^2}} - \frac{\sqrt{l^2 - b^2}}{l} \right] & b < l \leq \sqrt{a^2 + b^2}.
 \end{aligned}$$

For the rectangle, convergence to a thin plate was checked by taking lengths a and widths b such that $ab = 1$ (unit area). The length a was decremented from 1 by .1 to .1 to illustrate changes in both $\Omega(l)$ and $f_{T;\lambda}$. Results are shown in Figures 3.12 through 3.16 for various rectangles. Both methods provided fairly decent estimates, although the overlap function approach was better each time. For the ν -random chord density with length 0.2, neither method was suitable. An estimate from $\Omega(l)$ shot off to infinite close to zero, and the estimate from the segment λ -random density was useless.

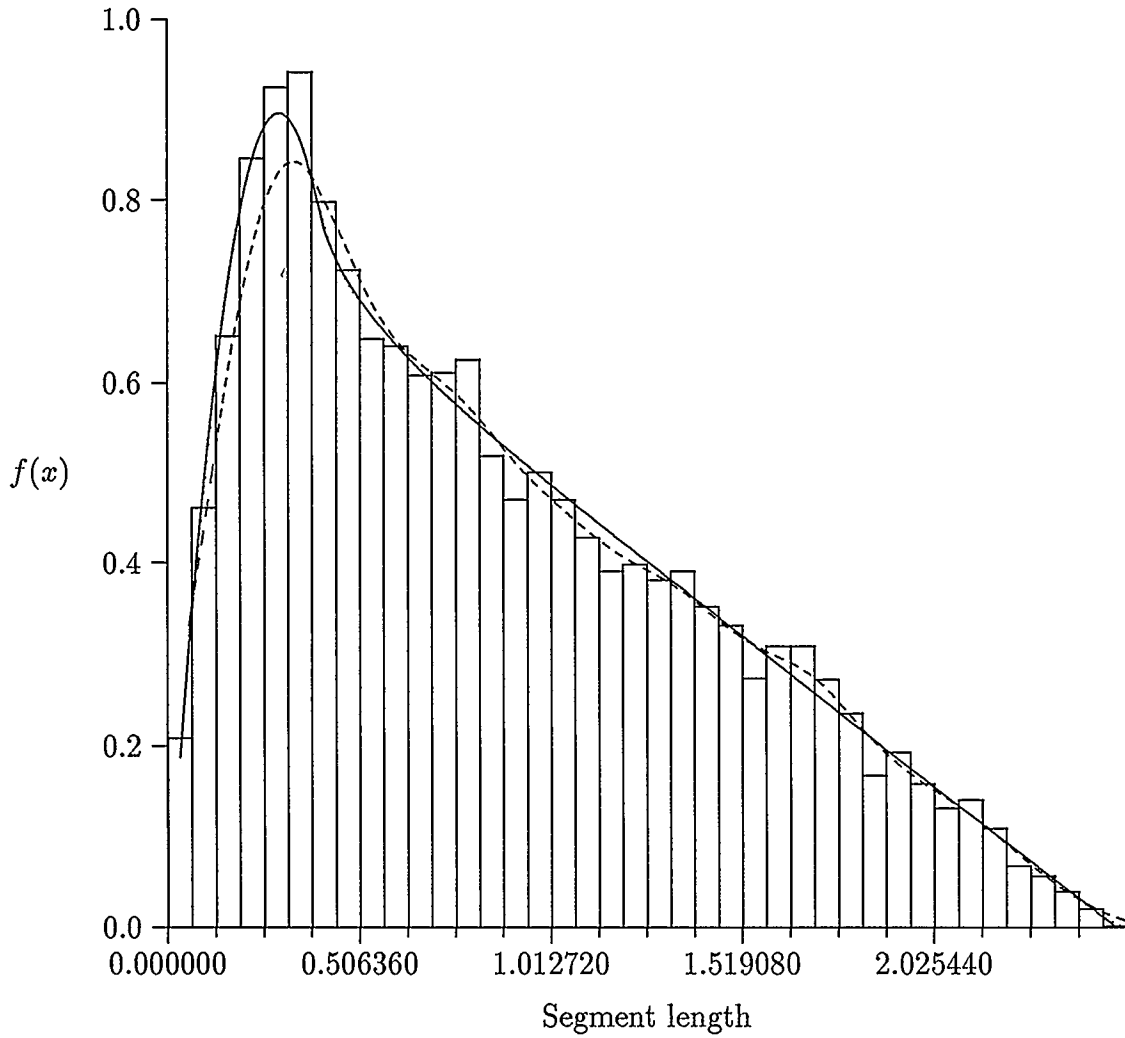
The Ω method provides an initial estimate of the segment density that is very

close to the actual curve (see Figures 3.12 and 3.13). This explains why fits are better for distributions requiring derivatives. For example, in Figure 3.14, the $f_{T;\lambda}$ method gives an estimate with right tail bias, although both methods provide decent estimates. In Figure 3.15 the $f_{T;\lambda}$ method cannot pick out the infinite jump in the density at the point of discontinuity. In Figure 3.16 neither method gave an adequate estimate — perhaps the dimensions of the rectangle differed too greatly.



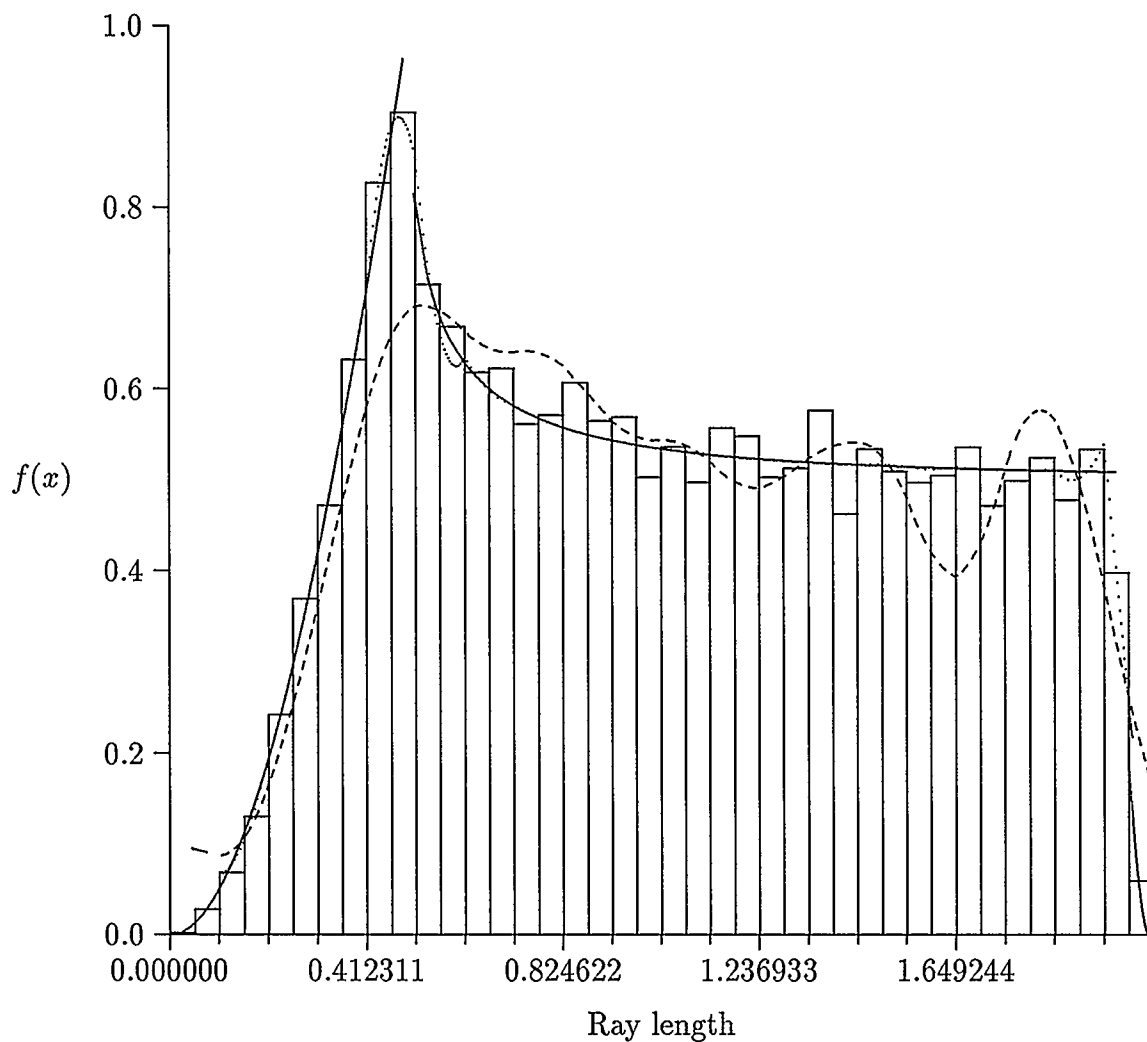
	Average	Variance		Symbol
Simulated	0.521742	0.061666	From $\Omega(l)$..
Analytical	0.521398	0.061478	$f_{T;\lambda}$	----
			Actual	—

Figure 3.12: $f_{T;\lambda}$ for the rectangle ($a = 1.0$) — fitted kernel smoother versus polygon program [actual curve and Ω method are indistinguishable]



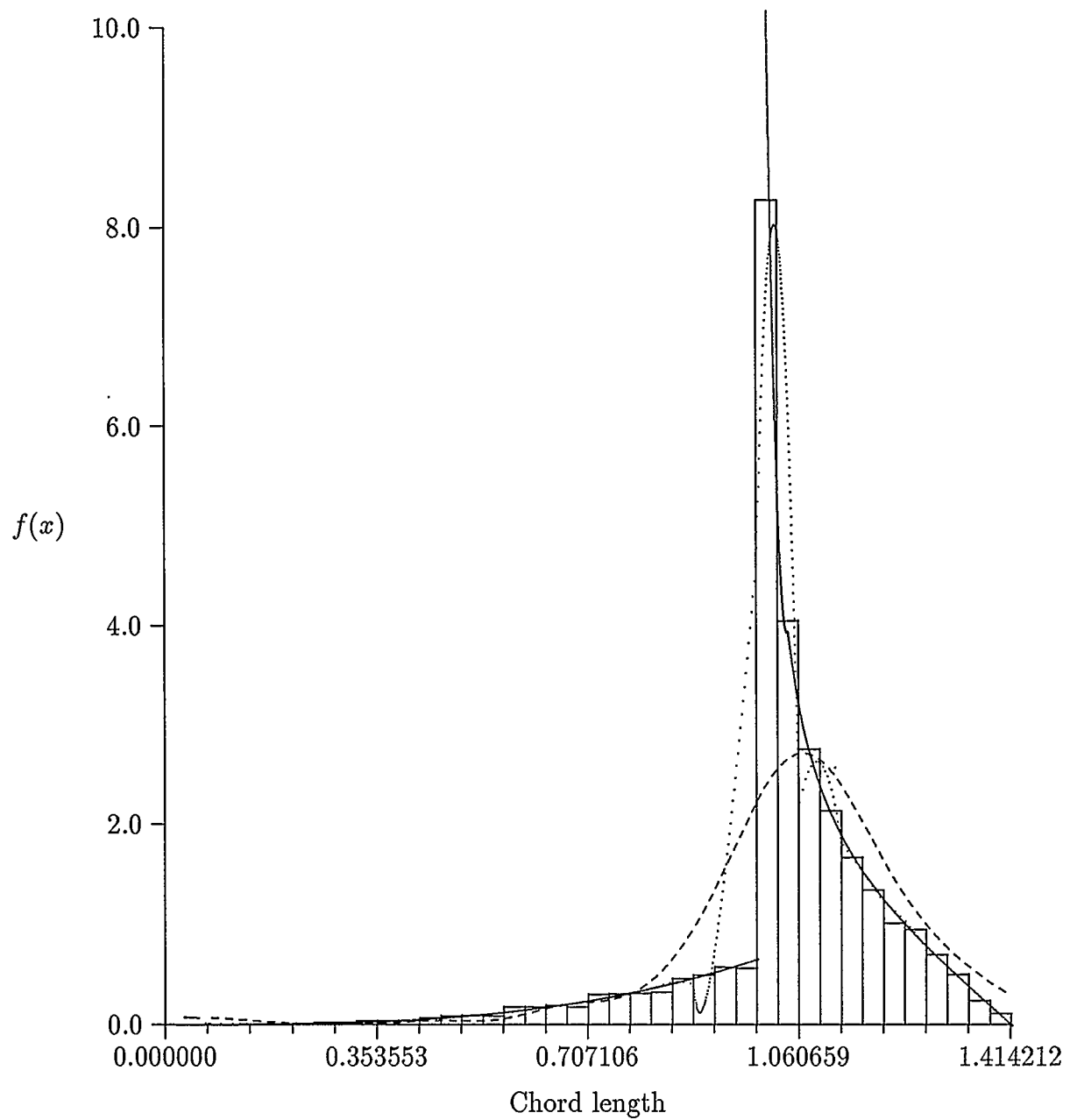
	Average	Variance		Symbol
Simulated	0.857725	0.324091	From $\Omega(l)$..
Analytical	0.861780	0.325585	$f_{T;\lambda}$	----
			Actual	—

Figure 3.13: $f_{T;\lambda}$ for the rectangle ($a = 0.4$) — fitted kernel smoother versus polygon program [actual curve and Ω method are indistinguishable]



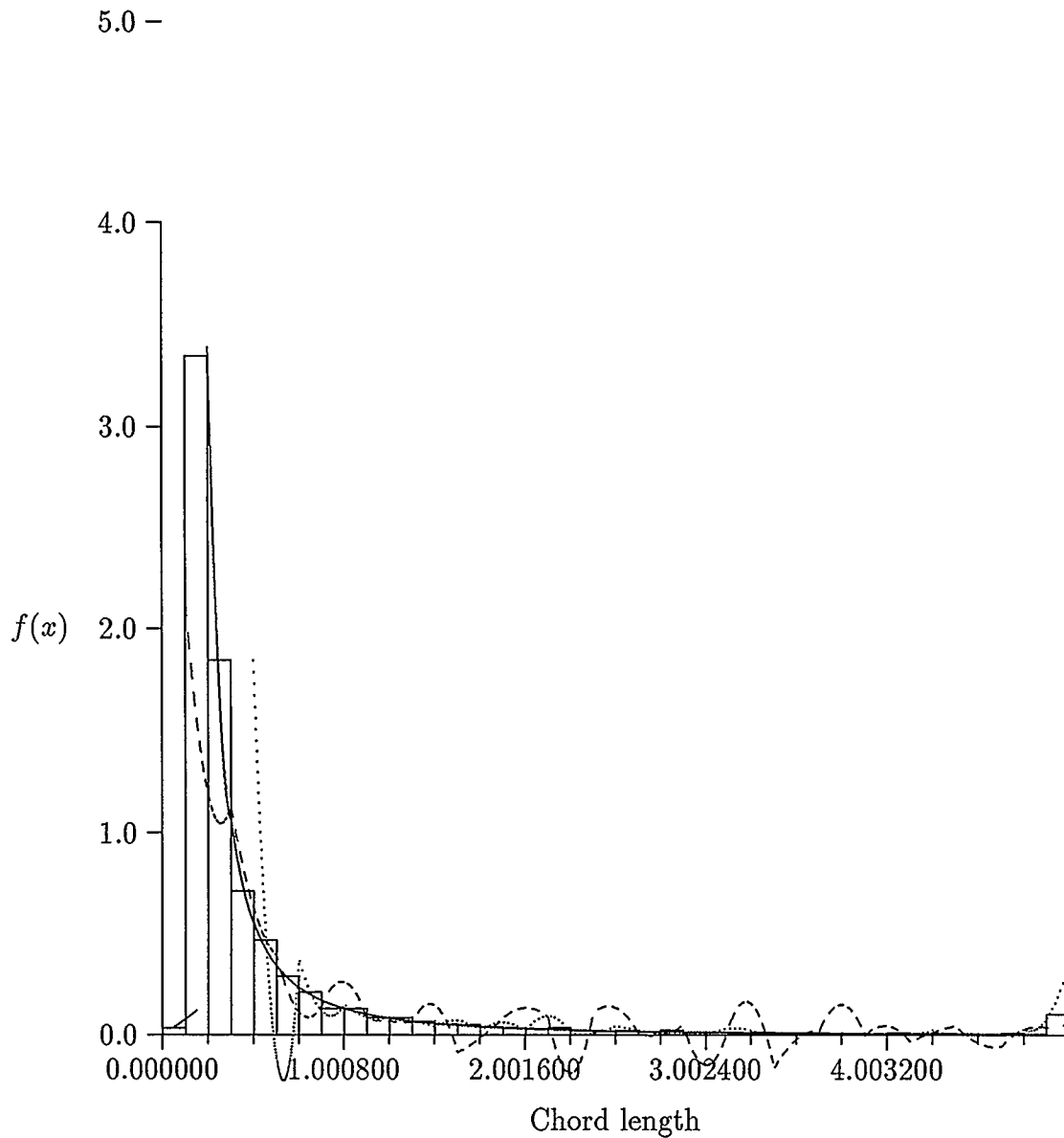
	Average	Variance		Symbol
Simulated	1.066234	0.266322	From $\Omega(l)$..
Analytical	1.070620	0.270443	From $f_{T;\lambda}$	----
			Actual	—

Figure 3.14: $f_{R,\lambda}$ for the rectangle ($a = 0.5$) — estimate via Ω versus estimate via $f_{T;\lambda}$



	Average	Variance		Symbol
Simulated	1.040538	0.024673	From $\Omega(l)$	· ·
Analytical	1.042811	0.023650	From $f_{T;\lambda}$	- - - -
			Actual	—

Figure 3.15: $f_{L,\lambda}$ for the rectangle ($a = 1.0$) — estimate via Ω versus estimate via $f_{T;\lambda}$



	Average	Variance		Symbol
Simulated	0.568252	0.634053	From $\Omega(l)$	· ·
Analytical	0.563450	0.637460	From $f_{T;\lambda}$	- - - -
			Actual	—

Figure 3.16: $f_{L,\nu}$ for the rectangle ($a = 0.2$) — estimate via Ω versus estimate via $f_{T;\lambda}$

3.5 The n -Sphere — Special Case: Circular Ovoid

Results for this “two-dimensional” body are presented here only because the circle was one body for which simulations were performed and overlaps calculated, but the theory is most presentable in its general form.

3.5.1 Theory

For the n -sphere of radius a , Enns and Ehlers (1978) have determined the overlap volume, whenever $0 \leq l \leq 2a$, as

$$\Omega(l) = \frac{2C_{n-1}}{C_n} \int_{l/2a}^1 dx (1-x^2)^{\frac{1}{2}(n-1)} = \frac{C_{n-1}}{C_n} B_\alpha \left(\frac{n+1}{2}, \frac{1}{2} \right), \quad (3.4)$$

where $\alpha = 1 - (l/2a)^2$ and $B_\alpha(p, q)$ is the incomplete beta function.

In particular, for ν -randomness, the distribution of chord lengths reduces to

$$f_{L,\nu}(l) = (n-1) \frac{C_{n-1}}{C_n} \frac{l^2}{4a^3} \left(1 - \frac{l^2}{4a^2} \right)^{\frac{1}{2}(n-3)} \quad 0 \leq l \leq 2a$$

$$= 0 \quad \text{otherwise.}$$

For distributions requiring $\epsilon(l)$ and $\omega(l)$, Enns and Ehlers have derived the expressions

$$\omega(l) = \Omega(l) + \frac{C_{n-1}}{nC_n} \left(\frac{l}{a} \right) \left(1 - \left(\frac{l}{2a} \right)^2 \right)^{(n-1)/2}, \quad (3.5)$$

and

$$\epsilon(l) = (n-1) C_{n-1} \frac{a^{n-1}}{l} \left(1 - \left(\frac{l}{2a} \right)^2 \right)^{(n-3)/2}. \quad (3.6)$$

These expressions give the entire spectrum of segment, ray and chord length distributions. These results, derived by $\Omega(l)$ above and the results of Chapter 2 (Table 2.6), are given in Table 3.2. For other references to analytical derivations for the circle, see Horowitz [43] and Coleman [12], [15].

Table 3.2: Actual distributions for the unit circle

Function	Expression	Function	Expression
$\Omega(l)$	$1 - \frac{2 \sin^{-1}(l/2)}{\pi} - \frac{l\sqrt{1-l^2/4}}{4\pi}$	$\omega(l)$	$1 - \frac{2 \sin^{-1}(l/2)}{\pi}$
$\epsilon(l)$	$\frac{2}{l\sqrt{1-l^2/4}}$	$f_{R;\alpha}$	$l - \frac{2l \sin^{-1}(l/2)}{\pi}$
$f_{R;\lambda}$	$\frac{2l^2\sqrt{1-l^2/4}}{\pi}$	$f_{R;\nu}$	$\frac{2\sqrt{1-l^2/4}}{\pi}$
$f_{L;\nu}$	$\frac{l^2}{2\pi\sqrt{1-l^2/4}}$	$f_{L;\mu}$	$\frac{l}{4\sqrt{1-l^2/4}}$
$f_{L;\alpha}$	$\frac{l^2}{2\pi\sqrt{1-l^2/4}}$	$f_{L;\gamma}$	$\frac{1}{\pi\sqrt{1-l^2/4}}$
$f_{L;\beta}$	$\frac{1}{\pi\sqrt{1-l^2/4}}$	$f_{L;\lambda}$	$\frac{l^4}{6\pi\sqrt{1-l^2/4}}$
$f_{T;\lambda}$	$2l\Omega(l)$		

3.5.2 Results for $n = 2$ — Circle

Direct simulations for the unit circle were performed for every distribution given in Table 2.6. In addition, for $f_{L;x}$, $x \in [\lambda, \mu, \nu]$ and for $f_{R;x}$, $x \in [\lambda, \nu]$, estimates based on both the $\Omega(l)$ and $f_{T;\lambda}$ methods were generated.

Interior point randomness was simulated by simply choosing a point in the square $[-1, 1] \times [-1, 1]$ and checking for $x^2 + y^2 < 1$. Surface randomness required choosing an angle θ in the interval $(0, 2\pi)$. The subsequent point $(\cos \theta, \sin \theta)$ was random on the surface of the circle.

Two polygonal approximations were considered. They are

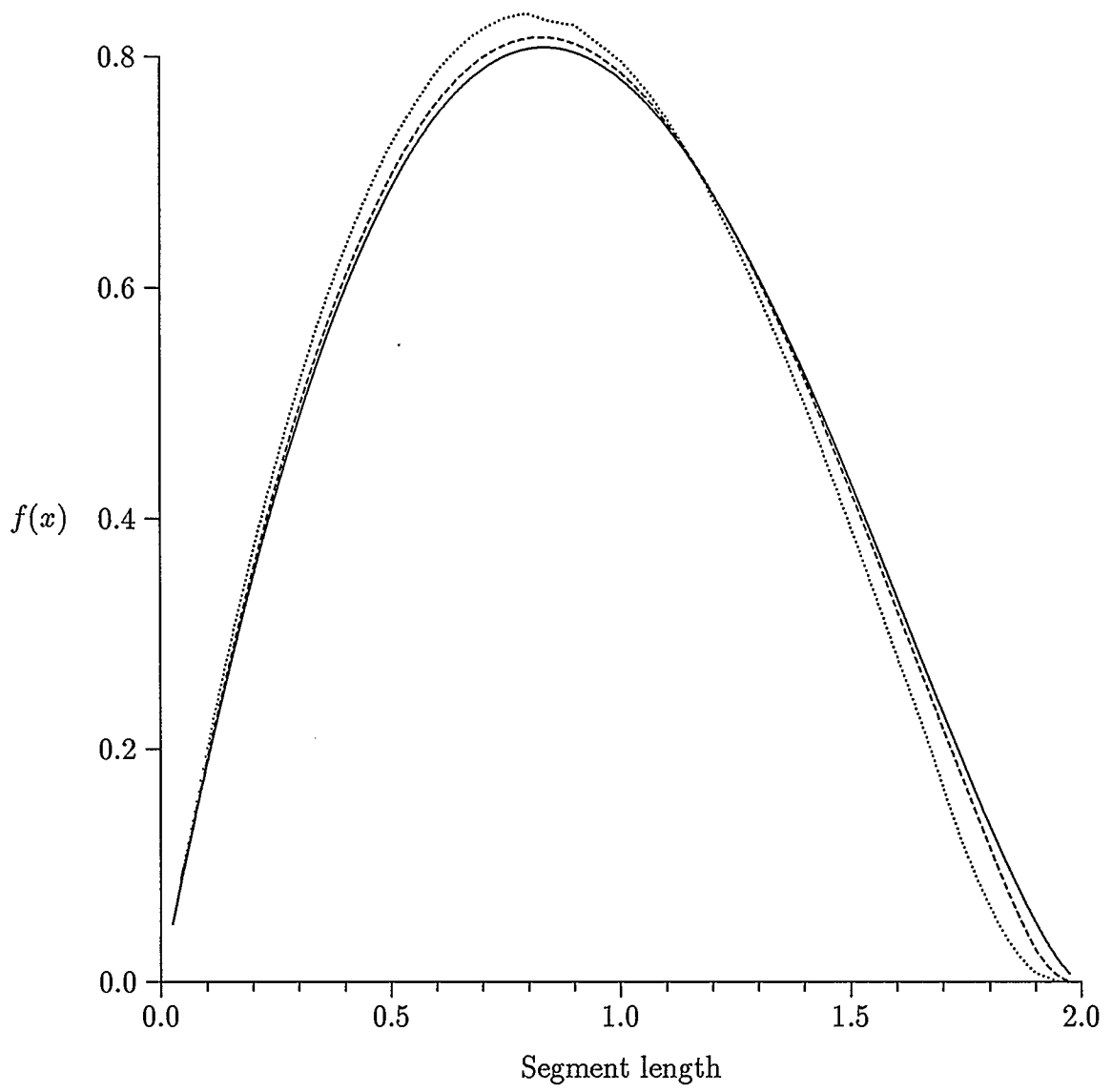
- (1) Estimate the circle by choosing points equally spaced on the unit circle. This gives an estimate of the true $\Omega(l)$ by inscribed polygons whose volume is always less than the volume of the circle. With a sufficient number of points, however, the approximation should be close enough to the circle to provide reasonable estimates.
- (2) Estimate the circle with regular polygons of area π . First the equilateral triangle, then the square, then the pentagon, and so on, up to the undecagon or the dodecagon. [This approach standardizes with respect to area. A regular n -gon of area π can be generated by taking n points on a circle of radius $\sqrt{2\pi / \sin(2\pi/n)}$, equally spaced.]

To illustrate these approaches, both were applied to simulation of the segment density $f_{T;\lambda}$. Figure 3.17 demonstrates convergence under the first, inscribed polygon, approach. Figure 3.19 demonstrates the second, regular polygon approach, starting at the equilateral triangle and ending with the hexagon. Convergence is swift in both

cases, and relatively few points should approximate the circle accurately. The first approach was used in the remaining simulations because it was easier to implement.

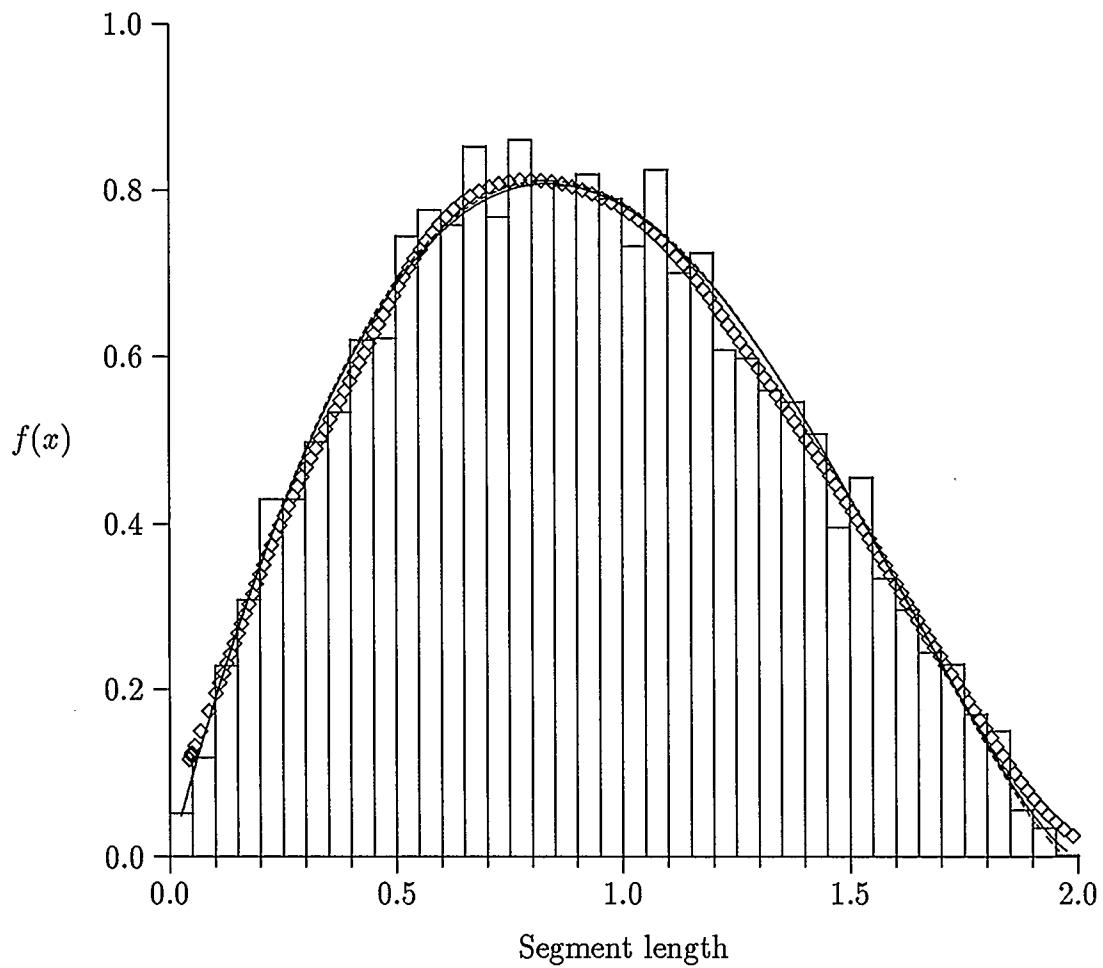
Now that $\Omega(l)$ is established in accuracy, $f_{T;\lambda}$ can be analyzed. In Figure 3.18 a comparison between $\Omega(l)$ generated with 40 points and the segment density kernel smoother as fits to the actual $f_{T;\lambda}$ are given. Note that the overlap function is here slightly better than the segment density for estimating other densities for which first and second derivatives are required that depend heavily on the initial estimate. However, even slight variations can cause severe fluctuations in estimated derivatives, and this explains why the Ω approach becomes a better estimator of distributions requiring derivatives.

It is no surprise, then, that $f_{R;\nu}$ (Figure 3.20) and $f_{R;\lambda}$ (Figure 3.21) are best estimated by the overlap function (polygon program). However, the $f_{T;\lambda}$ method exhibits bias in the left tail, as does the Ω method. For the chord densities under ν -, μ -randomness (Figures 3.22 and 3.23 respectively) the $f_{T;\lambda}$ method is inefficient with too many fluctuations. The Ω method in each of these cases provides reasonable estimates that exhibit bias throughout. The case is only slightly better for $f_{L;\lambda}$, where the fits from both the overlap function and the segment density are poor (Figure omitted).



	Symbol
Actual	—
10 Points Generated	...
20 Points Generated	- - - -

Figure 3.17: Convergence of $f_{T;\lambda}$ using Ω for inscribed polygons



	Symbol
Actual	—
From $\Omega(l)$	- - - -
Kernel Estimate (Gaussian)	◇ ◇ ◇

Figure 3.18: $f_{T,\lambda}$ for the unit circle — estimate via Ω versus estimate via direct simulation (best kernel fit) [actual curve and Ω method are indistinguishable]

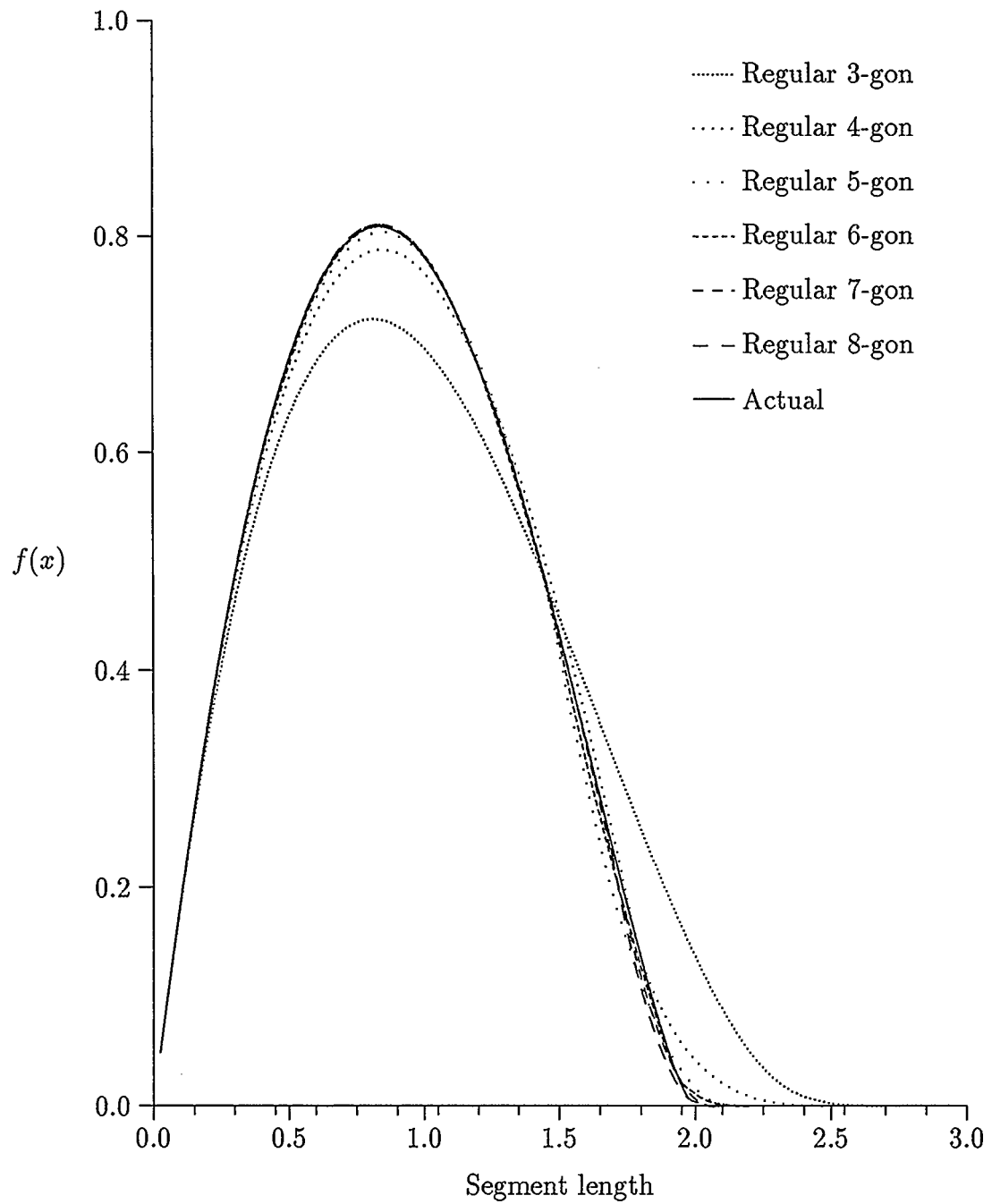
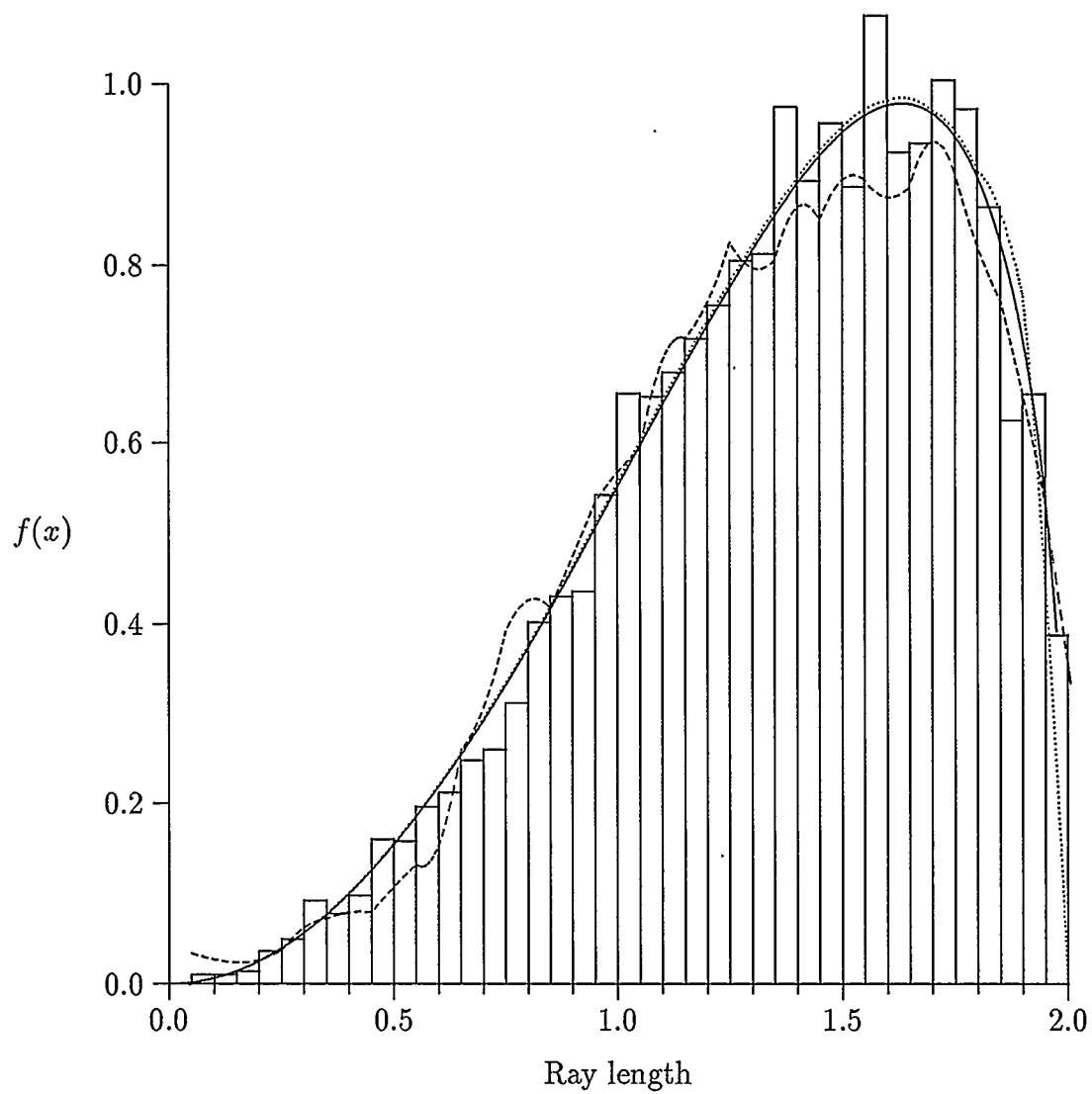
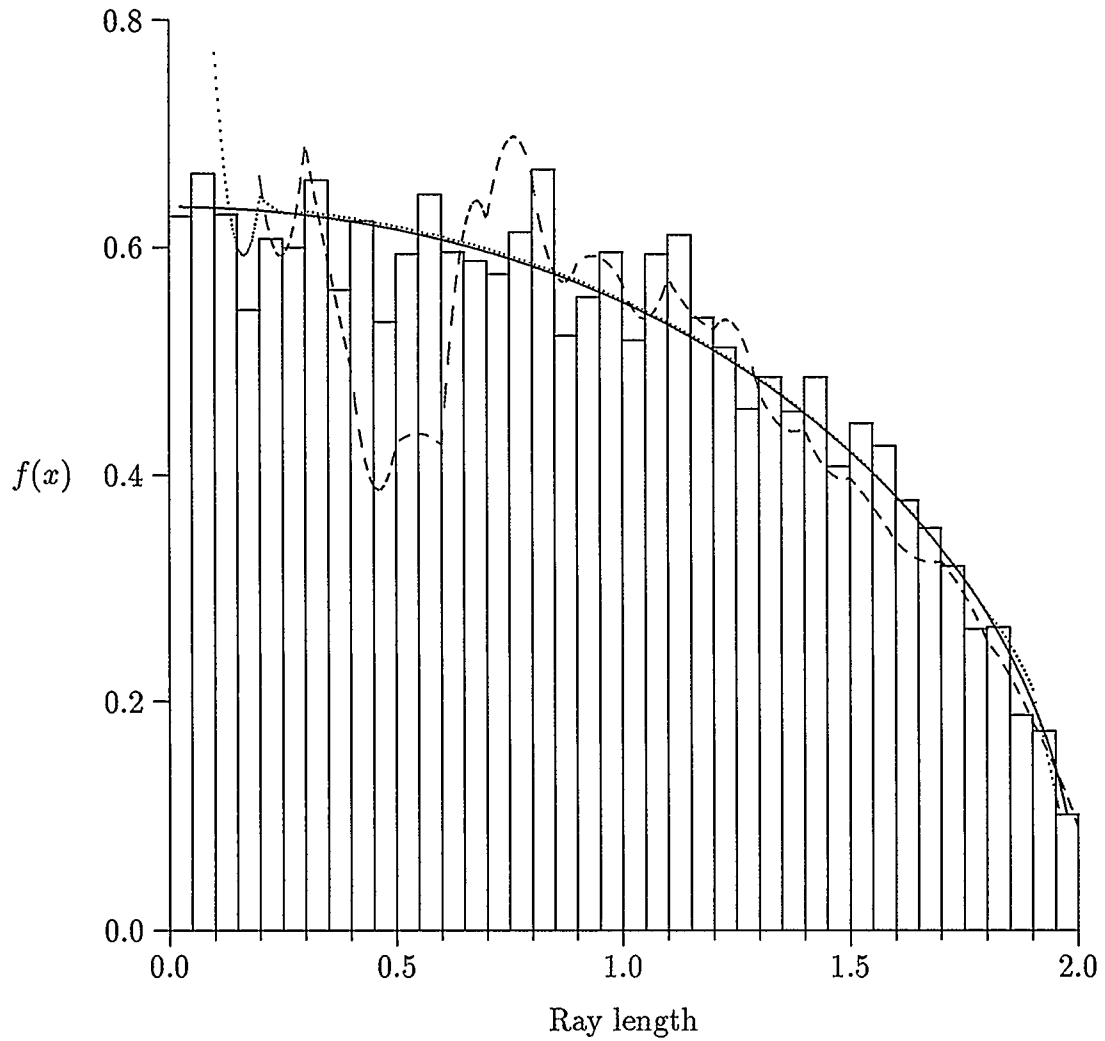


Figure 3.19: Convergence of $f_{T,\lambda}$ using Ω for equal-area polygons



	Symbol
Actual	—
From $\Omega(l)$...
From $f_{T,\lambda}$	- - - -

Figure 3.20: $f_{R,\lambda}$ for the unit circle — estimate via Ω versus estimate via $f_{T,\lambda}$



	Symbol
Actual	—
From $\Omega(l)$...
From $f_{T,\lambda}$	----

Figure 3.21: $f_{R,\nu}$ for the unit circle — estimate via Ω versus estimate via $f_{T,\lambda}$

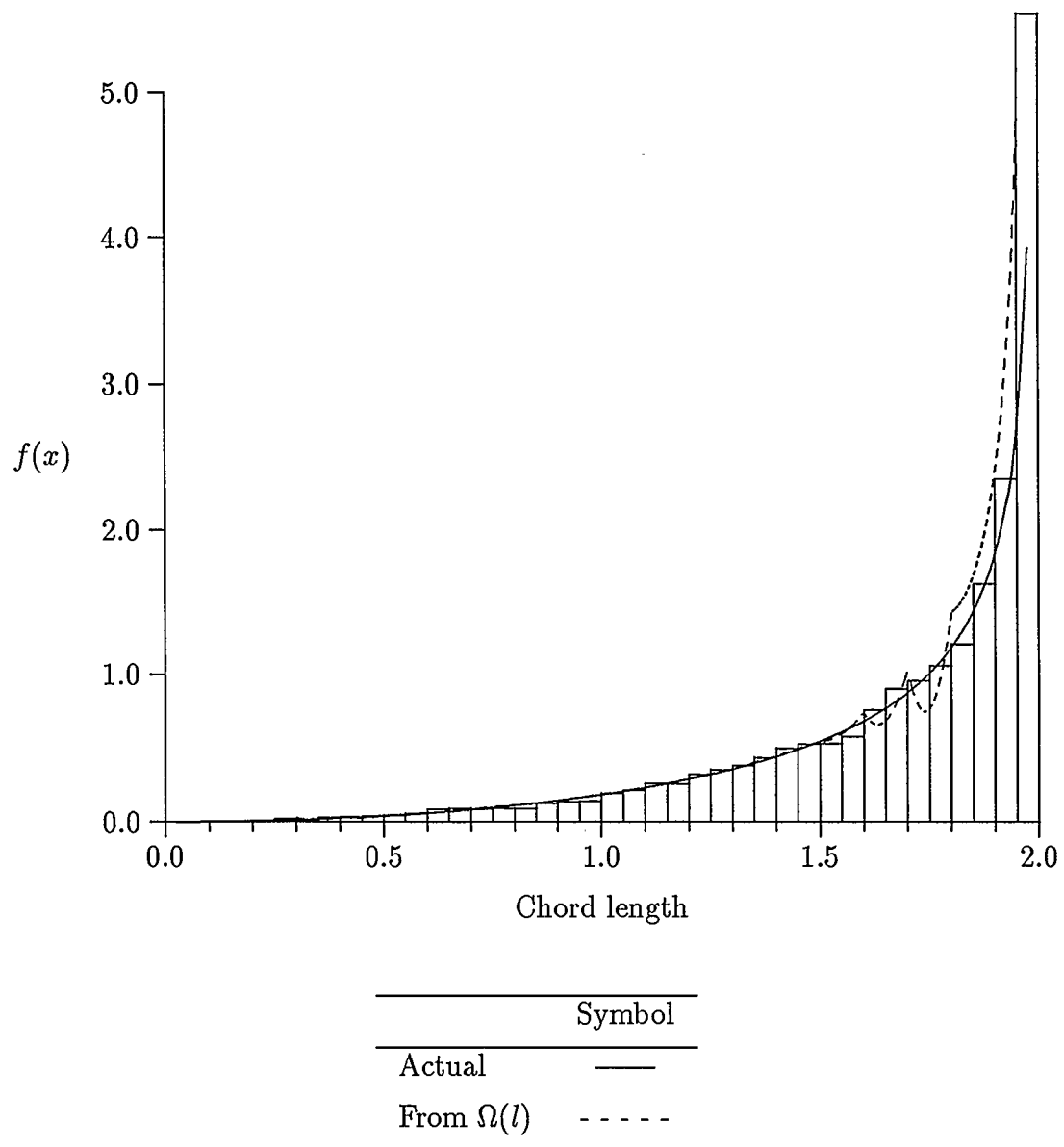


Figure 3.22: $f_{L,\nu}$ for the unit circle — estimate via Ω

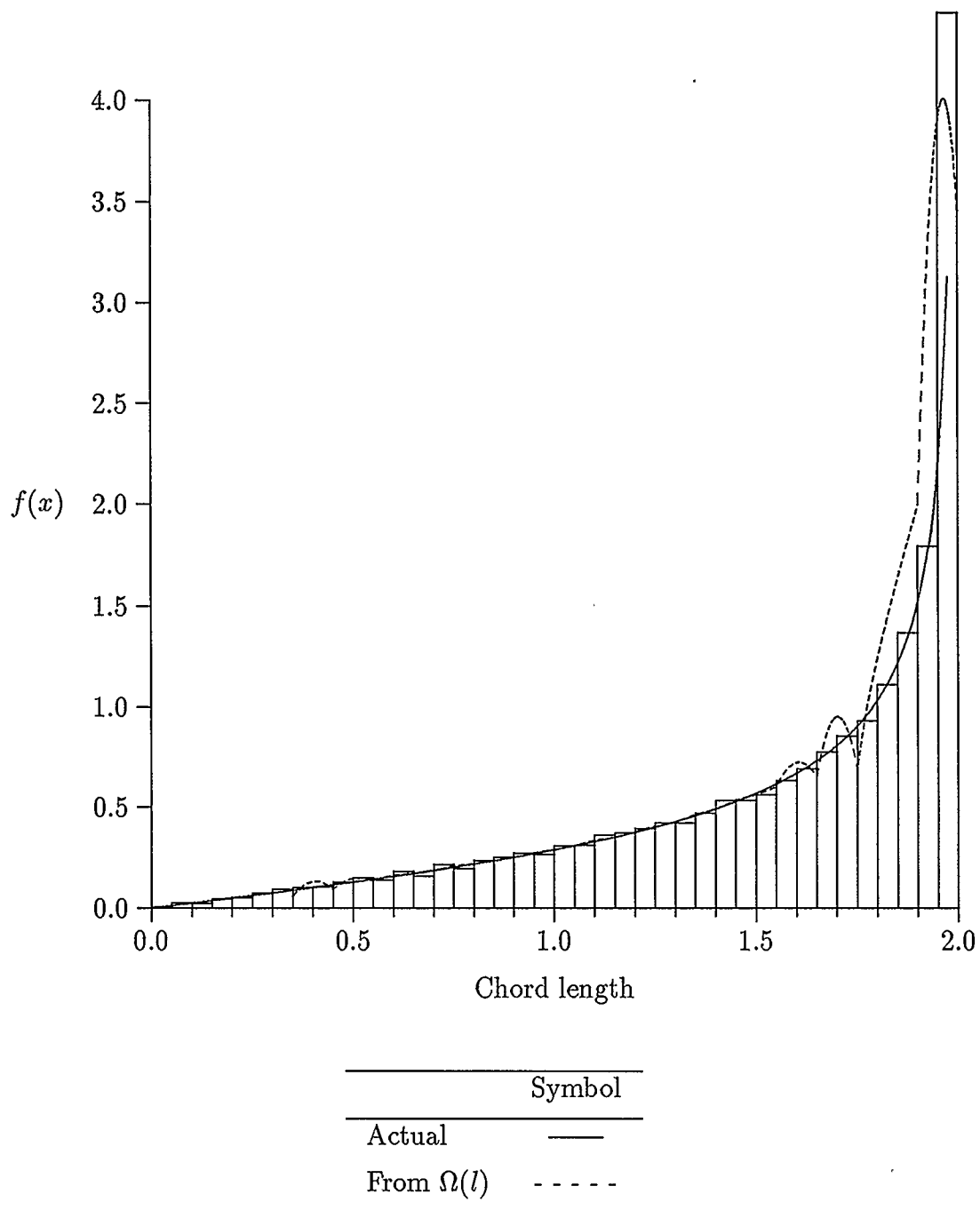


Figure 3.23: $f_{L,\mu}$ for the unit circle — estimate via Ω

3.6 Results For The Ellipse

For the ellipse surface-random chords cannot be dealt with theoretically and no published results exist. Surface randomness by simulation is therefore a step forward. Objects in reality do not appear as perfect circles and ellipses, and it is the purpose of this thesis to try and determine a methodology for dealing with non-trivial shapes, such as non-symmetric polygons and egg-shaped ovoids. Ellipse surface-random chords are a step in this direction.

We were required to develop an original methodology for generating uniform points on the surface of the ellipse. This methodology first involved parametrizing the ellipse

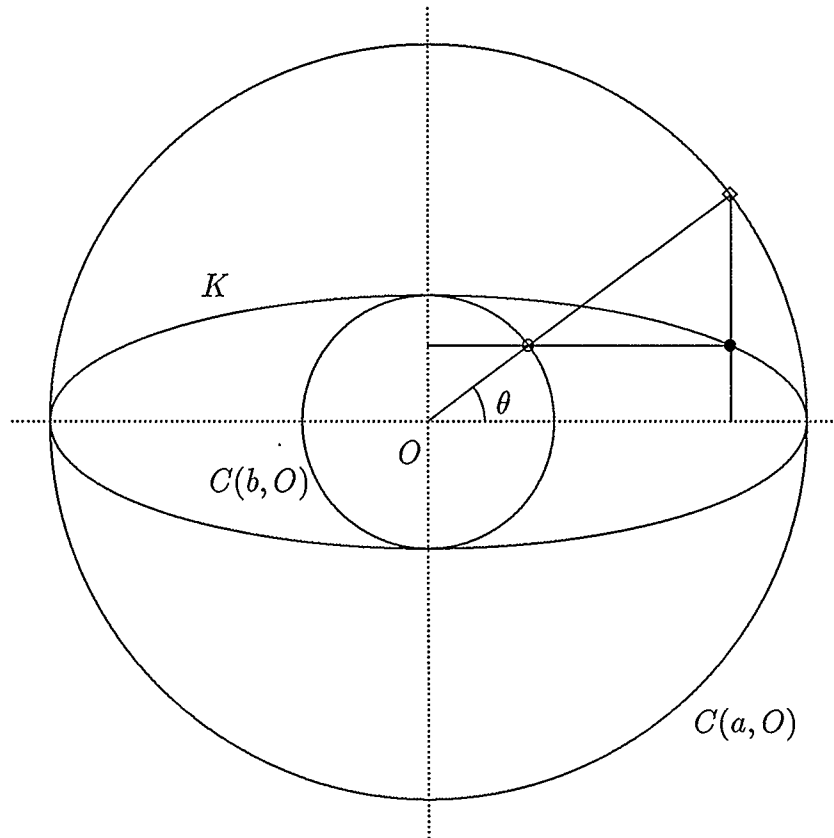
$$\frac{x^2}{a^2} + \frac{y^2}{b^2} = 1,$$

through the relations $x = a \sin(t)$ and $y = b \cos(t)$. Then the arc length is given by

$$S(t) = \int_0^t dS = \int_0^t \sqrt{a^2 \cos^2 \theta + b^2 \sin^2 \theta} d\theta \quad (3.7)$$

$$= \int_0^t a \cdot \sqrt{1 - \left(1 - \frac{b^2}{a^2}\right) \sin^2 \theta} d\theta, \quad (3.8)$$

the well-known Legendre elliptic integral of the second kind. What is required for surface randomness is to first choose a random number \tilde{s} in the interval $(0, S(2\pi))$. This gives a random point on the surface of the ellipse in terms of arc length. Then $\tilde{s} = S(t)$ can be inverted through the Jacobi elliptic function $S^{-1}(t)$ (simply the inverse of $S(t)$), to give $t = S^{-1}(\tilde{s})$, thus returning the coordinate $(a \sin t, b \cos t)$. Simulations for $a^2 = b^2 = 1$ return the unit circle (special case of the ellipse when $a = b = 1$) results. Figure 3.24 shows this methodology.

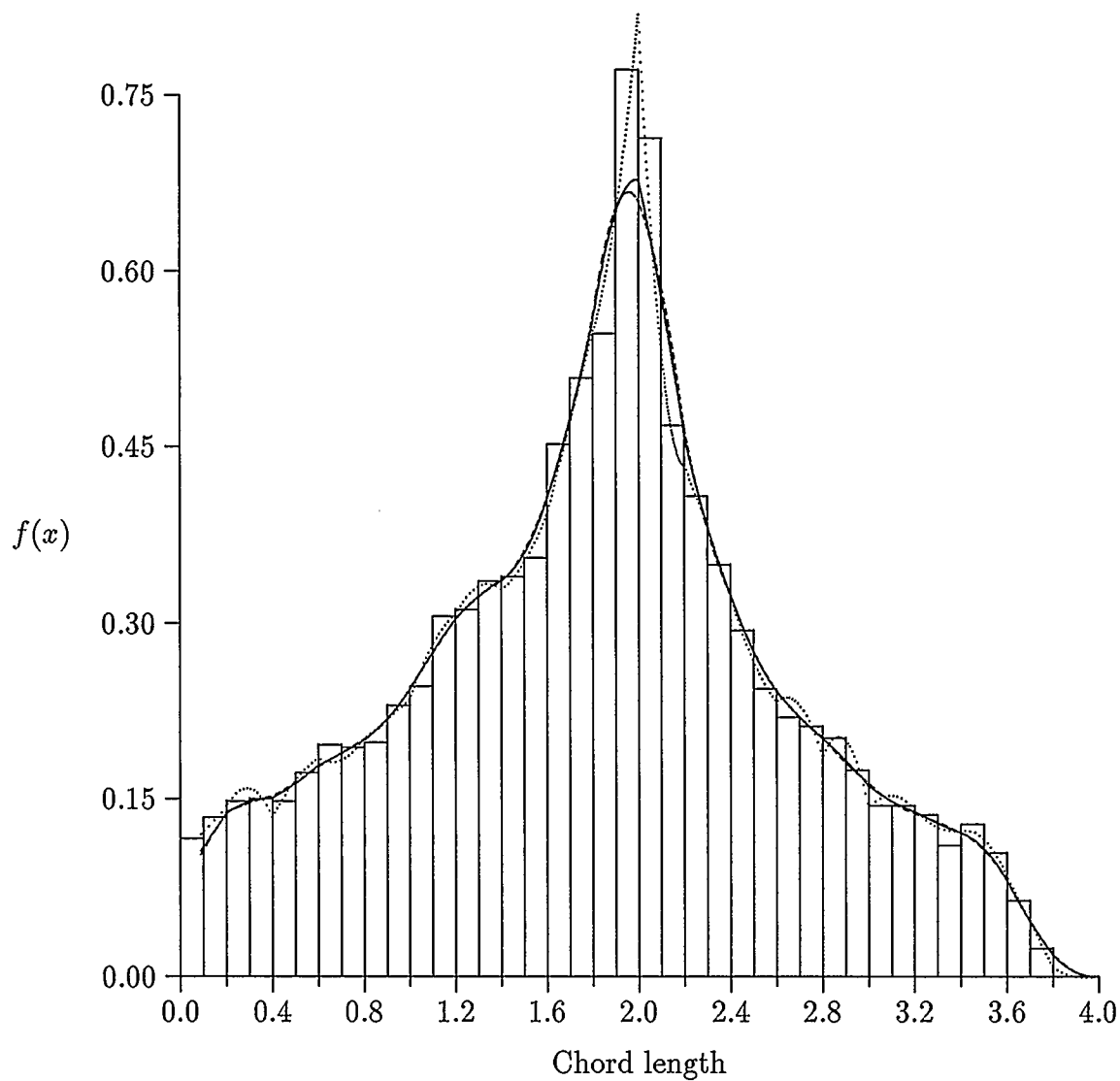


Symbol	Point
•	$(a \cos \theta, b \sin \theta)$
◦	$(b \cos \theta, b \sin \theta)$
◊	$(a \cos \theta, a \sin \theta)$

Figure 3.24: Ellipse Surface Randomness

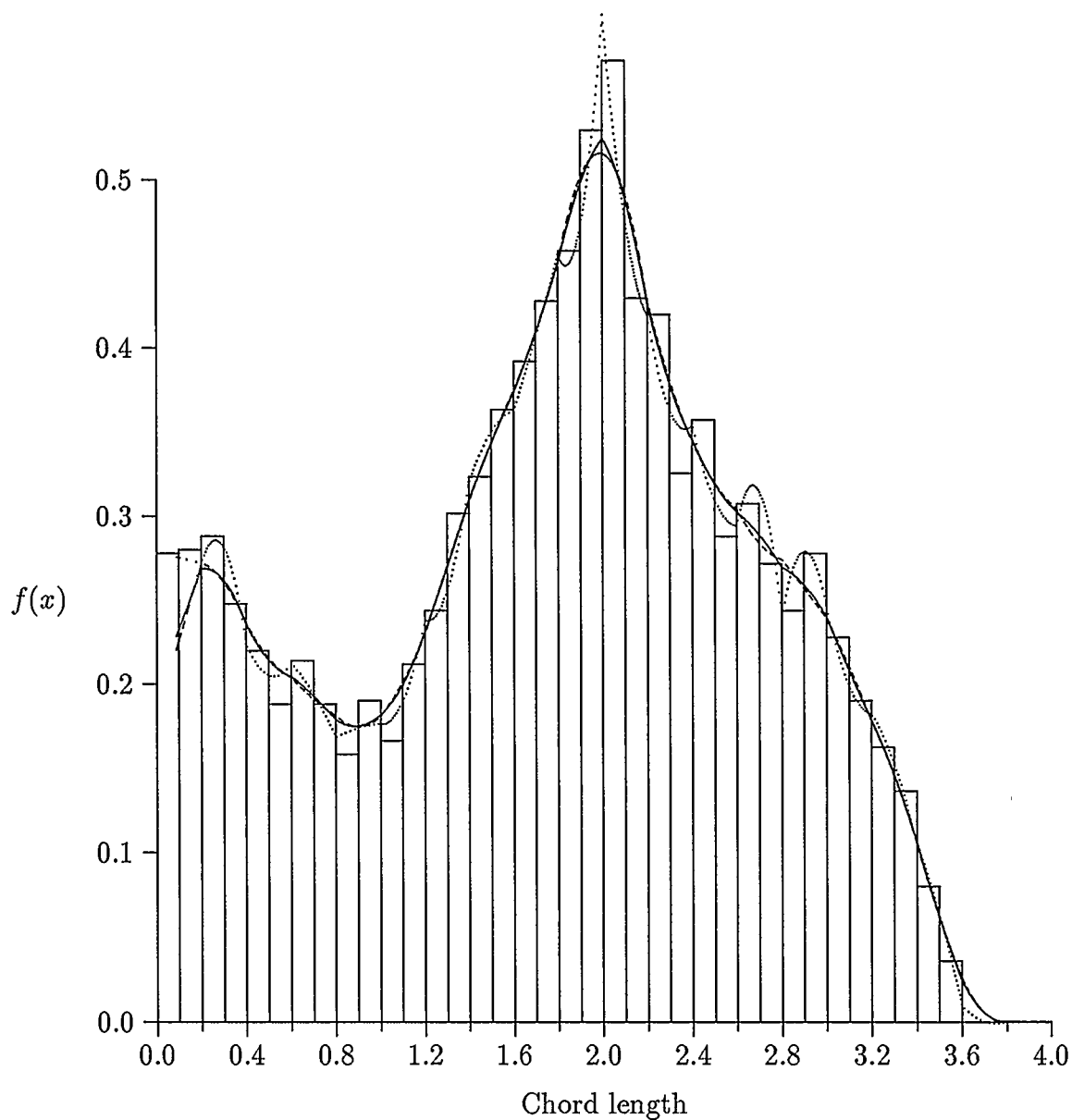
The distributions for surface randomness are given in Figures 3.25, 3.26, 3.27 and 3.28.

Other original work relates to the use of the polygon program to approximate the ellipse in generating chord and ray densities where appropriate under λ -, ν - or μ -randomness. The ellipse, like the circle, can be approximated through the polygon program by simply taking a number of points $(a \cos t, b \sin t)$ where t is incremented from 0 to 2π by some consistent level. Note that the kernel fit (from which derivatives are based in the $f_{T;\lambda}$ method) and the segment density from the Ω program are close (see Figure 3.29). There is no theoretical curve to compare with; however, the Ω program gives a much smoother estimate and its derivatives behave better (Figures omitted). [Theory for the ellipse has been developed by Piefke [74] for chords under μ -randomness. Gasparyan [29] basically recovers the overlap function for the ellipse.]



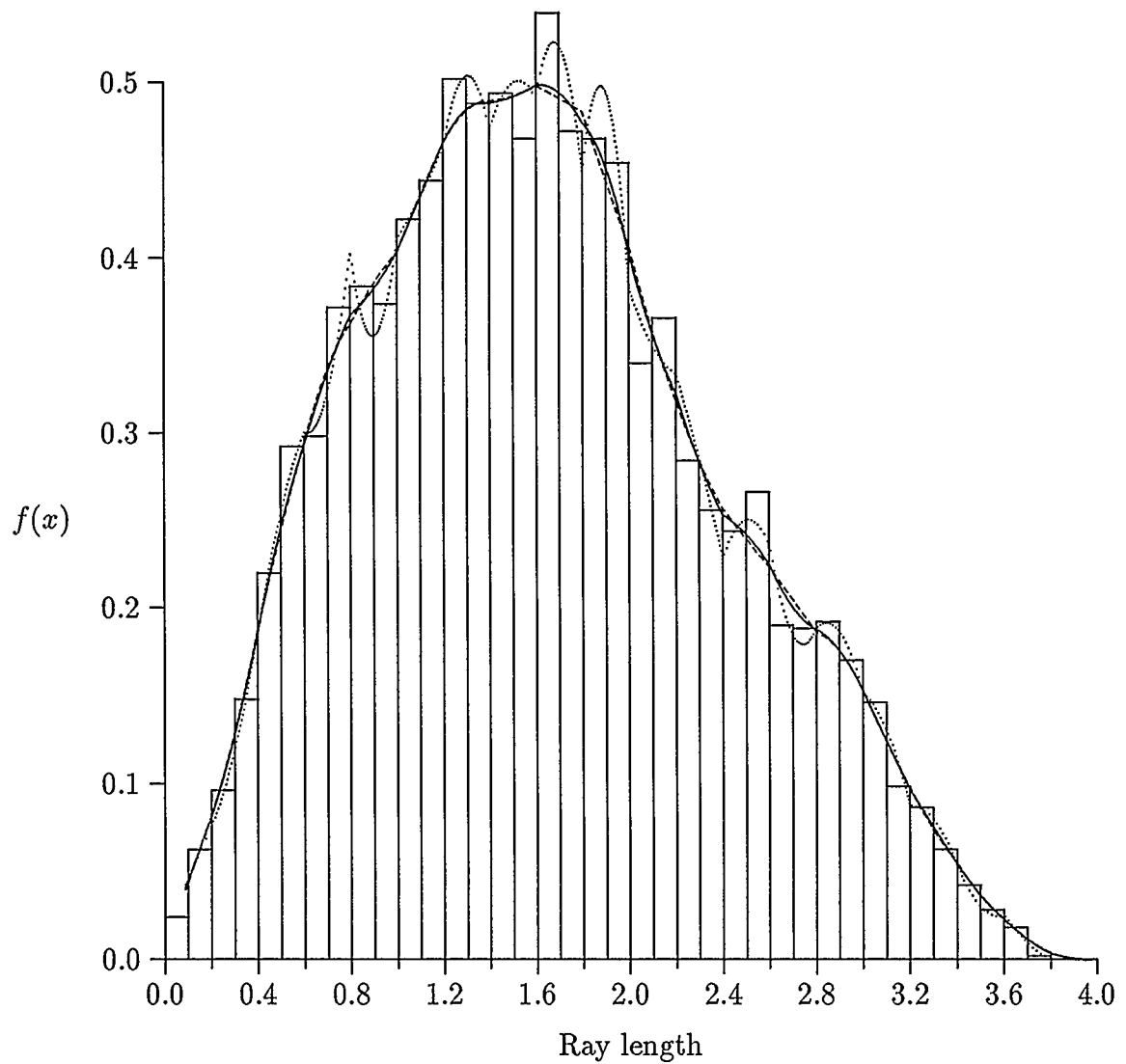
	Average	Variance		Symbol
Simulated	1.823404	0.663759	Gaussian	—
		$h = 0.1$	Epanechnikov	- - - -
			Biweight	· · ·

Figure 3.25: $f_{L,\gamma}$ for the ellipse ($a = 2, b = 1$) — several kernel fits



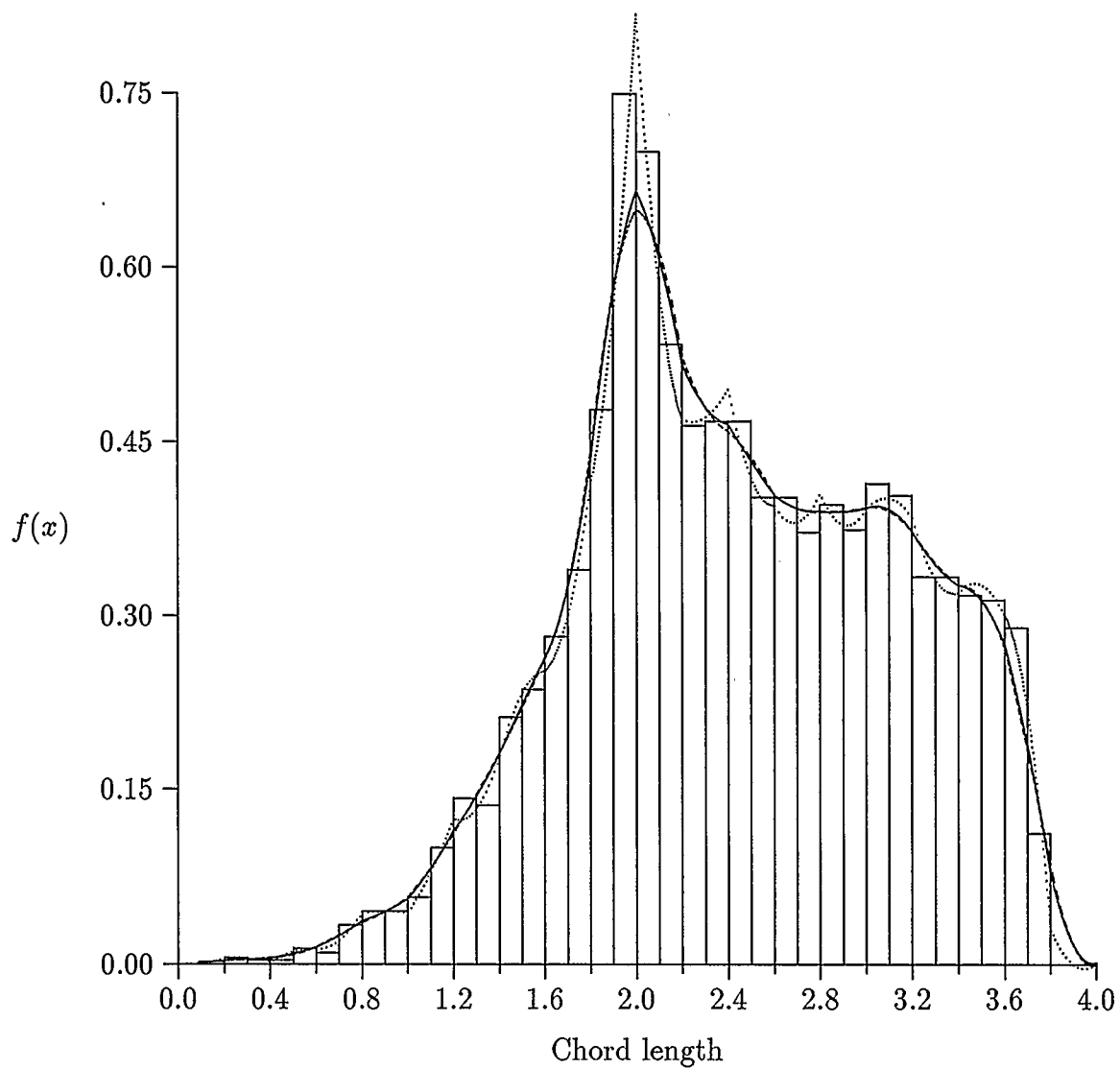
	Average	Variance		Symbol
Simulated	1.763113	0.806449	Gaussian	—
		$h = 0.1$	Epanechnikov	- - - -
			Biweight	...

Figure 3.26: $f_{L,\beta}$ for the ellipse ($a = 2, b = 1$) — several kernel fits



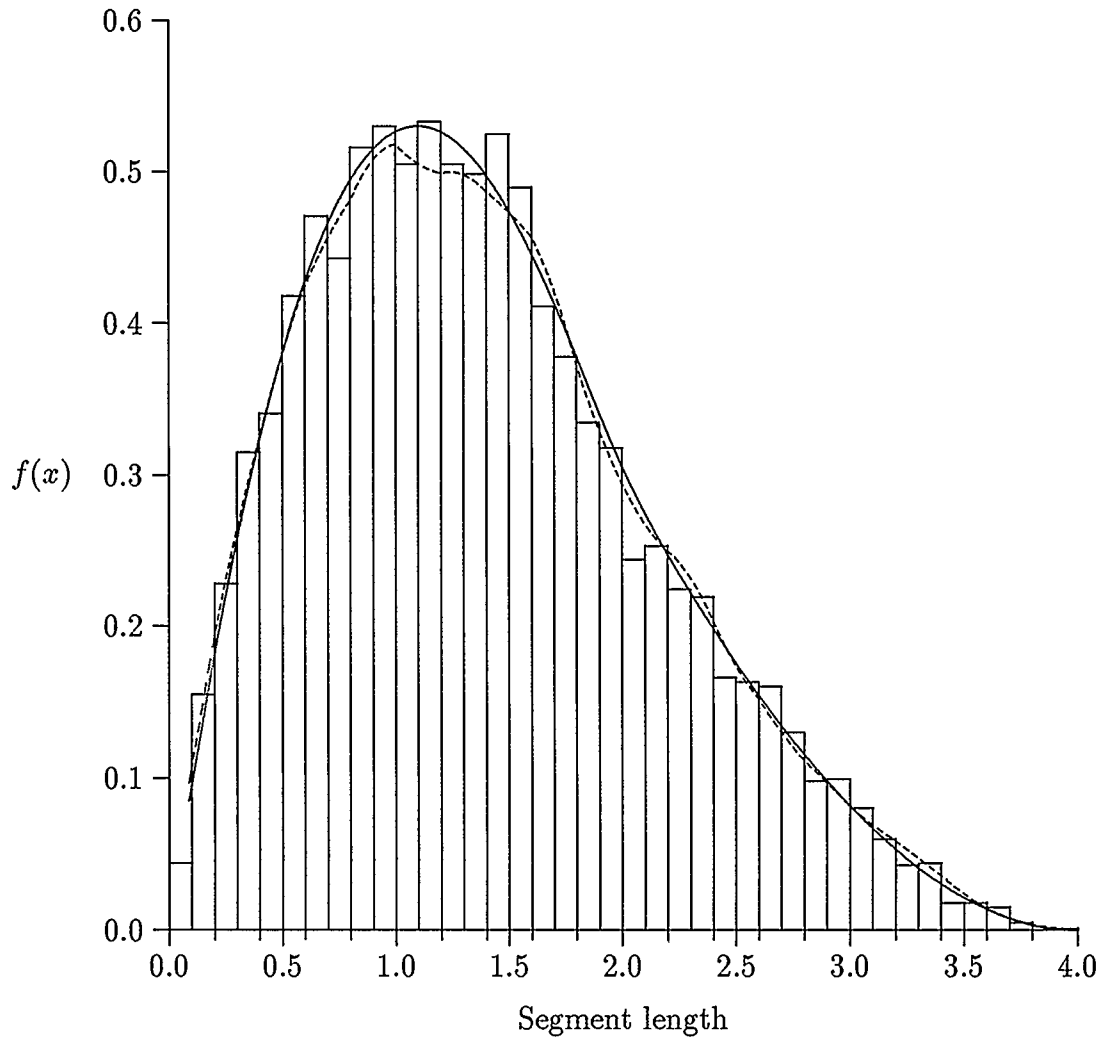
	Average	Variance		Symbol
Simulated	1.628292	0.574857	Gaussian	—
		$h = 0.1$	Epanechnikov	- - - -
			Biweight	· · ·

Figure 3.27: $f_{R,\alpha}$ for the ellipse ($a = 2, b = 1$) — several kernel fits



	Average	Variance		Symbol
Simulated	2.439189	0.475586	Gaussian	—
		$h = 0.1$	Epanechnikov	- - - -
			Biweight	· · ·

Figure 3.28: $f_{L,\alpha}$ for the ellipse ($a = 2, b = 1$) — several kernel fits



Symbol	
From $\Omega(l)$	—
$f_{T,\lambda}$	- - - -

Figure 3.29: $f_{T,\lambda}$ for the ellipse ($a = 2, b = 1$) — direct simulation versus estimate via Ω method

Chapter 4

Ovoids in Three Dimensions

In this chapter results for three-dimensional ovoids are presented. Ovoids considered here include the box, ellipsoid (and prolate spheroid), hemisphere, cylinder, and sphere. Since the Ω or polygon program was not extended to three dimensions, comparisons in this Chapter are limited to comparisons between the *direct simulation* and $f_{T;\lambda}$ methods. Distributions for surface-randomness for which the comparisons do not apply are included for the sphere to provide conclusions about kernel smoothers. Conclusions and recommendations involving analysis for both two- and three-dimensional ovoids are given at the end of this Chapter.

4.1 Results For The Box (Cube)

Simulations performed for the cube include all distributions listed in Table 2.6 [although figures for distributions involving surface-randomness were omitted]. Note that the simulations were done only for the cube – they were not generalized to boxes. However, generating both $\Omega(l)$ and $f_{T;\lambda}$ for arbitrary boxes is possible, and a natural place to start in extending the polygon program to higher dimensions.

This section also describes how to generate μ -random secants of a body K directly, using the procedure outlined by Itoh [44] for a cube to confirm his derived distribution. For all of the bodies studied in this thesis, including two-dimensional ovoids, his method was adapted to generate μ -random chords. The following para-

graphs describe Itoh's method for the cube.

First center the body K at some origin O and calculate the maximum intercept (or chord) length l_{max} . Choose a point (X_0, Y_0) in the interval $(-l_{max}/2, l_{max}/2)$. Next rotate the line through this point perpendicular to the z -axis around z by θ_1 , around y by θ_2 , around x by θ_3 , and finally incline the line to the z -axis with θ_2 . In this case, for U_i independent uniform $(0, 1)$ variates,

$$\theta_1 = 2\pi U_1, \quad \cos \theta_2 = 2U_2 - 1, \quad \text{and} \quad \theta_3 = 2\pi U_3.$$

Also, X_0 and Y_0 are chosen by picking two random uniform variate and then scaling to the appropriate interval. It remains to find the intersections of the rotated line with the boundary of K . However, this is a simple exercise since the points after rotation can be expressed as (with transformation matrices given)

$$\begin{pmatrix} x \\ y \\ z \end{pmatrix} = \begin{bmatrix} -C_3 & S_3 & 0 \\ -S_3 & C_3 & 0 \\ 0 & 0 & 1 \end{bmatrix} \begin{bmatrix} C_2 & 0 & -S_2 \\ 0 & 1 & 0 \\ S_2 & 0 & C_2 \end{bmatrix} \begin{bmatrix} C_1 & 0 & -S_1 \\ S_1 & C_1 & 0 \\ 0 & 0 & 1 \end{bmatrix} \begin{pmatrix} X \\ Y \\ Z \end{pmatrix},$$

with $C_i = \cos \theta_i$, $S_i = \sin \theta_i$ and $(X, Y, Z)^T$ being the original point with rotated coordinates $(x, y, z)^T$. These matrix relations give the equation

$$\begin{aligned} & \frac{x - x_0(C_1 C_2 C_3 - S_1 S_3) - y_0(S_1 C_2 C_3 + C_1 S_3)}{-S_2 C_3} \\ = & \frac{y - x_0(-C_1 C_2 S_3 - S_1 C_3) - y_0(-S_1 C_2 S_3 + C_1 C_3)}{S_2 S_3} \\ = & \frac{z - x_0 C_1 S_2 - y_0 S_1 S_2}{C_2}, \end{aligned}$$

which is more convenient when x , y and z are written as

$$x = x_1 + t(x_2 - x_1),$$

$$y = y_1 + t(y_2 - y_1),$$

$$z = z_1 + t(z_2 - z_1).$$

For the cube with side length a , Ehlers (1972) found

$$\begin{aligned}
4\pi\Omega(l) &= 4\pi - 6\pi\rho + 8\rho^2 - \rho^3 & 0 \leq \rho \leq 1 \\
&= \frac{(6\pi - 1)}{\rho} - 8\pi + 6\rho + 2\rho^3 - 8(1 + 2\rho^2)\frac{\sqrt{\rho^2 - 1}}{\rho} + 24\frac{\rho}{\cos^{-1}\rho} & 1 \leq \rho \leq \sqrt{2} \\
&= \frac{(6\pi - 5)}{\rho} - 8\pi + 6(\pi - 1)\rho - \rho^3 + 8(1 + \rho^2)\frac{\sqrt{\rho^2 - 2}}{\rho} - 24(1 + \rho^2) \\
&\quad \frac{\tan^{-1}(\sqrt{\rho^2 - 2})}{\rho} + 24 \tan^{-1}(\rho\sqrt{\rho^2 - 2}) & \sqrt{2} \leq \rho \leq \sqrt{3}
\end{aligned}$$

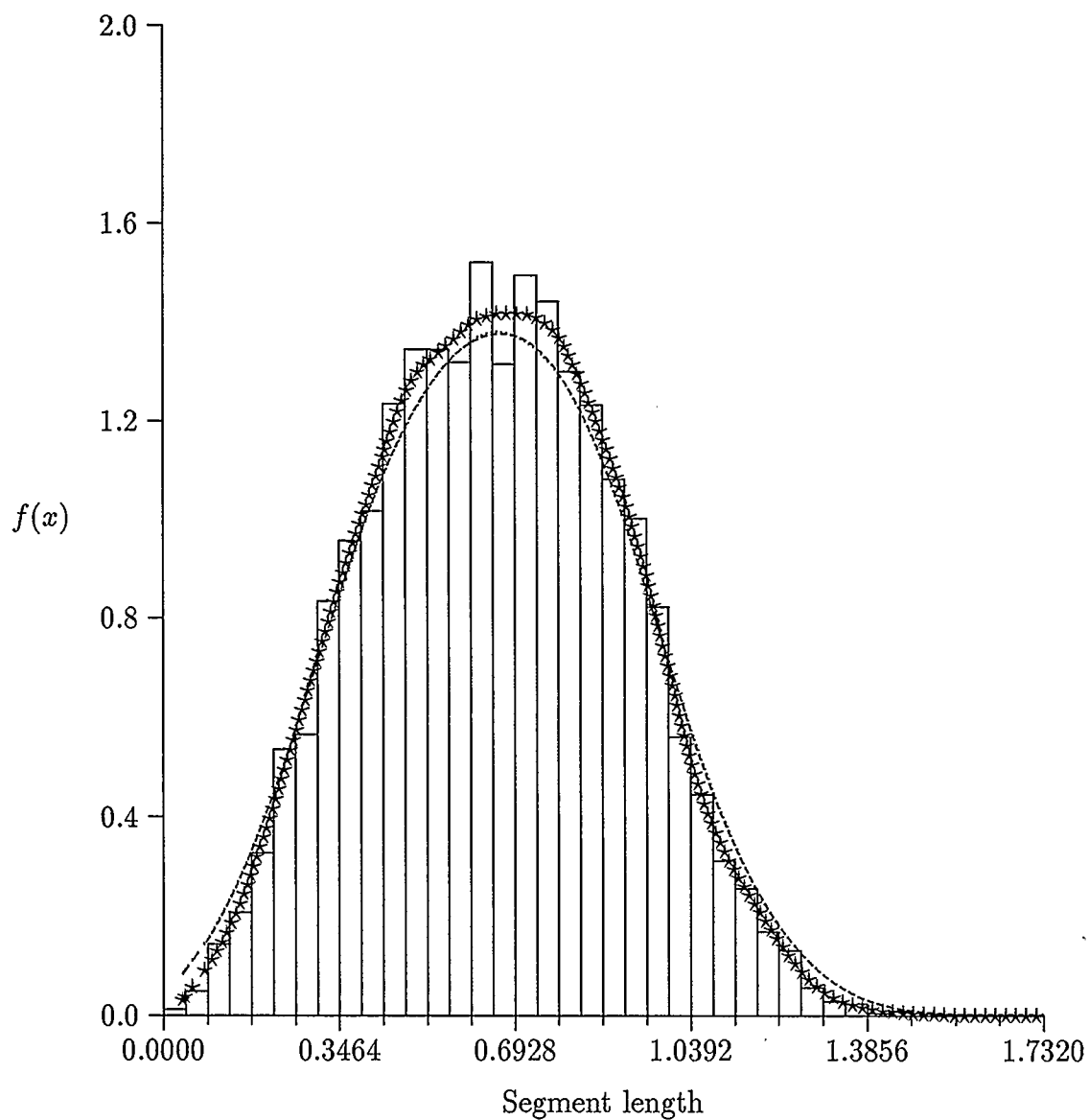
where $\rho = l/a$. [Analytical results for the cube can also be found in Horowitz [43], Coleman [13], [14], Ehlers and Enns [22], Gille [31] and Bendel [3].]

For α - and γ -random rays,

$$\omega(l) = \Omega(l) + \frac{a}{3} \frac{\delta\Omega(l)}{\delta a}. \quad (4.1)$$

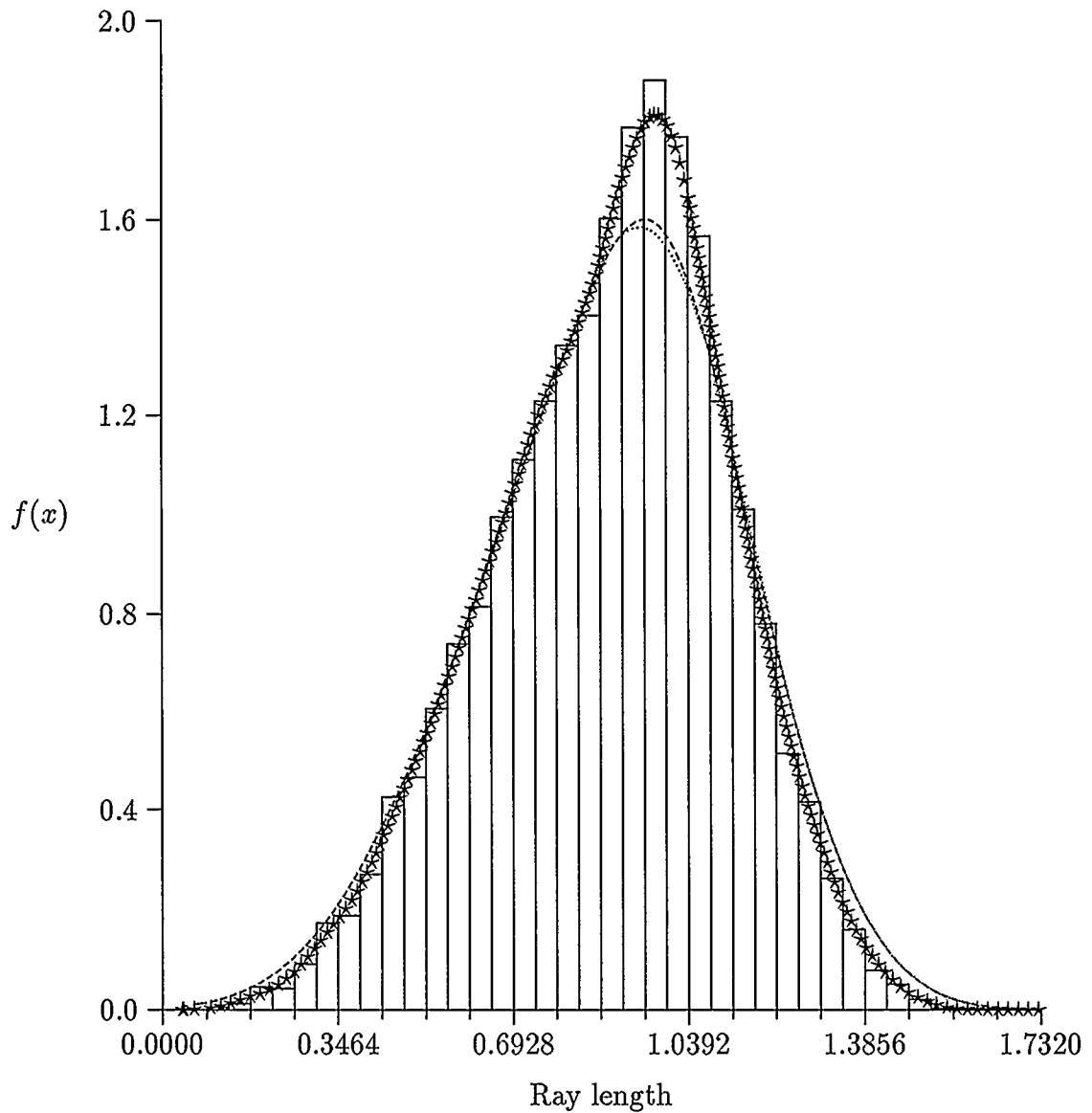
Simulation results are given in Figures 4.1 through 4.11. Figure 4.1 shows an adequate fit, no better than some of the other segment length fits for other ovoids. However, Figure 4.3 is unusually excellent. Recall that this fit is from a derivative of the smoothed version of the segment density shown in Figure 4.1. Figure 4.5 is also a good fit, although some of the poor tail properties are beginning to show to the left. Figure 4.9 is also quite good compared to some of the other derivative-based densities seen in Chapter 4.

An interesting question is then why are the fits so perfect here and not elsewhere? After much deliberation and checking of results, we could not find a clear answer. The segment density seems to be appropriate in some cases of which the cube is one. Note also that Figures 4.7, 4.11 are again poor fits, but still closer than for most other three-dimensional ovoids.



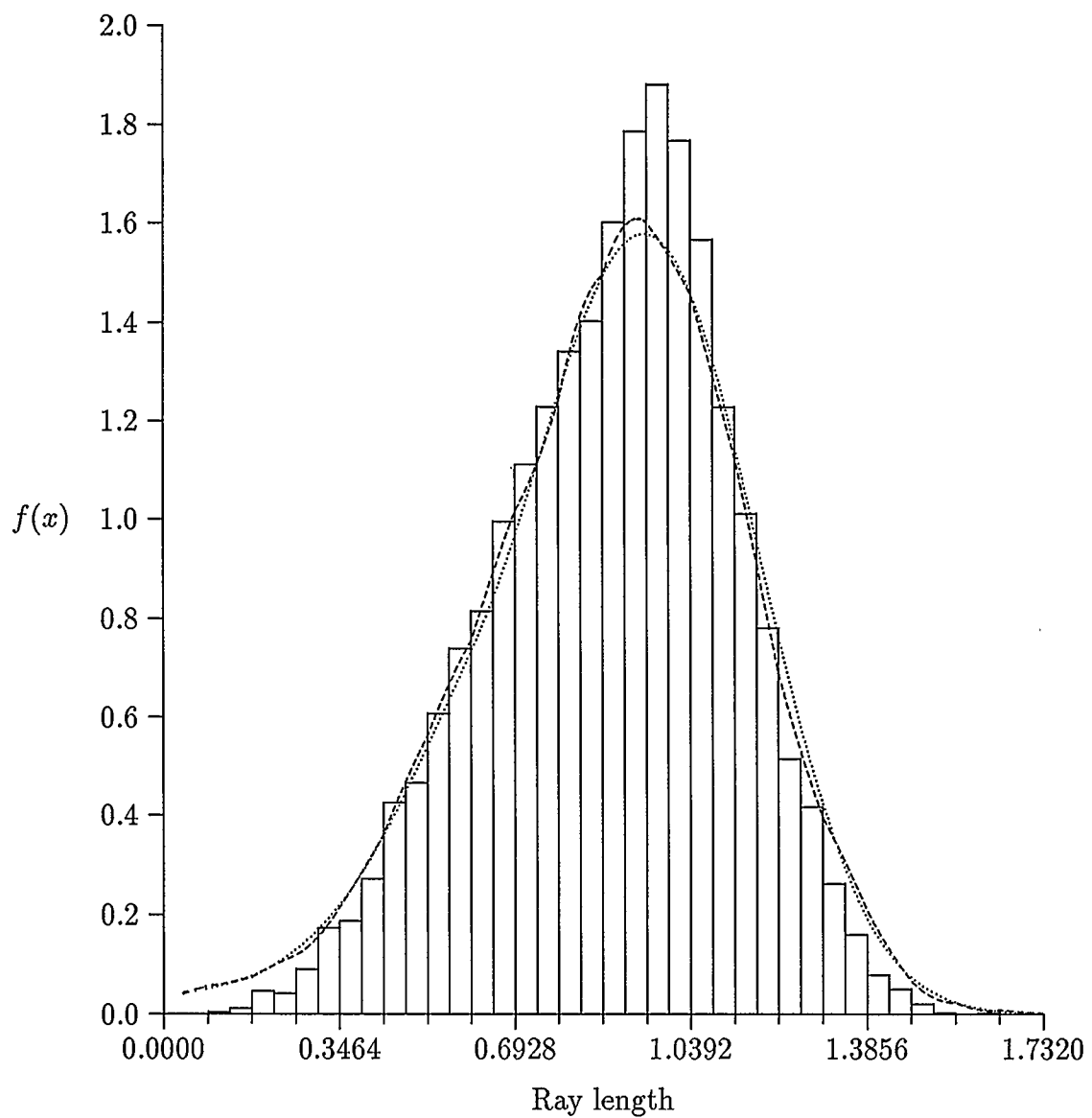
	Average	Variance		Symbol
Simulated	0.656182	0.061652	Epanechnikov	· ·
			Biweight	*
		$h = 0.1$	Gaussian	- - - -

Figure 4.1: $f_{T,\lambda}(l)$ for the cube — several kernel fits



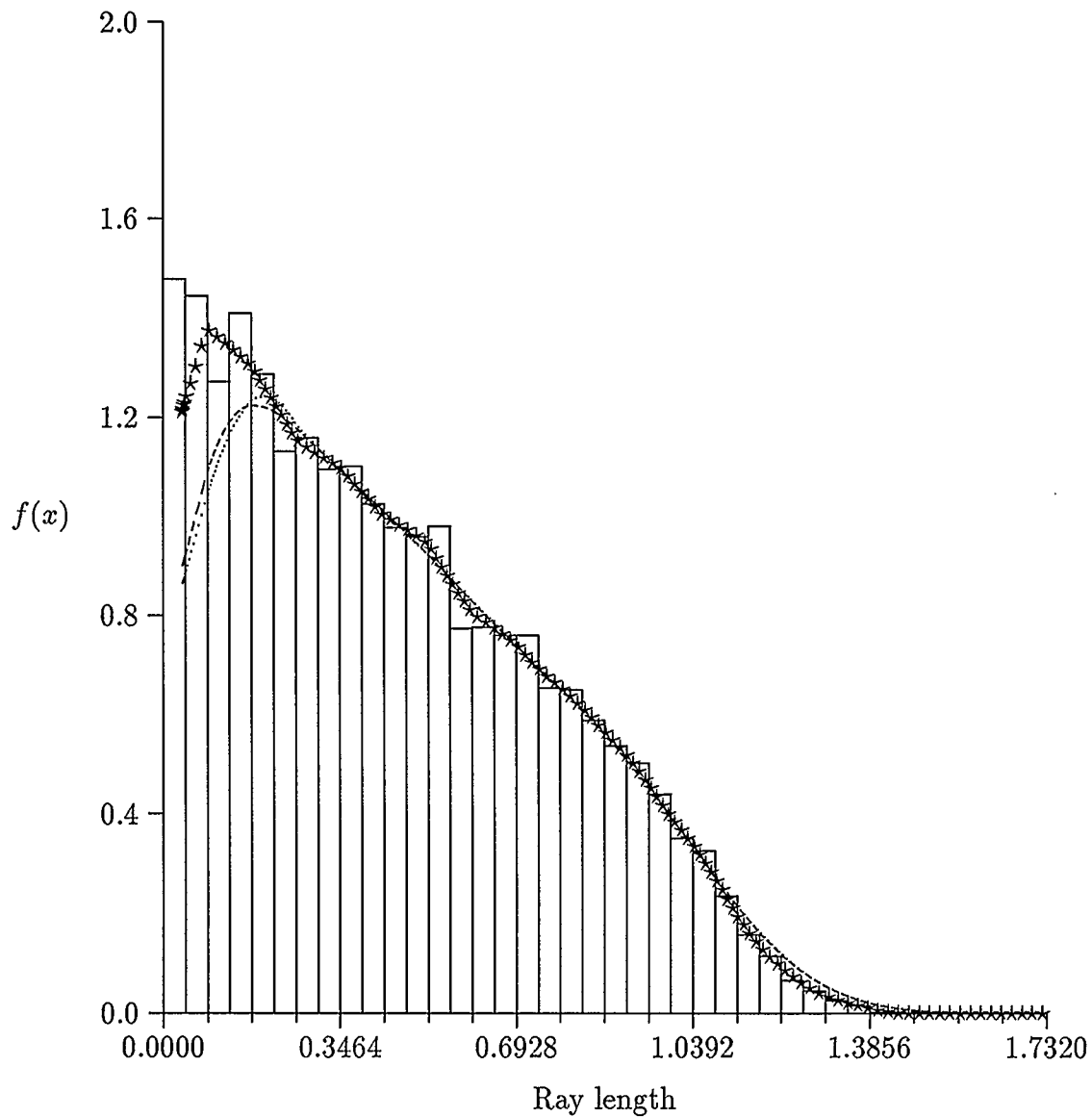
	Average	Variance		Symbol
Simulated	0.883980	0.054244	Epanechnikov	· ·
			Biweight	*
		$h = 0.1$	Gaussian	- - - -

Figure 4.2: $f_{R,\lambda}(l)$ for the cube — several kernel fits



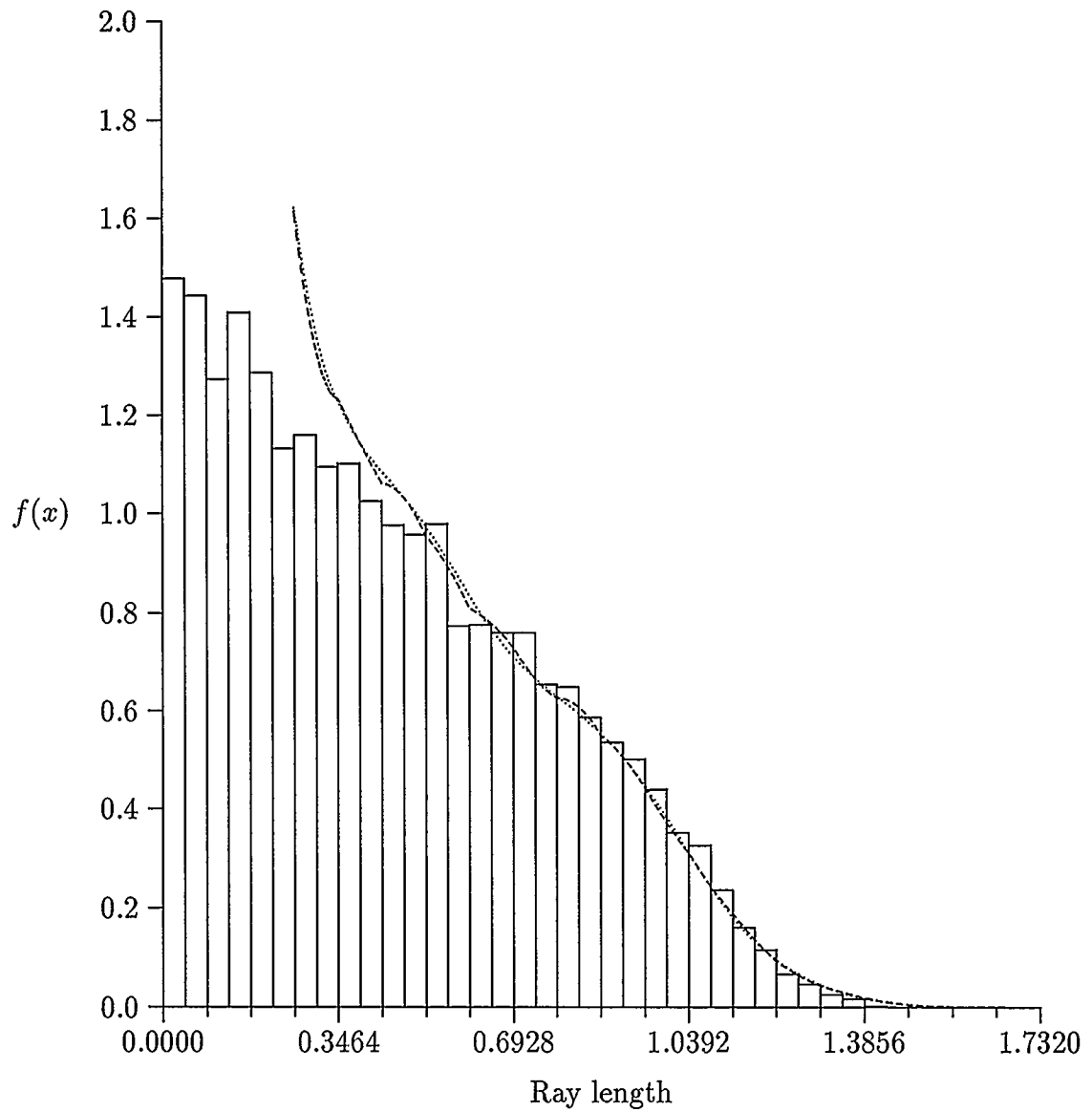
	Symbol
From $f_{T,\lambda}$ — Gaussian	-----
From $f_{T,\lambda}$ — Epanechnikov

Figure 4.3: $f_{R,\lambda}$ for the cube — estimates via the $f_{T,\lambda}$ method



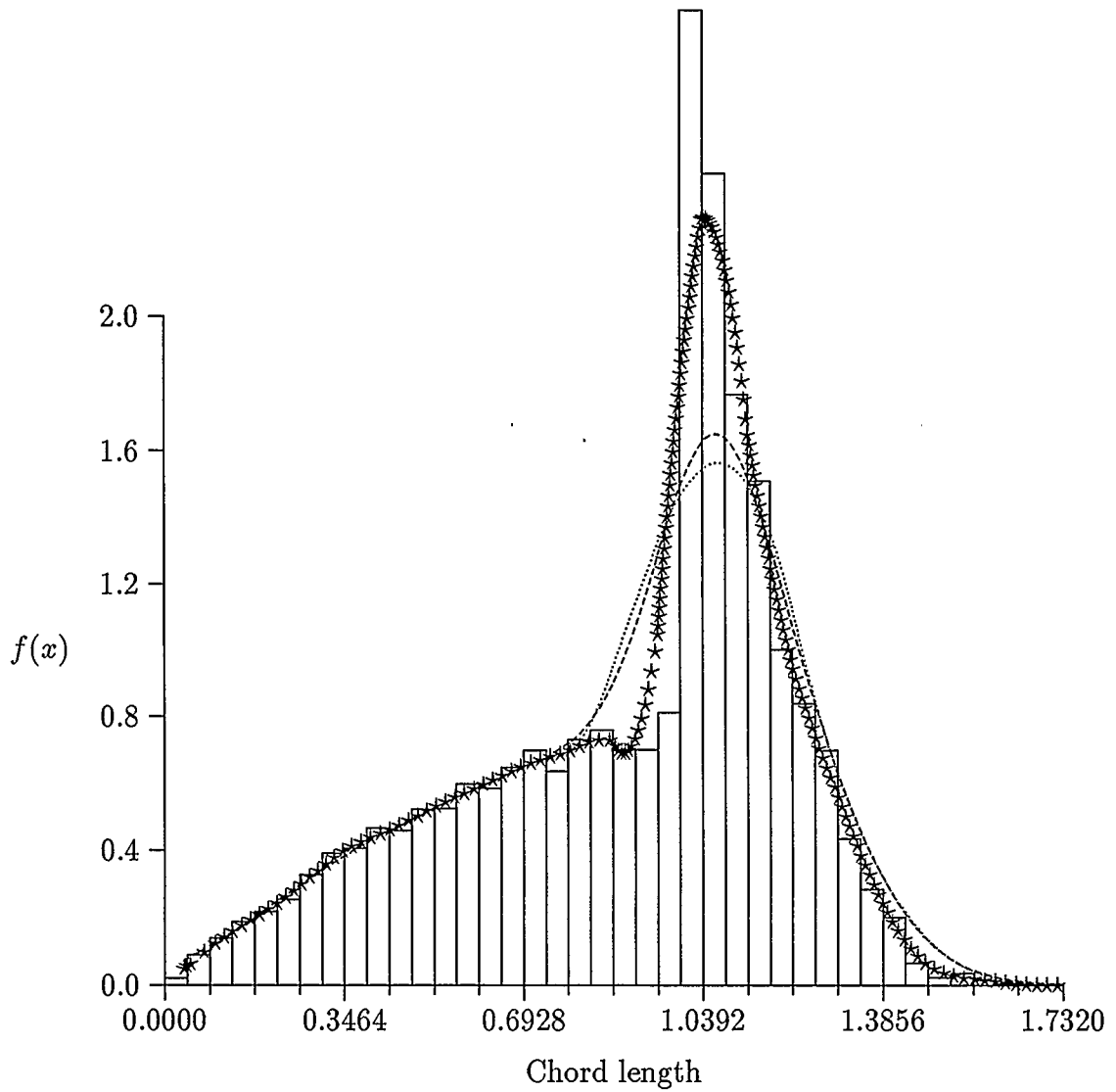
	Average	Variance		Symbol
Simulated	0.446373	0.097440	Epanechnikov	· ·
			Biweight	*
		$h = 0.1$	Gaussian	- - - -

Figure 4.4: $f_{R,\nu}(l)$ for the cube — several kernel fits



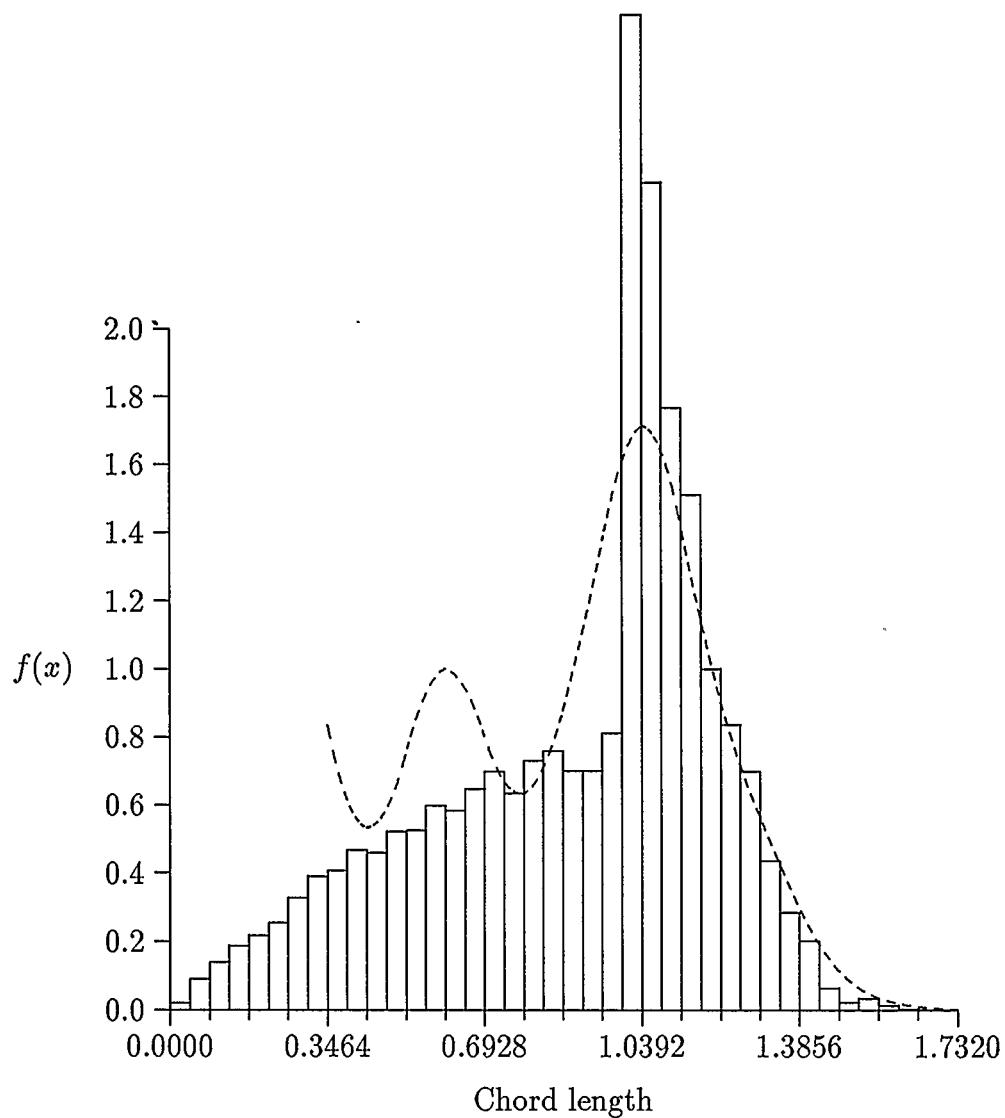
	Symbol
From $f_{T,\lambda}$ — Gaussian	-----
From $f_{T,\lambda}$ — Epanechnikov

Figure 4.5: $f_{R,\nu}$ for the Cube — estimates via $f_{T,\lambda}$ method



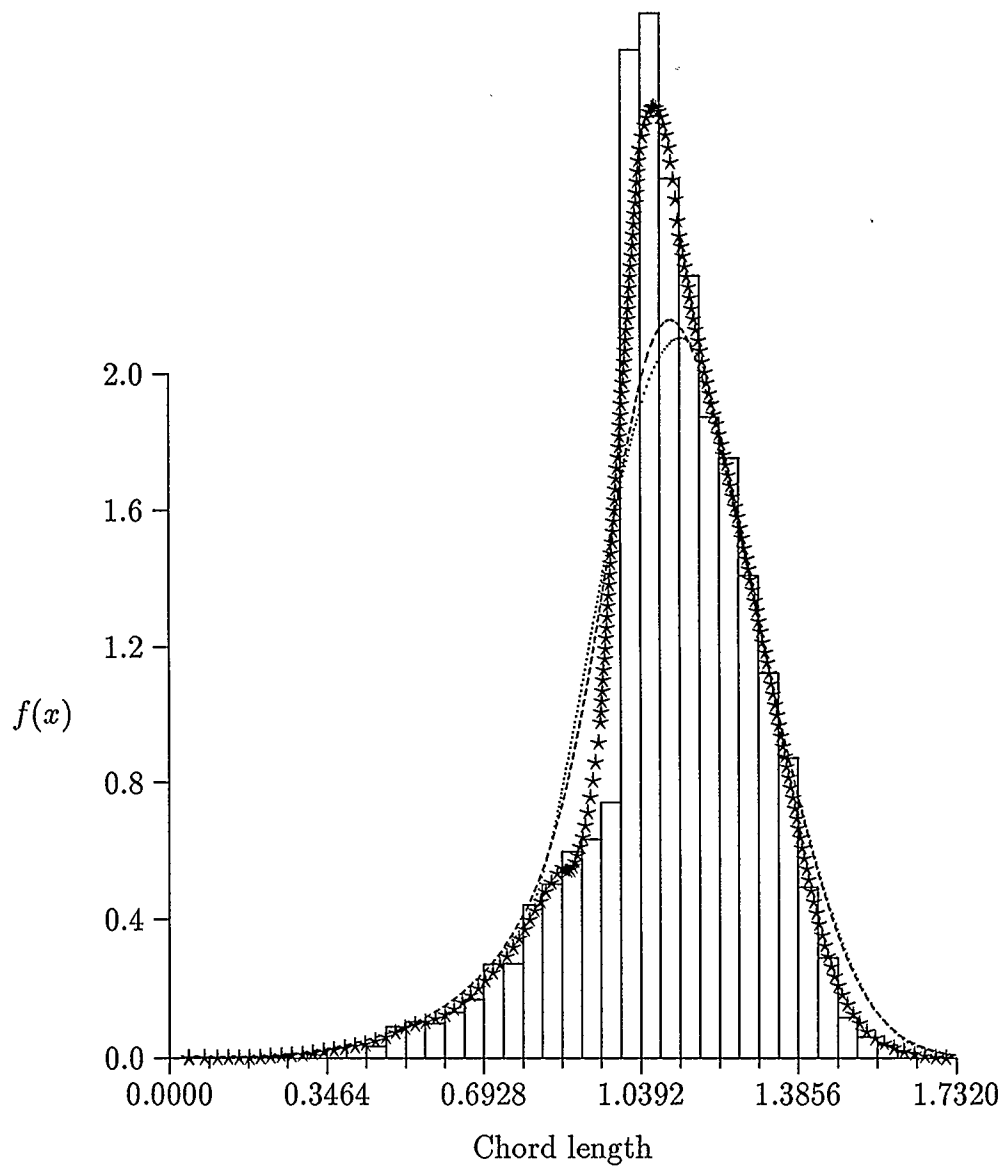
	Average	Variance		Symbol
Simulated	0.895993	0.094561	Epanechnikov	· ·
			Biweight	*
		$h = 0.1$	Gaussian	- - - -

Figure 4.6: $f_{L,\nu}(l)$ for the cube — several kernel fits



Symbol	
From $f_{T,\lambda}$	-----

Figure 4.7: $f_{L,\nu}$ for the Cube — estimates via $f_{T,\lambda}$ method



	Average	Variance		Symbol
Simulated	1.102829	0.033582	Epanechnikov	· ·
			Biweight	*
		$h = 0.1$	Gaussian	- - - -

Figure 4.8: $f_{L,\lambda}(l)$ for the cube — several kernel fits

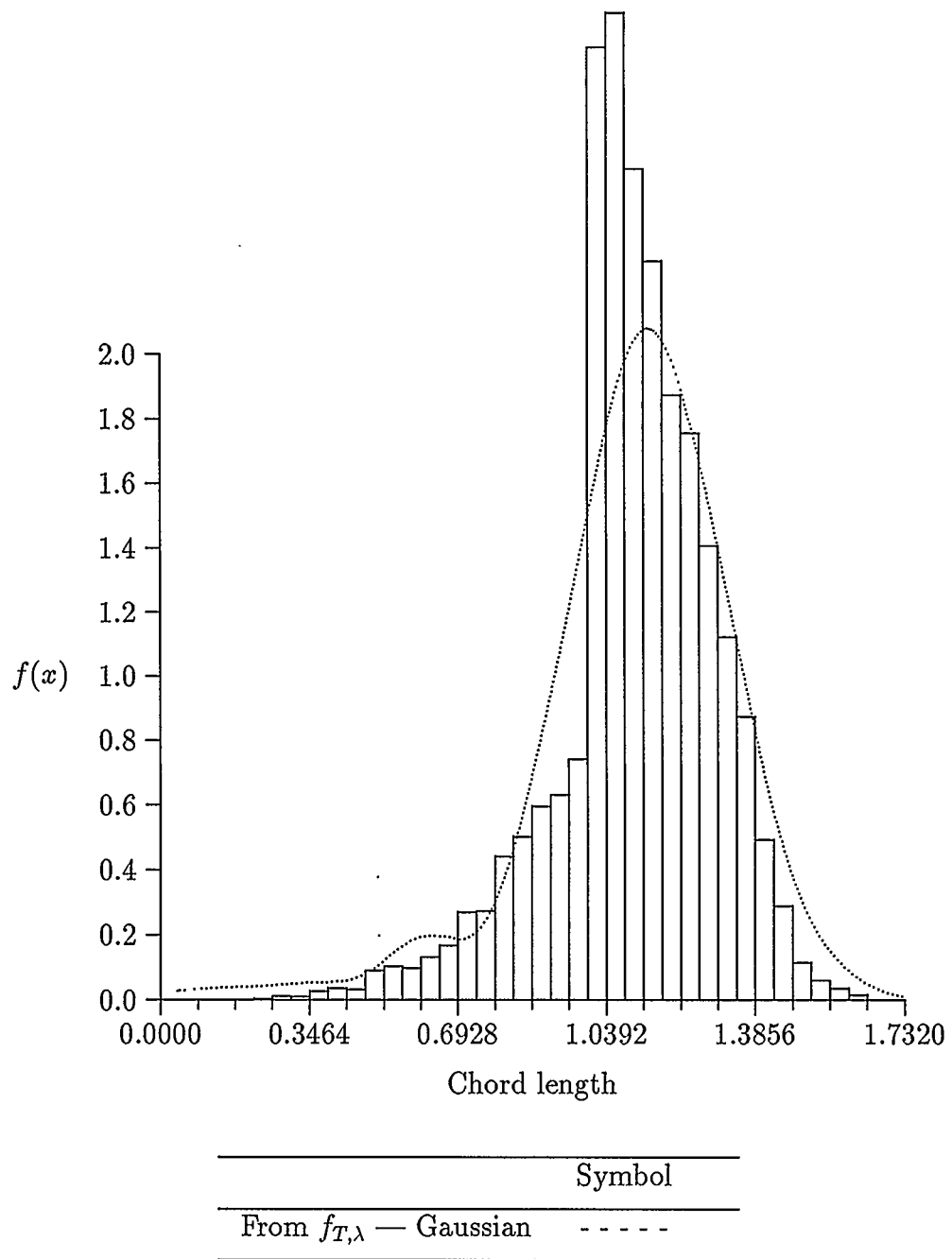
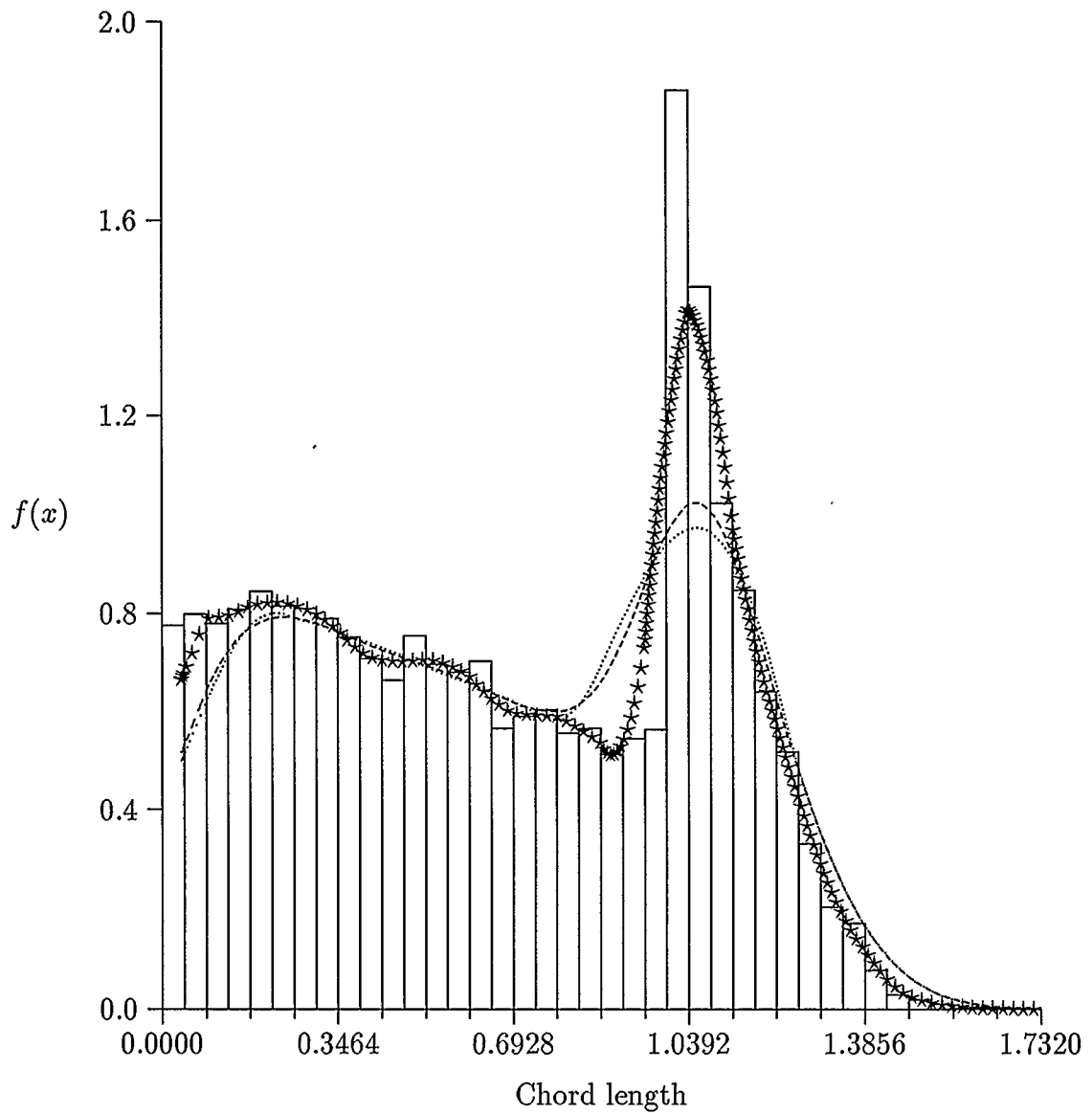
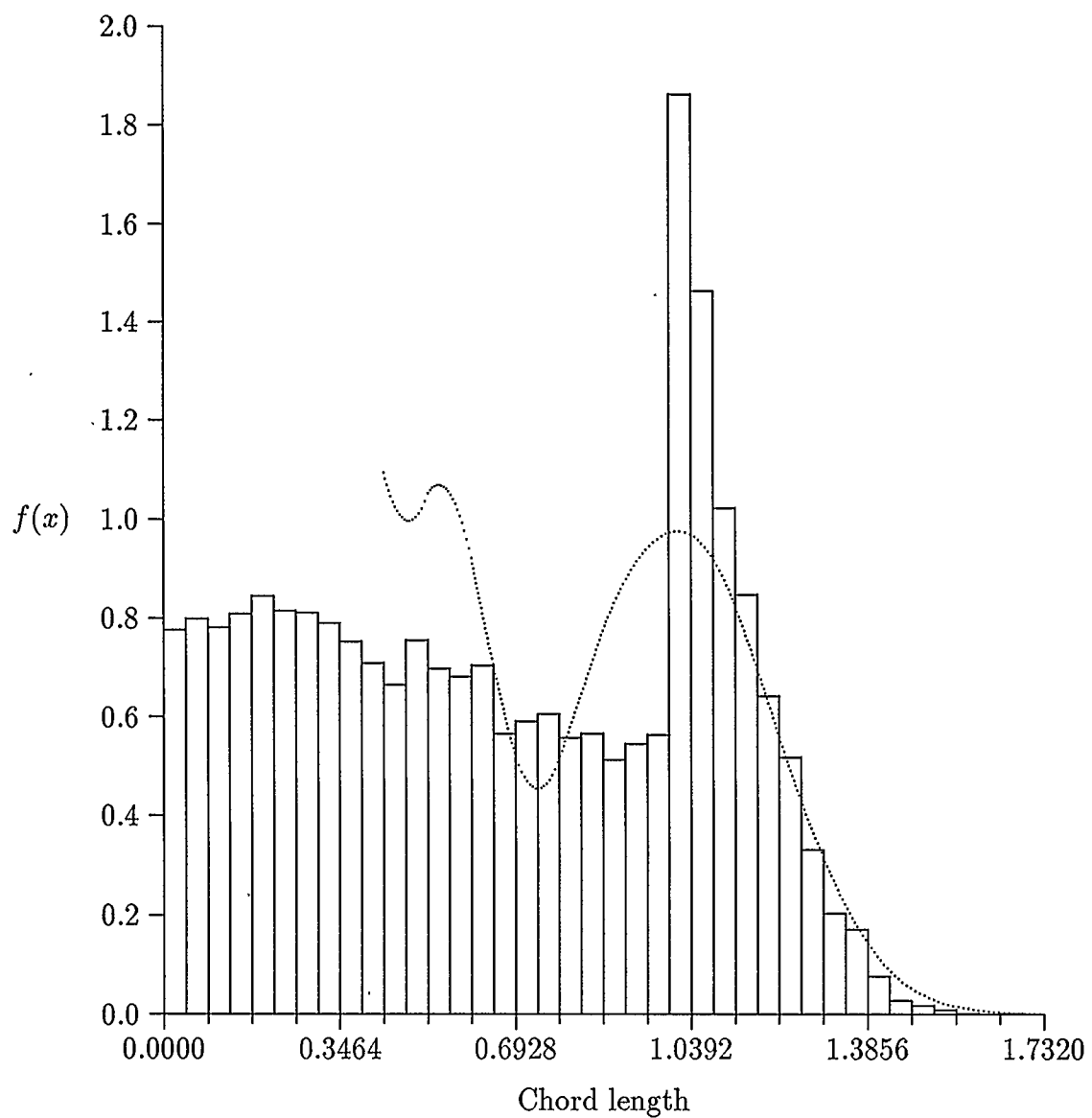


Figure 4.9: $f_{L,\lambda}$ for the cube — estimates via $f_{T,\lambda}$ method



	Average	Variance		Symbol
Simulated	0.664864	0.152314	Epanechnikov	· ·
			Biweight	*
		$h = 0.1$	Gaussian	- - - -

Figure 4.10: $f_{L,\mu}(l)$ for the cube — several kernel fits



Symbol	
From $f_{T,\lambda}$ — Gaussian	- - - - -

Figure 4.11: $f_{L,\mu}$ for the cube — estimates via $f_{T,\lambda}$ method

4.2 Results For The Ellipsoid

No distributions involving surface randomness for the ellipsoid were simulated. For a spheroid (two of a, b, c equal) the problem is simple. Choose a random point on one of the x, y , or z axes. Cut the body perpendicular to that axis and then choose a point on the resulting ellipse (the cut will be elliptical, so simply choose on the surface of this cut) as outlined in Chapter 4. For the general ellipsoid the problem is more difficult because the integral giving partial ellipsoid surface area cannot be inverted to obtain a random surface point.

4.2.1 The Prolate Spheroid

For the three-dimensional prolate spheroid with semi-axes a, b and c with $a > b = c$, the ν -random density of L is (see Enns and Ehlers [23])

$$\begin{aligned}
 f_{L;\nu}(l) &= \frac{3}{8} \frac{l^2}{b^3} g \left(1 - \frac{b^2}{a^2} \right) & 0 \leq l \leq 2b \\
 &= \frac{3}{8} \frac{l^2}{b^3} \left[g \left(1 - \frac{b^2}{a^2} \right) - \left(\frac{1 - 4b^2 l^{-2}}{1 - b^2 a^{-2}} \right)^{\frac{1}{2}} g \left(1 - \frac{4b^2}{l^2} \right) \right] & 2b < l \leq 2a \\
 &= 0 & \text{otherwise}
 \end{aligned}$$

where

$$g(x) = \frac{1}{4}(1-x)^{3/2} + \frac{3}{8}(1-x)^{1/2} + \frac{3}{8} \left(\frac{\sin^{-1} \sqrt{x}}{\sqrt{x}} \right).$$

Note that Table 2.6 provides a useful way to derive the distributions $f_{L;\lambda}$ and $f_{L;\mu}$ from $f_{L;\nu}$.

The k th moment of chord length is

$$E_\nu(L^k) = \frac{3}{(k+3)} \cdot \frac{(2b)^k}{\gamma} \int_0^{\sin^{-1} \gamma} (\sec \theta)^{k-1} d\theta, \quad (4.2)$$

where $\gamma = \sqrt{1 - b^2/a^2}$.

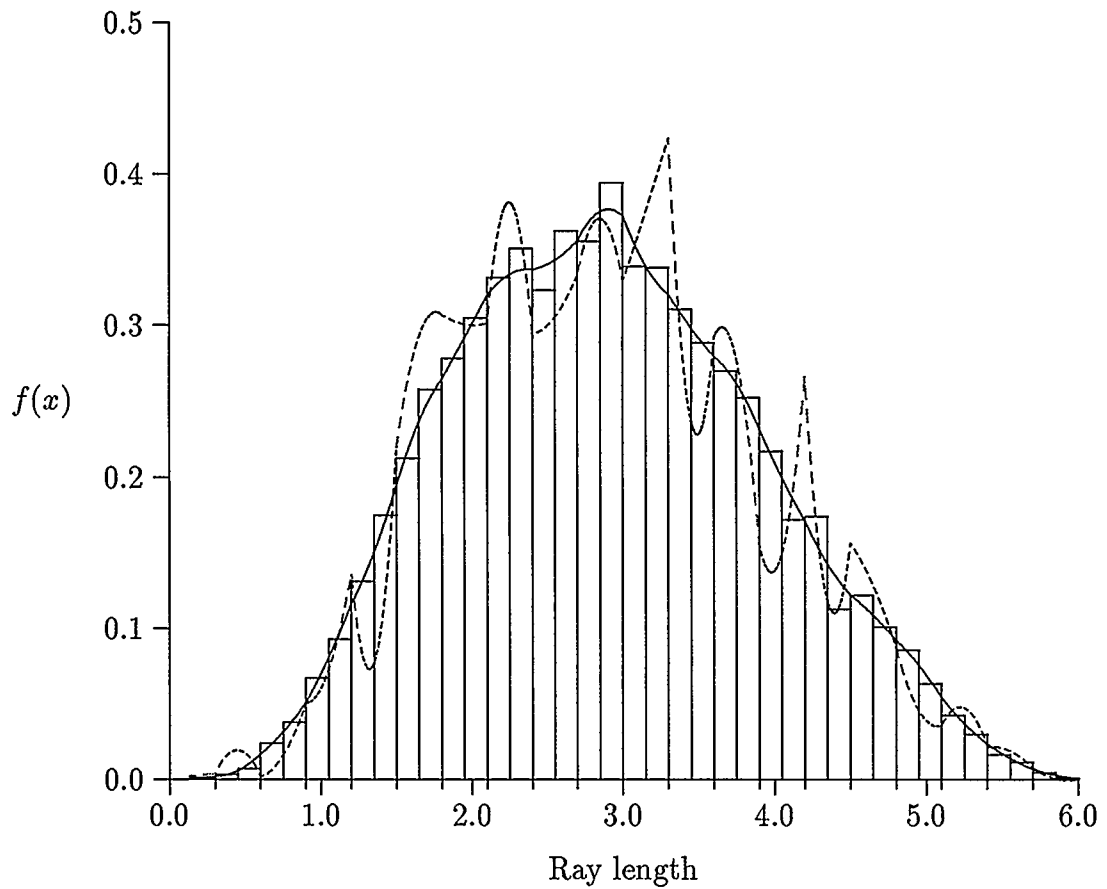
Similarly, for λ -random rays, the moments are

$$E_\lambda(R^k) = \frac{32^{k+3}b^{k+1}}{(k+4)(k+6)\gamma a} \int_0^{\sin^{-1}\gamma} (\sec\theta)^{k+2} d\theta. \quad (4.3)$$

Moments of R_ν follow from Table 2.6.

Previous work for the ellipsoid includes Gundersen and Jensen [34], who derive a rather complicated formula for $f_{L;\nu}$ for the general three-dimensional ellipsoid. DeHoff and Bousquet [18] consider linear intercepts through triaxial ellipsoidal particles. Kellerer [49] works with spheroids.

All simulations were performed for $a = 3$ and b and c varying from 1 to 3 (both triaxial and prolate spheroids were considered here). The segment density $f_{T;\lambda}$ was not an efficient estimator of the densities to which it is related. A clear example of this is Figure 4.12, which gives the $f_{R;\lambda}$ distribution. The huge variations in the curve resulting from the derivative of the segment density demonstrates the inadequacy of the segment density as estimator. Figure 4.13 shows several μ -random distributions for various choices of a , b and c .



	Average	Variance		Symbol
Simulated	2.895473	1.034804	Kernel Est.	—
			From $f_{T;\lambda}$	- - - -

Figure 4.12: $f_{R,\lambda}(l)$ for the ellipsoid ($a = 3, b = 2, c = 1$) — kernel fit versus estimate via $f_{T;\lambda}$ method

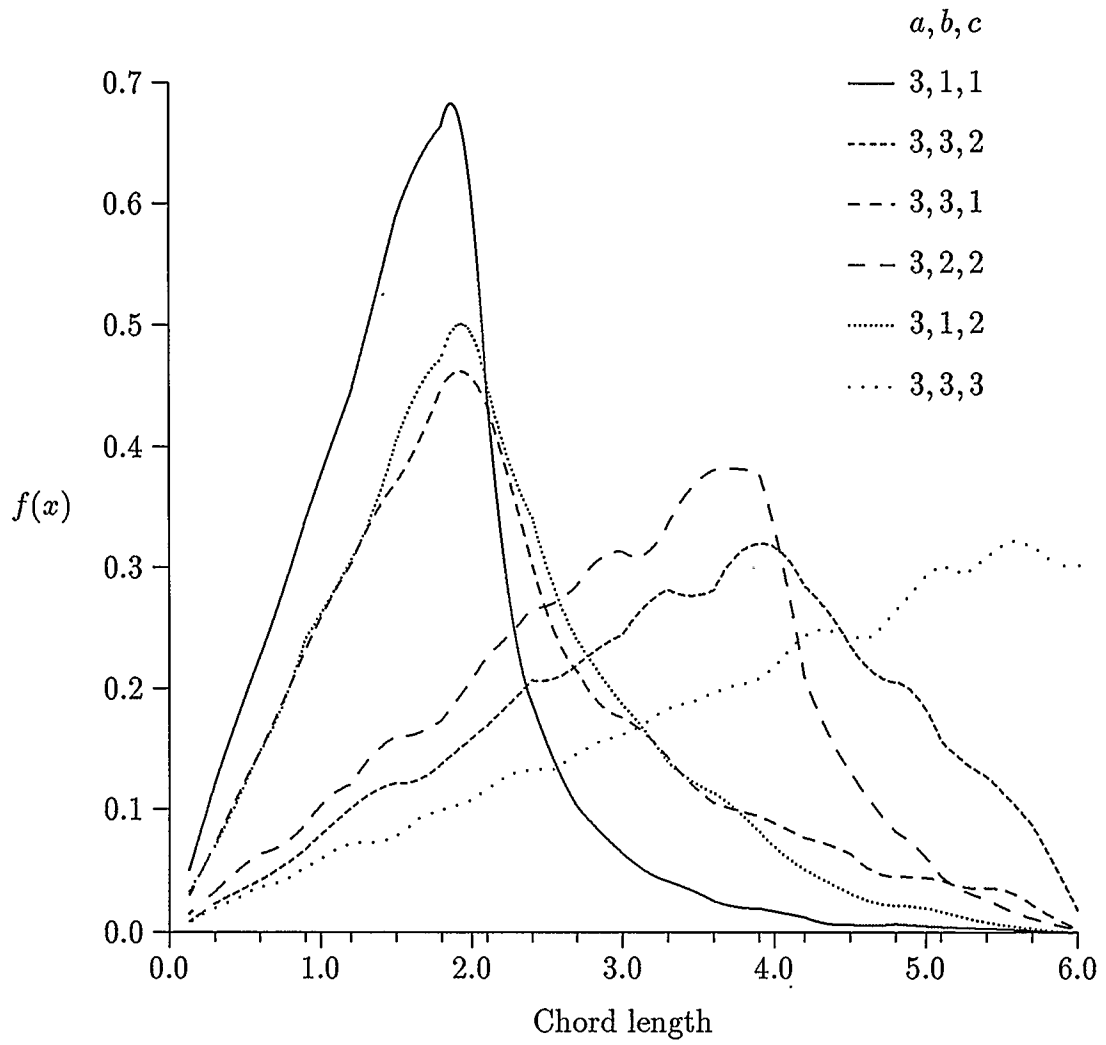


Figure 4.13: $f_{L,\mu}(l)$ for some ellipsoids

4.3 Results For The Sphere

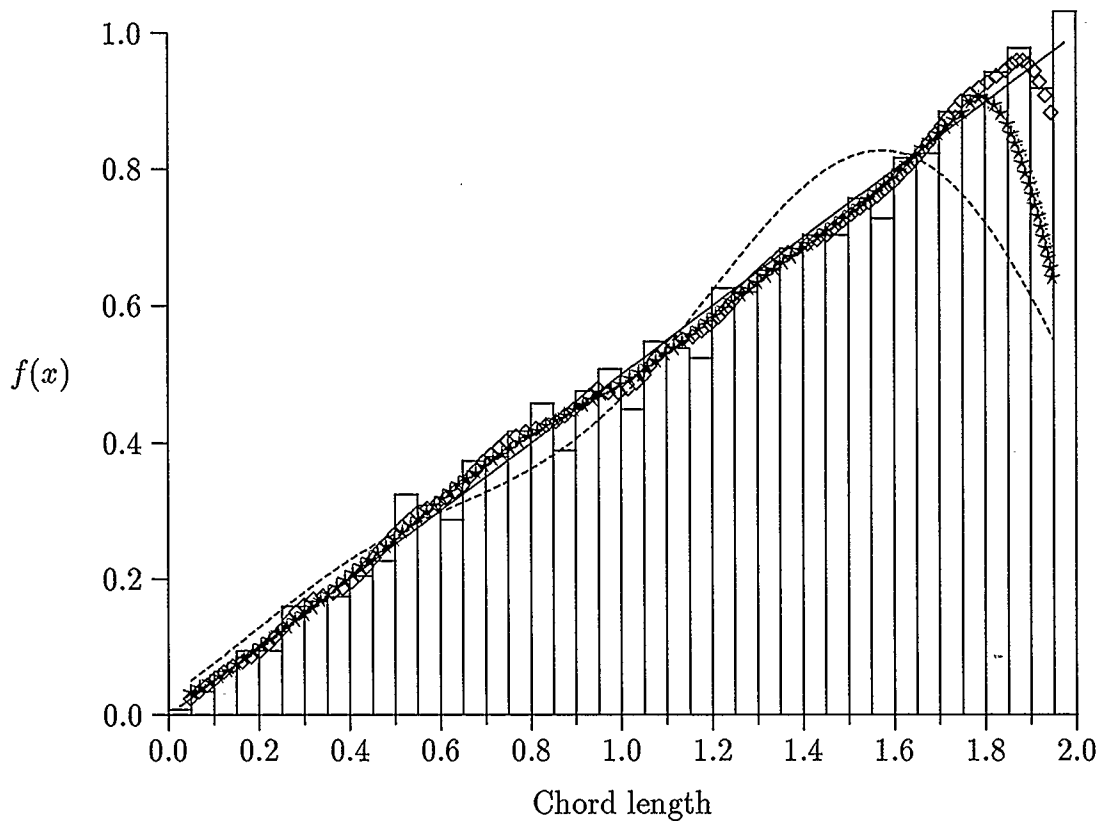
Although theory was already presented in Chapter 4, a note should be made here about surface randomness for the sphere. Marsaglia ([66]) considered this problem. He gave several methods, the most efficient including

Method	Description
1	Choose V_1, V_2 and V_3 independently and uniformly in the interval $(-1, 1)$ until $S = V_1^2 + V_2^2 + V_3^2 < 1$. The point is then given by $(V_1/\sqrt{S}, V_2/\sqrt{S}, V_3/\sqrt{S})$. This method chooses a point in the cube which is inside the sphere, and then projects the point outward to the surface of the sphere.
2	Choose V_1 and V_2 in the interval $(-1, 1)$ until $S = V_1^2 + V_2^2 < 1$. Then the point on the surface is given by $(2V_1(1 - S)^{-1/2}, 2V_2(1 - S)^{-1/2}, 1 - 2S)$.

For the sphere, all distributions given in Table 2.6 were simulated directly, and derivatives of the segment density $f_{T,\lambda}$ were used to estimate densities depending on $\Omega(l)$. All distributions for the sphere are included here. The actual sphere distributions are all fairly “regular” in the sense that Equation 3.4 reduces to a simple polynomial when $n = 3$. The sphere is therefore the perfect opportunity to weed out those kernel or series estimators that fail to even fit a simple polynomial. Parameters used include $\kappa = 15$, the cutoff for the Hermite series estimator, and $h = 0.1$, the window width for the kernel smoothers.

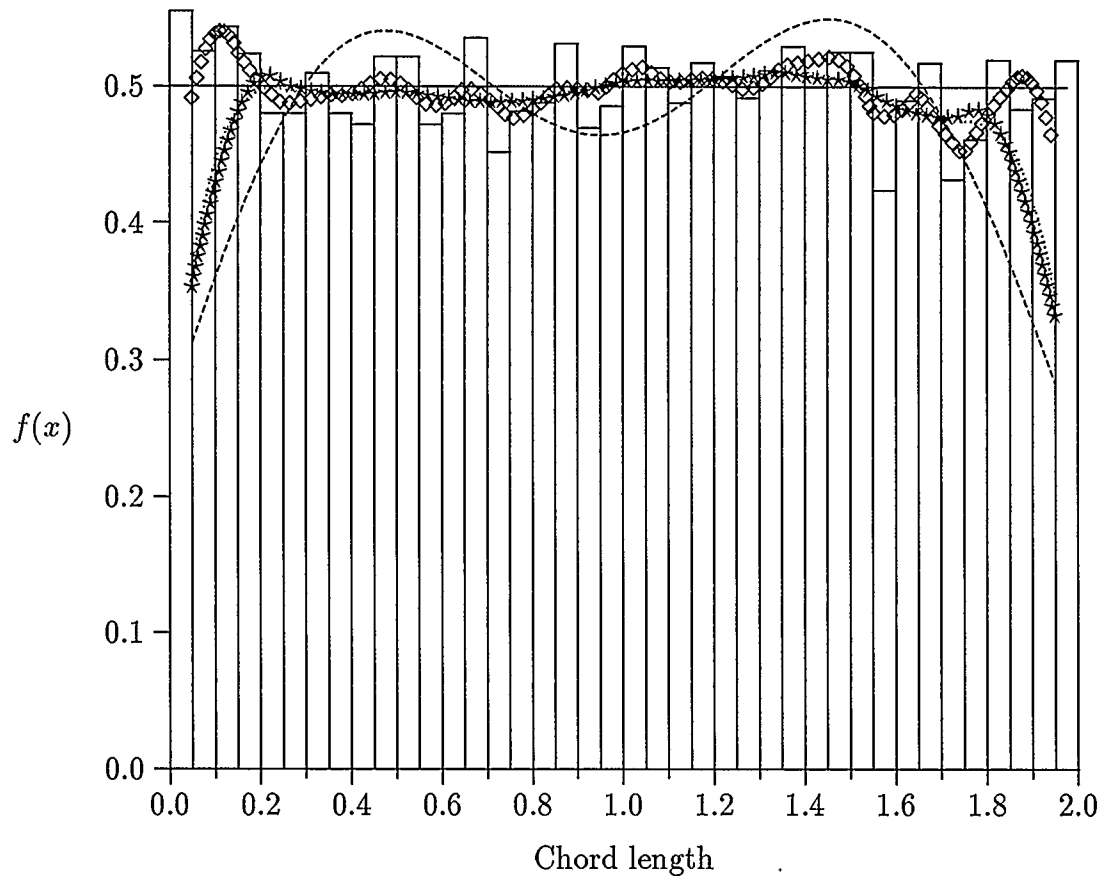
Figures 4.14 through 4.22 give these distributions. Note that the Hermite series estimator in each case smooths too much, and that the tails, particularly for the chord distributions, seem to taper off prematurely. Fits for the ray and segment distributions seem very good.

Figures 4.24 and 4.23 show the actual distribution (solid line) versus the distribution resulting from the derivative of a smoothed estimate of $f_{T;\lambda}$. In Figure 4.23 in particular, the left tail is a very poor fit, but the curve rebounds to make a decent fit for the right tail. In Figure 4.24, the fit is generally good. Note that the accuracy of these estimates (from $f_{T;\lambda}$) depend on the initial accuracy of the smoothed estimate of $f_{T;\lambda}$, which is very good (see Figure 4.21).



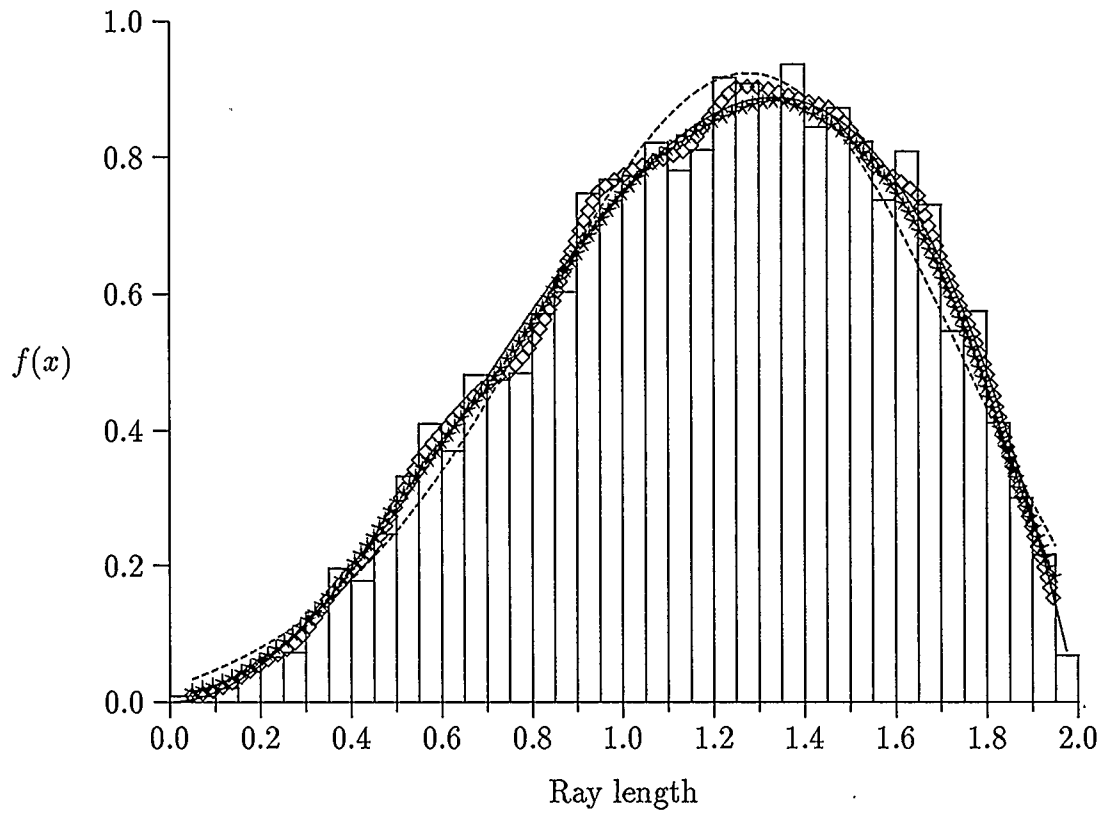
	Average	Variance		Symbol
Simulated	1.332404	0.225712	Gaussian	· ·
Analytical	1.333333	0.221841	Epanechnikov	*
			Hermite	- - - -
		$\kappa = 15$	Actual	—
		$h = 0.1$	Biweight	◇

Figure 4.14: $f_{L,\mu}(l)$ for the sphere — several kernel fits



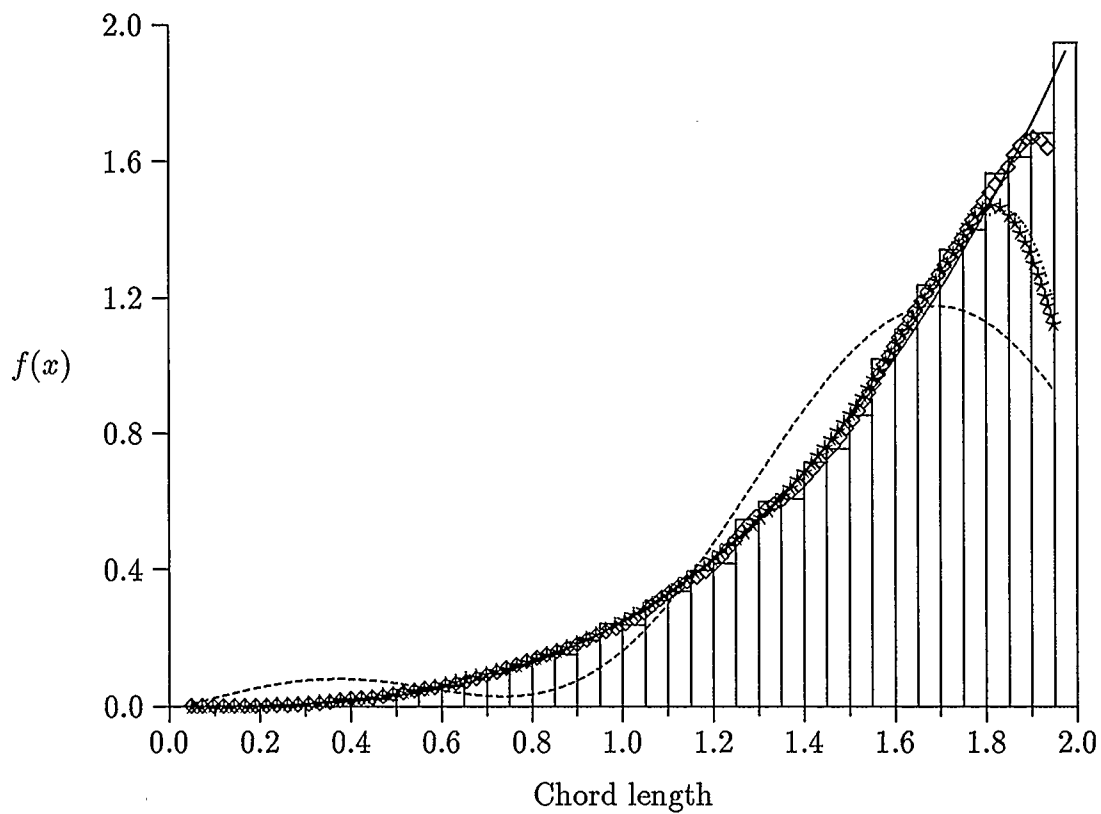
	Average	Variance		Symbol
Simulated	0.993371	0.335788	Gaussian	· ·
Analytical	1.000000	0.333333	Epanechnikov	*
			Hermite	- - - -
		$\kappa = 15$	Actual	—
		$h = 0.1$	Biweight	◇

Figure 4.15: $f_{L,\gamma}(l)$ for the sphere — several kernel fits



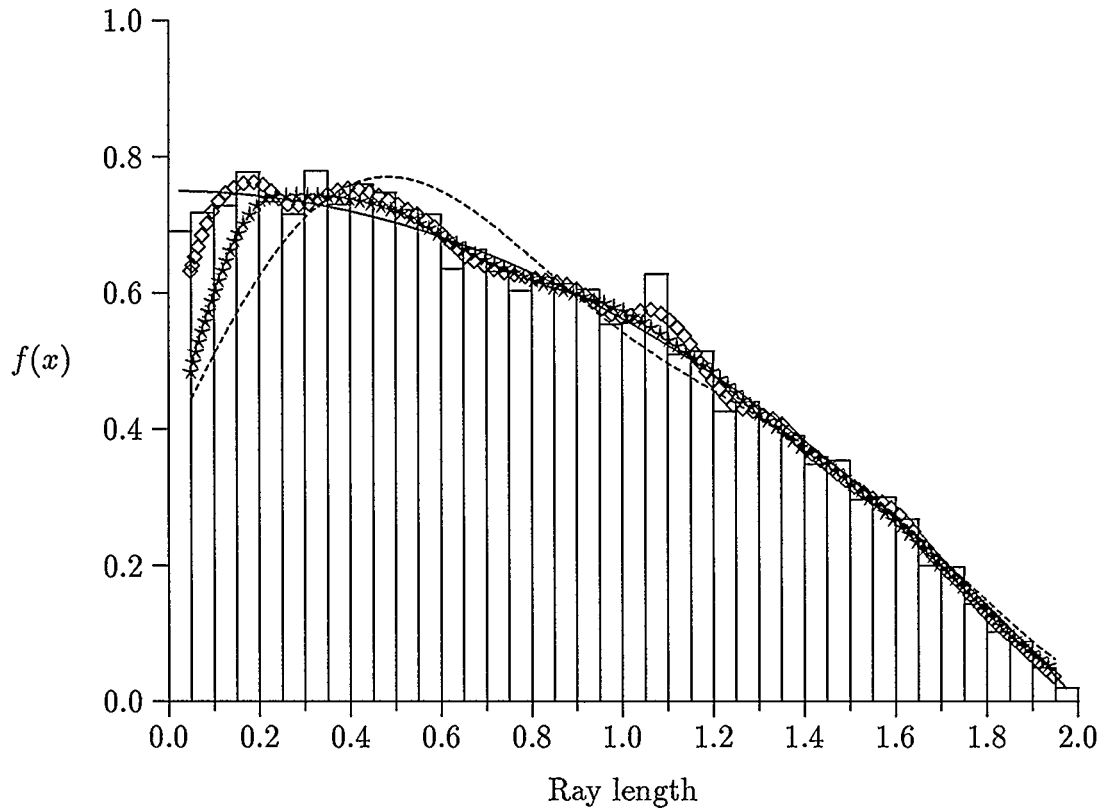
	Average	Variance		Symbol
Simulated	1.201504	0.158712	Gaussian	· ·
Analytical	1.200000	0.160000	Epanechnikov	*
			Hermite	- - - -
		$\kappa = 15$	Actual	—
		$h = 0.1$	Biweight	◇

Figure 4.16: $f_{R,\alpha}(l)$ for the sphere — several kernel fits



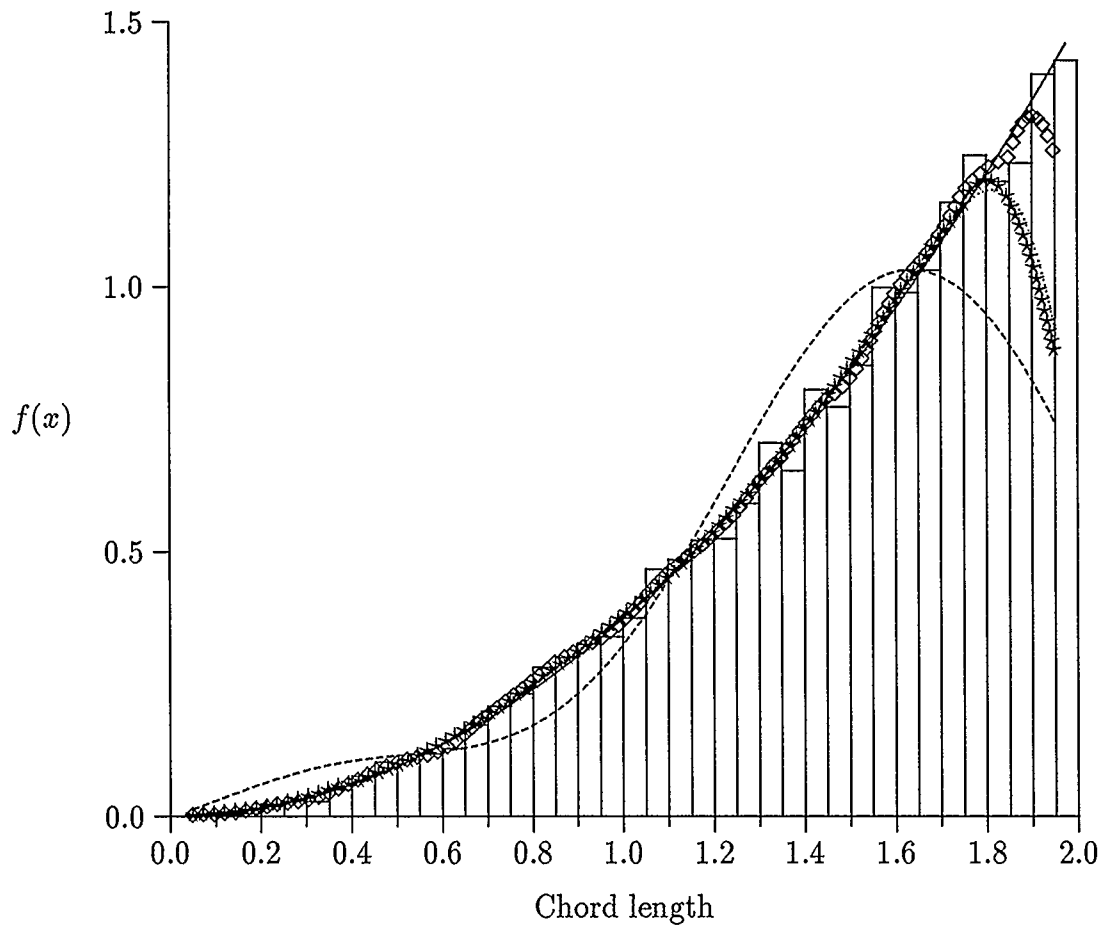
	Average	Variance		Symbol
Simulated	1.600893	0.106628	Gaussian	· ·
Analytical	1.600000	0.106667	Epanechnikov	*
			Hermite	- - - -
		$\kappa = 15$	Actual	—
		$h = 0.1$	Biweight	◇

Figure 4.17: $f_{L,\alpha}(l)$ for the sphere — several kernel fits



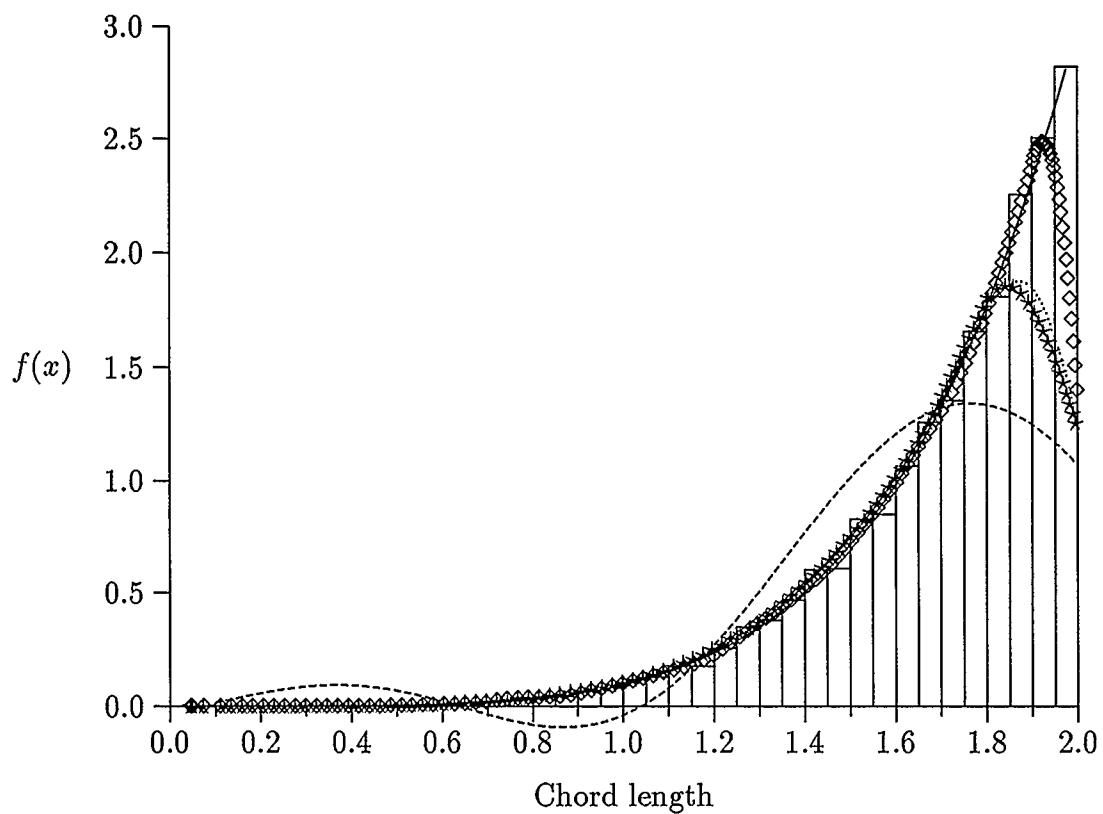
	Average	Variance		Symbol
Simulated	0.748258	0.233004	Gaussian	· ·
Analytical	0.750000	0.237500	Epanechnikov	*
			Hermite	- - - -
		$\kappa = 15$	Actual	—
		$h = 0.1$	Biweight	◇

Figure 4.18: $f_{R,\nu}(l)$ for the sphere — several kernel fits



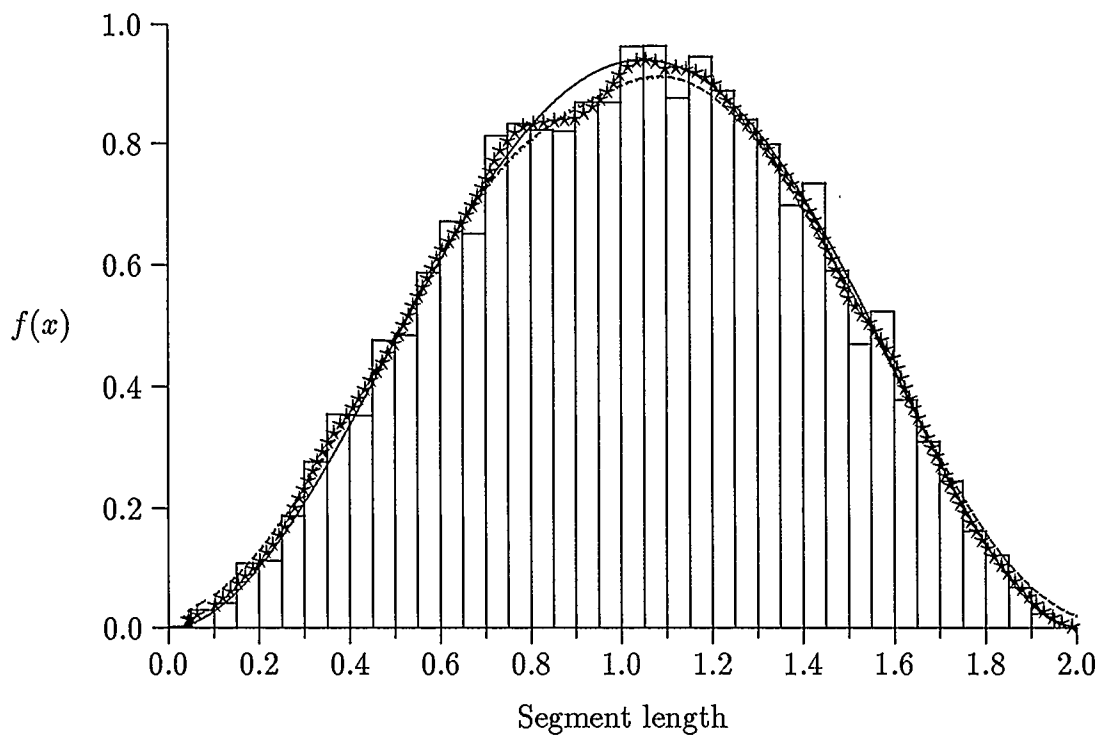
	Average	Variance		Symbol
Simulated	1.497223	0.150177	Gaussian	· ·
Analytical	1.500000	0.150000	Epanechnikov	★
			Hermite	- - - -
		$\kappa = 15$	Actual	—
		$h = 0.1$	Biweight	◇

Figure 4.19: $f_{L,\nu}(l)$ for the sphere — several kernel fits



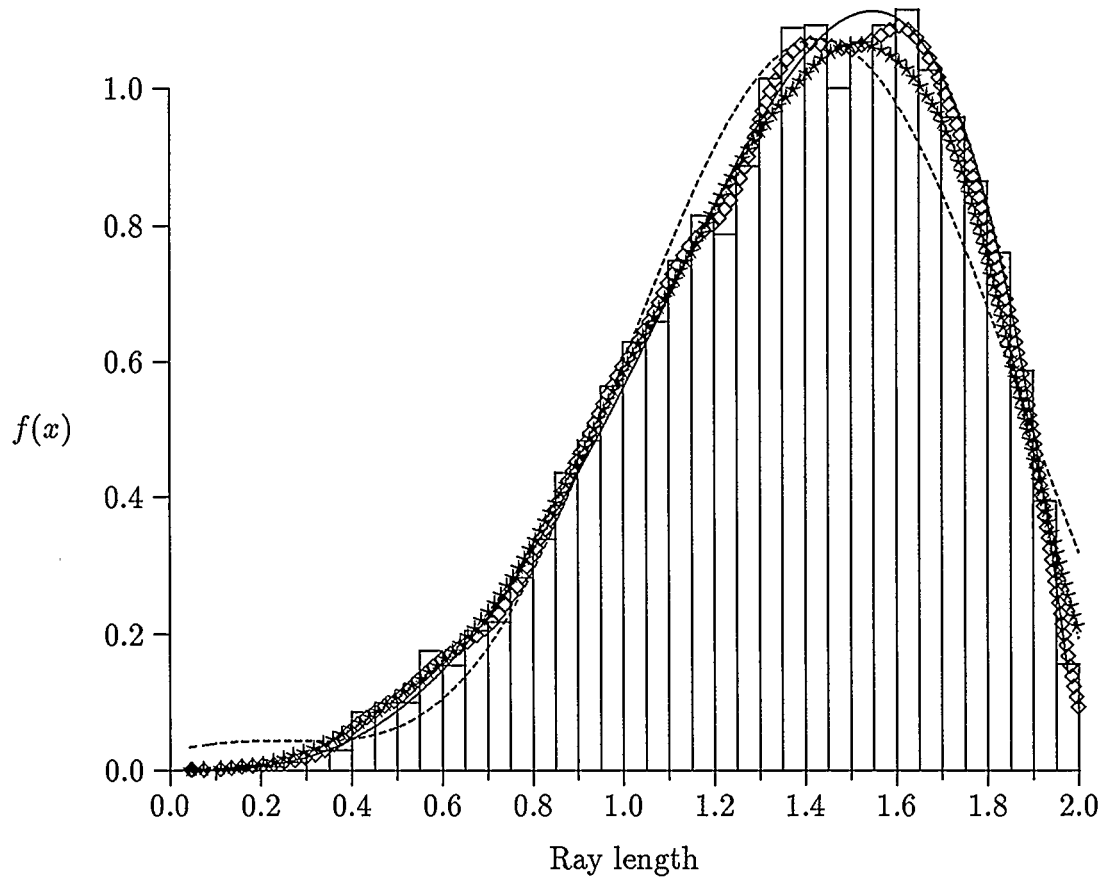
	Average	Variance		Symbol
Simulated	1.714013	0.062108	Gaussian	· ·
Analytical	1.714286	0.061009	Epanechnikov	*
			Hermite	- - - -
		$\kappa = 15$	Actual	—
		$h = 0.1$	Biweight	◇

Figure 4.20: $f_{L,\lambda}(l)$ for the sphere — several kernel fits



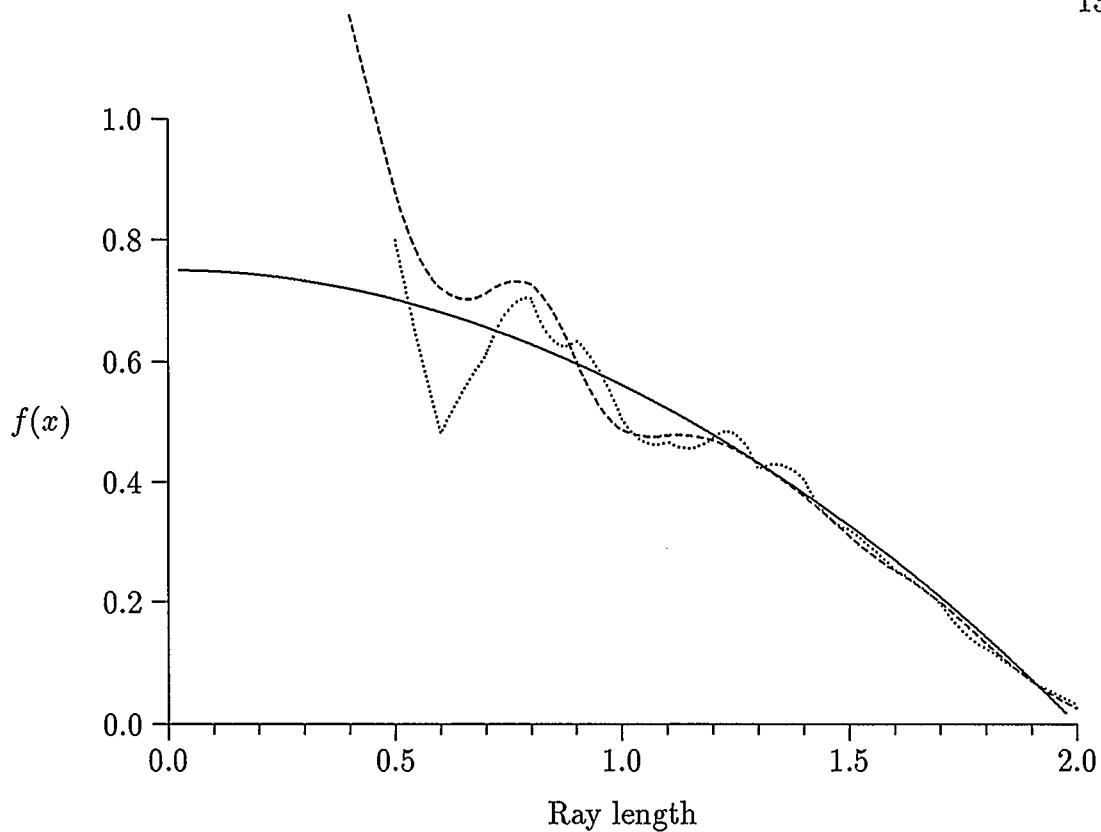
	Average	Variance		Symbol
Simulated	1.023659	0.145289	Epanechnikov	· ·
Analytical	1.028571	0.142041	Biweight	*
		$h = 0.1$	Gaussian	- - - -
		$\kappa = 15$	Actual	—

Figure 4.21: $f_{T,\lambda}(l)$ for the sphere — several kernel fits



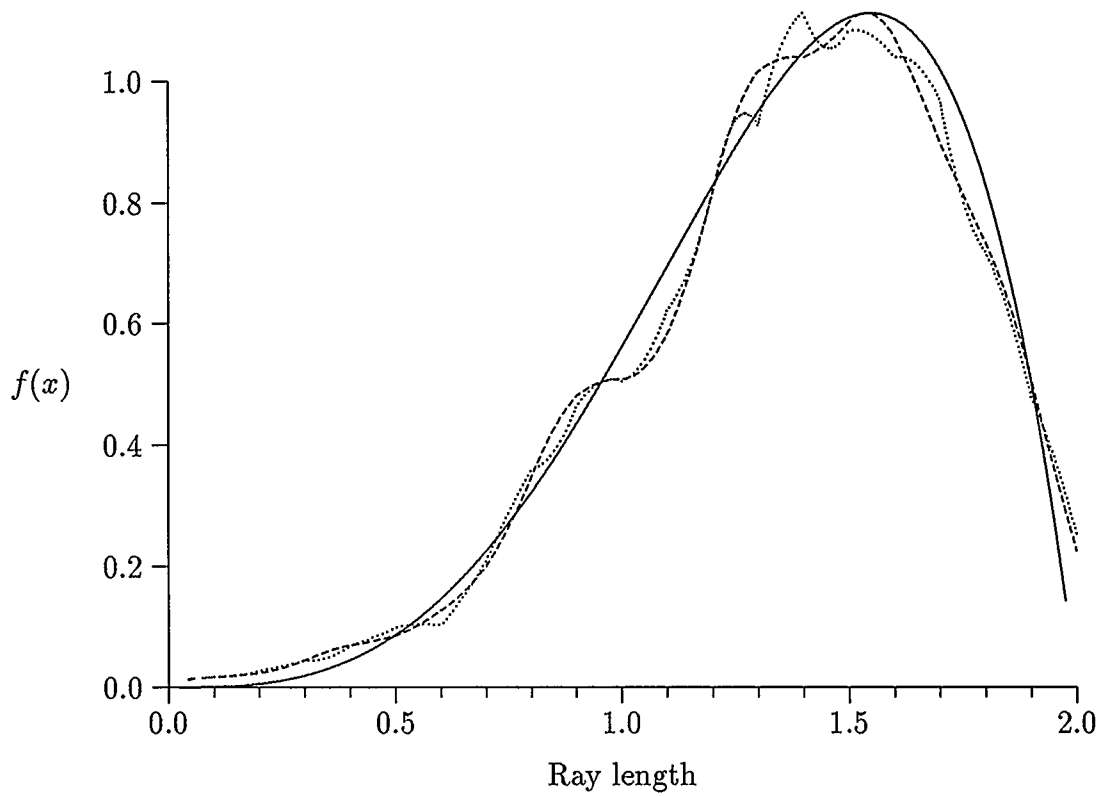
	Average	Variance		Symbol
Simulated	1.366085	0.121621	Gaussian	· ·
Analytical	1.371429	0.119184	Epanechnikov	*
			Hermite	- - - -
		$\kappa = 15$	Actual	—
		$h = 0.1$	Biweight	◇

Figure 4.22: $f_{R,\lambda}(l)$ for the sphere — several kernel fits



	Symbol	Parameters
Actual	—	
From $f_{T,\lambda}$ — Gaussian	- - - - -	$h = 0.1$
From $f_{T,\lambda}$ — Epanechnikov	. . .	$h = 0.1$

Figure 4.23: $f_{R,\nu}$ for the sphere — estimates via $f_{T,\lambda}$ method



	Symbol	Parameters
Actual	—	
From $f_{T,\lambda}$ — Gaussian	- - - - -	$h = 0.1$
From $f_{T,\lambda}$ — Epanechnikov	. . .	$h = 0.1$

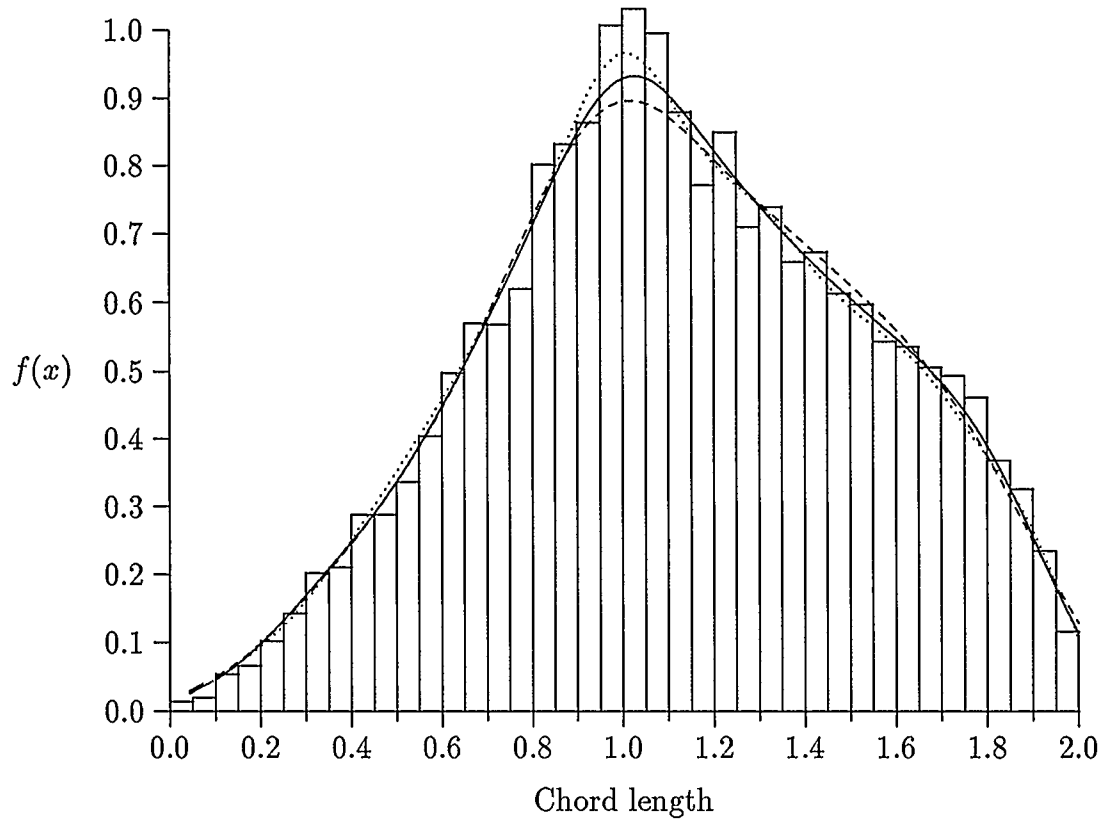
Figure 4.24: $f_{R,\lambda}$ for the sphere — estimates via $f_{T,\lambda}$ method

4.4 Results For The Hemisphere

Simulations for the hemisphere were performed for all surface and interior point random distributions from Table 2.6. However, only the ν -random chord distribution is reproduced in this thesis.

Interior randomness for the hemisphere was naturally easy. Surface randomness required weighting a random number to choose either the spherical cap or the flat bottom of the hemisphere. Once this was done, points were generated from the bottom by simply choosing a point inside a circle, and a point generated from the spherical cap by slightly modifying the sphere surface randomness procedure.

Nothing interesting came out of the analysis. The segment density $f_{T;\lambda}$ was not a good estimator of even the ray length distributions for ν - and λ -randomness. However, as can be seen in Figure 4.25, the ν -random chord distribution, the general shape of the distribution first discovered by Langworthy [60] is repeated (this distribution is indicative of most of the chord distributions, including the μ -random distribution which he considers).



	Average	Variance		Symbol	h
Simulated	1.125241	0.169048	Kernel Est.	—	0.100
				0.075
				- - - - -	0.125

Figure 4.25: $f_{L,\nu}(l)$ for the hemisphere — several Gaussian kernel fits for different window widths

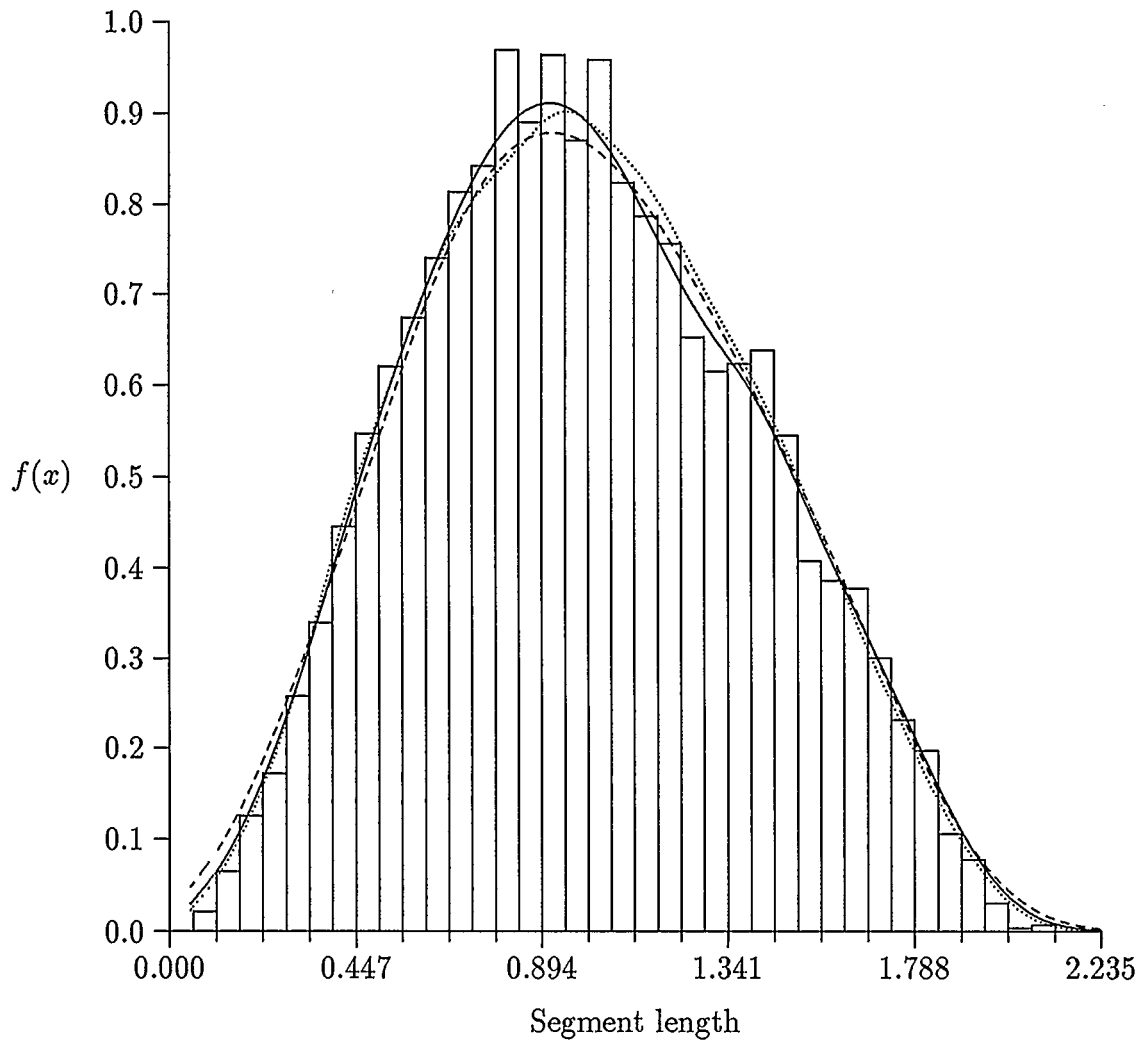
4.5 Results For The Cylinder

For the cylinder, programs were developed to directly simulate each of the distributions listed in Table 2.6. No actual curves were calculated, although Kellerer [47] derives the μ -random chord distribution in cylinders having arbitrary cross section, and Langworthy [59] and Mäder [64] present numerical results for right circular cylinders. See also Gille [30] and Kellerer [48].

All simulations were performed for a cylinder of unit height and radius with the exception of the μ -random chord distribution, which was done for arbitrary height and radius (i.e. height and radius could be set at arbitrary values).

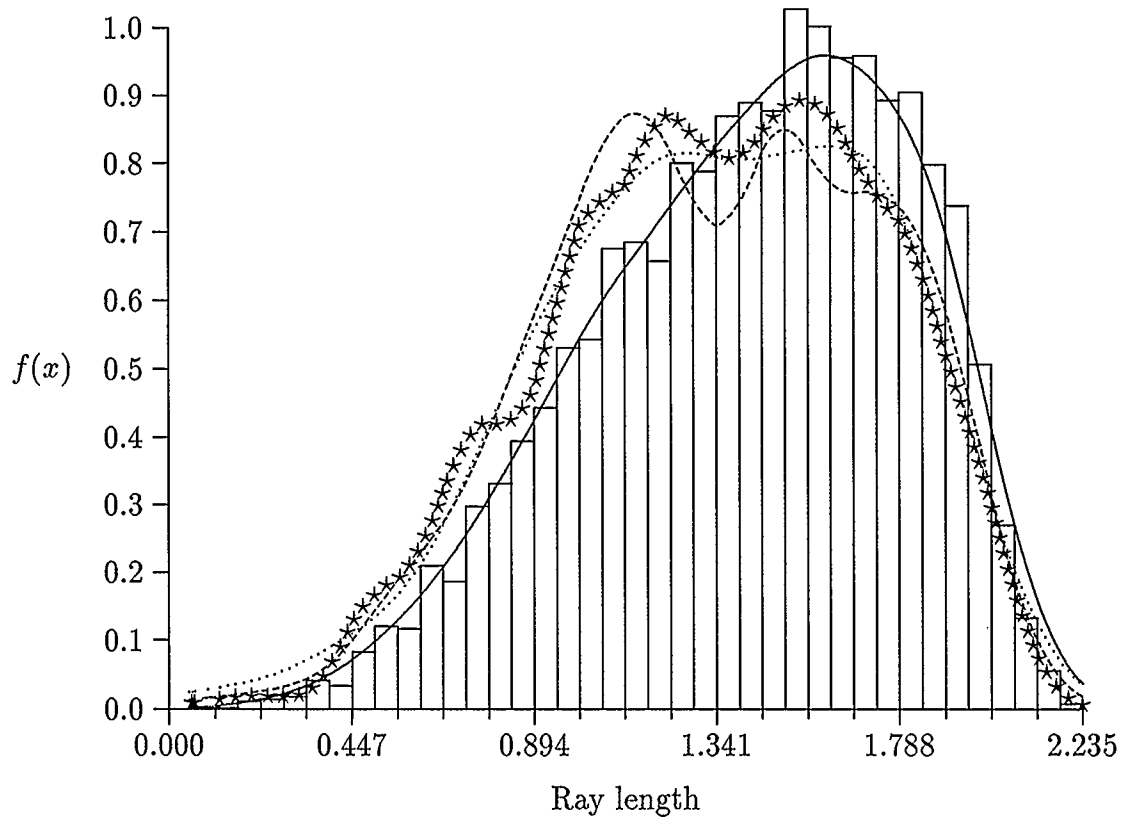
Interior randomness was done by simply choosing a z -coordinate, thus slicing the cylinder. With the remaining circle, a point (x, y) was chosen as points internal to a circle are chosen. Surface randomness for the cylinder constituted weighting the endcaps and the “wall” of the cylinder appropriately. Once this was done, points could be chosen on the caps as points are chosen interior to a circle, and points on the “wall” as points are chosen on the surface of the circle, once a z -coordinate is chosen.

Results to be demonstrated here include the λ -random segment density (Figure 4.26) with several Gaussian kernel fits. In Figure 4.26 the crucial nature of the initial estimate of $f_{T,\lambda}$ is demonstrated. First derivatives of the segment density are demonstrated in Figure 4.27. Note the fluctuation in this curves derived from the segment density for small changes in the window width h . The segment density was also not a good estimator of the chord length distributions or of the $f_{R,\nu}$ distribution.



	Average	Variance	Symbol	h
Simulated	1.001133	0.158182	—	0.100
			⋯⋯	0.125
			****	0.075

Figure 4.26: $f_{T,\lambda}$ for the cylinder — several Gaussian kernel fits for different window widths



	Average	Variance		Symbol
Simulated	1.421905	0.145719	Kernel Est.	—
			From $f_{T,\lambda}$	---- $h = 0.1$
			 $h = 0.125$
				**** $h = 0.075$

Figure 4.27: $f_{R,\lambda}$ for the cylinder — estimates via $f_{T,\lambda}$ method from Gaussian parent kernel

4.6 $\Omega(l)$ versus $f_{T;\lambda}$ — A Brief Summary

Single and double derivatives of either the Ω or $f_{T;\lambda}$ functions depend heavily on the accuracy of the initial estimate. The behaviour of generated distributions, then, depends on the behaviour of the methods used to generate $f_{T;\lambda}$ (kernels) or Ω (splines).

Recall that comparisons were evaluated visually although there is a great need for a quantitative measure to support the Ω method over the $f_{T;\lambda}$ method. However, as alternatives to direct simulation for generating distributions, the Ω and $f_{T;\lambda}$ methods show great promise.

In particular, the Ω method generated an initial estimate of the density $f_{T;\lambda}$ that agreed to within four or five decimal places of the analytical density. Kernel fits to the $f_{T;\lambda}$ (from which derivatives are calculated) were not as accurate. It was no surprise, then, that Ω provided a better estimate than $f_{T;\lambda}$ for ray densities (ν, λ) and chord densities (ν, λ, μ) . The Ω method also provided excellent estimates when approximating the circle.

Generation time, also an important comparison measure, was much quicker for the Ω program *when* the number of vertices of the polygon was 20 or less. This fact is easily explained by three things. First, the segment densities require a large number of calls to a random number generator. Second, computations involving the segment density are more computer-intensive, with many more square roots and trigonometric functions required. Third, and most important, many points for non-square regions (in two dimensions) are thrown away because they do not fall within the required body K , especially when K differs greatly from a rectangle.

Recommendations:

- (1) Pursue LRSs (Chapter 3) as an alternative to kernels as estimators of $f_{T;\lambda}$,
- (2) Use weighted splines for estimating Ω ,
- (3) Continue analysis by extending the Ω method to three dimensions.

With slight modifications to the Ω and $f_{T;\lambda}$ programs incorporating these recommendations, these two new methods can become efficient generators of the ray densities with measure $\in [\lambda, \nu]$ and chord densities with measure $\in [\lambda, \nu, \nu]$.

Chapter 5

Future Directions

In this chapter some mention will be made of possible future directions. Once the simulation was completed for two-dimensional arbitrary polygons, a natural extension would be three-dimensional arbitrary polyhedra. Other natural extensions include bivariate rays, non-convex regions and embedded bodies.

Also, in keeping with the methods employed in this thesis, it would be reasonable to generate surface-random chords and rays from surfaces of arbitrary bodies. For the ellipsoid problems arose when points could not be chosen from the surface — that is, the ellipse surface-randomness procedure could not be extended to higher dimensions. Currently there is little if any theory developed for β -random chords for the general ellipsoid. As future work, then, simulation of β -random chords is important as a step in developing theory.

5.1 Polyhedra

The main objective of this thesis has been to determine the feasibility of developing a computer program that can generate chord length distributions of arbitrary two- and three-dimensional ovoids. For such regions, a program has been developed that deals with arbitrary polygonal regions, and bodies such as circles or ellipses that can be closely approximated by choosing a polygon with enough edges.

For three-dimensional regions, an extension to the polygon approach is certainly

possible for a box but was not attempted here.

The algorithm used to determine if points are interior to a polygon can be extended to polyhedra, and indeed to n -dimensional simplexes defined by $(n+1)$ points. Two methods exist, each of them unchecked but both with applications to generating $f_{T;\lambda}$ for general polyhedra.

First, for a convex n -hedron, describe each of the surfaces in the form

$$\sum_{k=1}^n a_k x_k = c.$$

Let the ordered n -tuple formed by a_k be vector A . If $P \cdot A < c$ for each surface, the point is inside.

Second, observe that each subset of n points defines an $(n-1)$ -dimensional hyperplane; the test point is inside the polytope (n -dimensional polygon) if and only if it is on the appropriate side of each of these hyperplanes. Let the points defining the polytope be P_1, P_2, \dots, P_{n+1} where $P_i = (p_{i,1}, p_{i,2}, \dots, p_{i,n})$. Let Q be the point whose position must be determined. Then form the linear equations given by

$$\sum_i \lambda_i P_i = Q \quad \text{and} \quad \sum_i \lambda_i = 1,$$

which form a system of $(n+1)$ equations. If all $\lambda_i \geq 0$, then the point is inside.

However, the generalization of the area formula from vertices (Stone [94]) is not so straightforward when applied in three dimensions. Schaer and Stone [85] devised a method for calculating the area of a polyhedron when a traverse is known. A traverse is simply a sequential list of all of the faces so that adjacent faces in the list share exactly two vertices. This fact could not be used to calculate Ω for arbitrary polyhedra since a traverse is not always guaranteed.

5.2 Bivariate Rays

Bivariate rays have received some attention lately. In particular Misi ([68]) considered various types of randomness and defined a new overlap function which arises out of his research.

Types of randomness include $\hat{\nu}$, where a point P is chosen from within K . Two directions θ_1 and θ_2 are then chosen independently and uniformly random to define two rays R and S .

Another randomness is $\hat{\lambda}$, where three points P , Q and O are chosen independently and uniformly random from within K , giving two rays $U = \overline{PQ}$ and $V = \overline{PO}$.

A description of the new bivariate overlap function is given in Figure 5.1. The shaded region defines this new overlap function.

This overlap function is defined as the intersection volume of K with two independent translates $K(r, \theta_1)$ and $K(s, \theta_2)$, averaged over θ_1 and θ_2 , that is

$$\Omega_K(r, s) = E_{\theta_1, \theta_2} \left\{ \frac{V[K \cap K(r, \theta_1) \cap K(s, \theta_2)]}{V(K)} \right\}. \quad (5.1)$$

Consideration of bivariate rays could have some immediate applications in many of the areas for which chord distributions are now exclusively used.

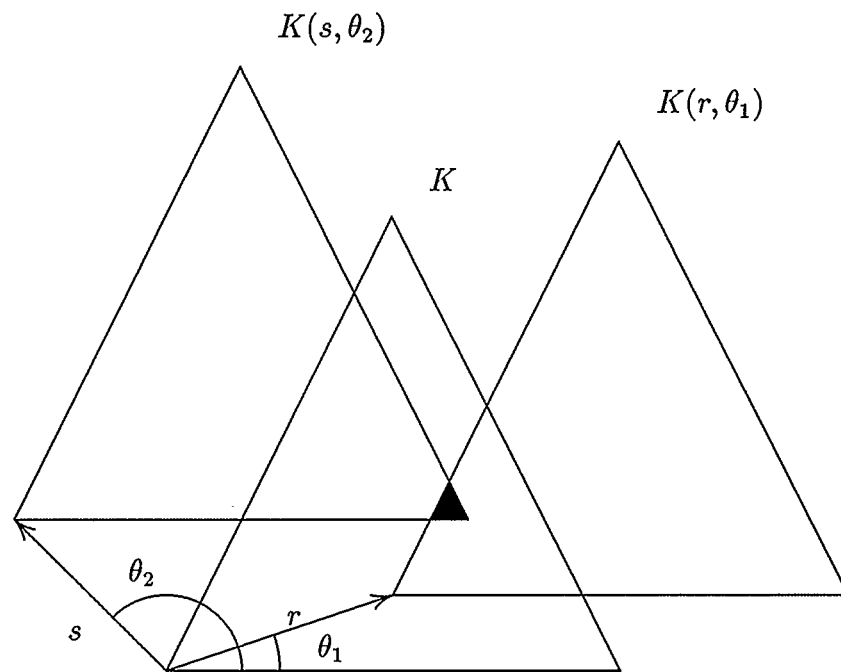


Figure 5.1: Bivariate overlap function

5.3 Non-uniform Directions

This thesis has not considered chords generated by non-uniform angular measures. The author is not aware of any published results regarding such anisotropic measures. It should be relatively simple to modify our simulation techniques to accommodate anisotropy. For example, γ -random chords might be chosen with θ chosen according to a (multivariate) normal law. Simulation would be all the more important because analytical results may be expected to be extremely difficult.

5.4 Exotic and Embedded Bodies

Single-body results can be extended to the case of one body embedded in another. One possible application is the case of nucleated particles — essentially convex particles containing a (possible non-convex) nuclear region. Below, we review the theory of embedded bodies as developed by Enns and Ehlers [25].

Let K be some body completely embedded within some convex body G . Line segments can then be generated on K , or on both K and G , and then projected outward. Define the overlap function as

$$\Omega_{K,G}(l) \equiv \frac{E_{\theta}[V(K(l, \theta) \cap G)]}{V(K)}. \quad (5.2)$$

For example, consider the randomness measure defined by choosing a point $P \in K$ and a point $Q \in G$, where G is not necessarily convex. The distance between P and Q defines a segment length T (see Figure 5.2). Recall that $B(l, P)$ is the n -ball of radius l with centre P and surface $\partial B(l, P)$. Then

$$P(T \leq l) = \frac{E_{P_K}[V(B(l, P) \cap G)]}{V(G)}, \quad (5.3)$$

where P is uniformly averaged over the region K . Writing this in terms of the total solid angle subtended at P by $G \cap \partial B(l, P)$ one obtains

$$f_T(l) = \frac{E_{P_K}[l^{n-1}\Phi(l, P)]}{V(G)}. \quad (5.4)$$

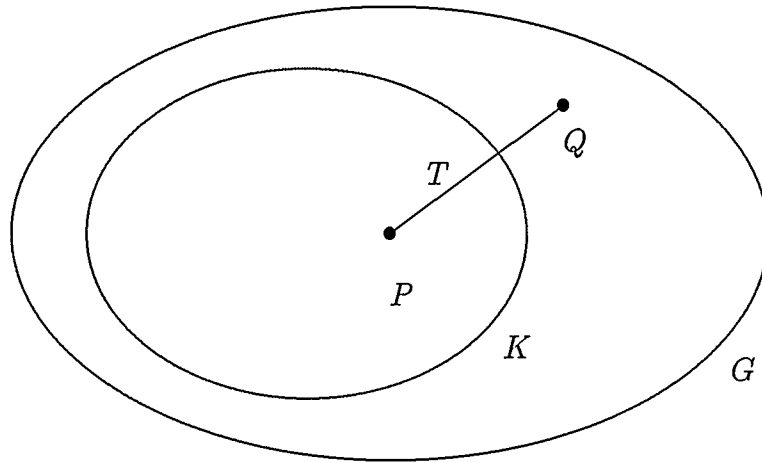


Figure 5.2: Embedded body — generation of T

Equation (2.22) is easily generalized to

$$\frac{E_{P_K}[\Phi(l, P)]}{nC_n} = \Omega_{K,G}(l), \quad (5.5)$$

giving as segment density

$$f_T(l) = \frac{nC_n \Omega_{K,G}(l)}{V(G)} \cdot l^{n-1}. \quad (5.6)$$

When $K = G$, this density recovers the Chapter 2 result (see Table 2.6).

Rays and secants in G can also be generated from within K . Assume G convex and K to be some non-empty subset of G . Select a point $P \in K$ and a direction θ , thus defining ν -randomness (see Figure 5.3).

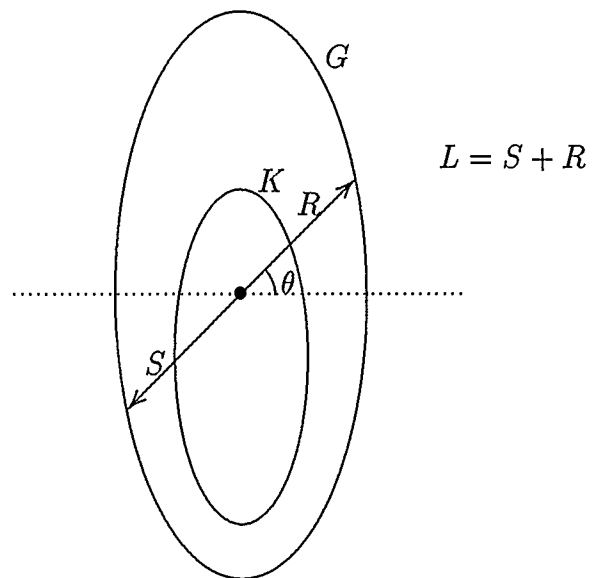


Figure 5.3: Embedded body — generation from within K

Two rays are thereby formed. The first, a forward ray R , starts at P and ends at ∂G (surface of G) in direction θ . The second, a backward ray S , begins at P and ends at ∂G in direction $-\theta$. A secant L of G is formed when the forward and backward components are combined. Clearly

$$P(R \geq l) = P(S \geq l) = \Omega_{K,G}(l), \quad (5.7)$$

and therefore

$$P(R \geq l) = \frac{V(G)f_T(l)}{nC_n l^{n-1}}. \quad (5.8)$$

Given this relationship, moments are related by

$$E(R^{m+n}) = \frac{n+m}{nC_n} V(G)E(T^m). \quad (5.9)$$

Note, when $K = \partial G$, the connection between γ -random chords and α -random rays can be recovered, since then $P(R \geq l) = P(L_\gamma \geq l)$ and $f_T(l) = f_{R,\alpha}(l)$ (Table 2.6).

The final type of ray to be considered here is defined when two points $P \in K$ and $Q \in G$ are chosen where $K \subseteq G$ and G is convex. Then Q clearly lies in G with probability $V(K)/V(G)$. Define W as the length of the ray formed from P through Q to the boundary of G .

To derive the distribution of W for this type of randomness, place an n -ball of radius l having centre at P (see Figure 5.4). Let $C(l,P)$ be the union of conical subsets of $B(l,P)$ subtended by $\Phi(l,P)$ at P . In this way, $C(l,P)$ is then those conical portions of the n -ball whose caps fall inside G .

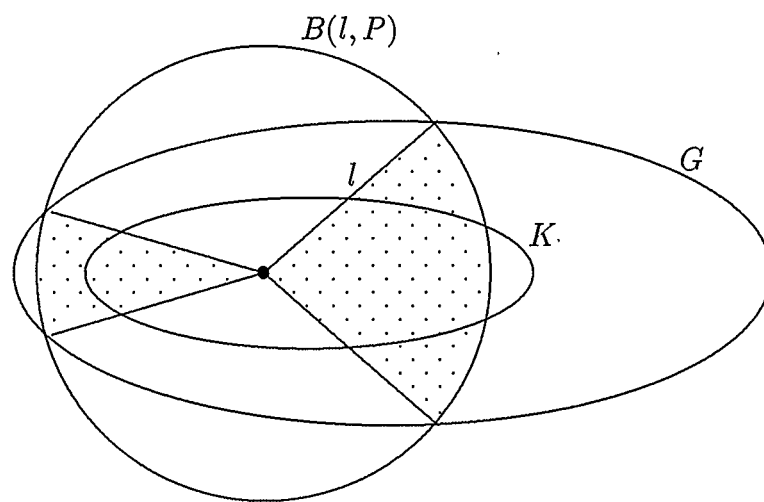


Figure 5.4: Rays in G generated by two points in K and G

Then $V(C(l, P)) = l^n \Phi(l, P)/n$ and

$$P(W > l|P) = P(T > l|P) + P(T \leq l, W > l|P) \quad (5.10)$$

$$= P(T > l|P) + \frac{l^n \Phi(l, P)}{nV(G)}, \quad (5.11)$$

a conditional distribution, that, when averaging over the point P becomes

$$P(W > l) = P(T > l) + \frac{l^n E_{P_K}[\Phi(l, P)]}{nV(G)} \quad (5.12)$$

$$= P(T > l) + \frac{C_n l^n}{V(G)} \Omega_{K,G}(l). \quad (5.13)$$

The density of W is thus

$$f_W(l) = \frac{-C_n l^n}{V(G)} \frac{d}{dl} \Omega_{K,G}(l) \quad (5.14)$$

$$= \frac{C_n l^n f_R(l)}{V(G)}. \quad (5.15)$$

Finally, moments of W , R and T are related by

$$E(W^m) = \frac{C_n}{V(G)} E(R^{n+m}) = \frac{n+m}{n} E(T^m). \quad (5.16)$$

In this type of randomness, $K = G$ gives λ -randomness in the Chapter 2 setting.

Bibliography

- [1] Barbery, G. (1974) Determination of Particle Size Distribution from Measurements on Sections. *Powder Technology* **9**, 231-240.
- [2] Bate, A.E. and M.E. Pillow (1947). Mean free path of sound in an auditorium. *Proc. Phys. Soc. London* **59**, 535-541.
- [3] Bendel, W.L. (1984). Length Distribution of Chords Through a Rectangular Volume. *Naval Research Laboratory Memorandum Report 5369*.
- [4] Birkhoff, R.D. Turner, J.E. et al. (1970). The Determination of LET Spectra from energy-proportional pulse-height measurements I. Track-length distributions in cavities. *Health Physics* **18**, 1-14.
- [5] Bos, L.P. Computer Code in FORTRAN for Weighted Splines.
- [6] Breiman, L. and S. Peters (1992). Comparing Automatic Smoothers (A Public Service Enterprise). *International Statistical Review* **60**, pp. 271-290.
- [7] Buckland, S.T. (1992). Fitting Density Functions with Polynomials. *Appl. Statist. (JRSS (Series C))* **41**, 63-76.
- [8] Buckland, S.T. (1992). Algorithm AS270 — Maximum Likelihood Fitting of Hermite and Simple Polynomial Densities. *Appl. Statist. (JRSS (Series C))* **41**, 241-266.
- [9] Butler, T.W. (1960). An Investigation of Particle Size Analyses as Applied to WC-Co. *Metallography* **2**, 289-292.
- [10] Caswell, R.S. (1966). Deposition of Energy by Neutrons in Spherical Cavities. *Radiation Research* **27**, 92-107.
- [11] Cleveland, W.S. (1979). Robust locally weighted regression and smoothing scatterplots. *J. Amer. Statist. Assoc.* **74**, 829-836.
- [12] Coleman, R. (1969). Random Paths Through Convex Bodies. *J. Appl. Prob.* **6**, 430-441.
- [13] Coleman, R. (1973). Random Paths Through Rectangles and Cubes. *Metallography* **6**, 103-114.
- [14] Coleman, R. (1981). Intercept Lengths of Random Probes Through Boxes. *J. Appl. Prob.* **18**, 276-282.

- [15] Coleman, R. (1989). Random Sections of a Sphere. *The Canadian Journal of Statistics* **17**, 27-39.
- [16] Cowan, R. A Collection of Problems in Random Geometry. Teubner Texte zur Mathematik – Band 65, pp. 64-68. [Stochastic Geometry, Geometric Statistics, Stereology. Proceedings of a Conference held at Oberwolfach, 1983. Rm. Ambartzumian and W. Weil, eds. B.C. Teubner Verlagsgesellschaft, Leipzig.]
- [17] Davy, P.J. (1984). Inequalities for Moments of Secant Length. *Z. Wahrscheinlichkeitstheorie verw. Gebiete* **68**, 243-246.
- [18] DeHoff, R.T. and P. Bousquet (1970). Estimation of the size distribution of triaxial ellipsoidal particles from the distribution of linear intercepts. *Journal of Microscopy* **92**, 119-135.
- [19] DeHoff, R.T. and F.N. Rhines (1961). Determination of Number of Particles Per Unit Volume From Measurements Made on Random Plane Sections: The General Cylinder and the Ellipsoid. *Trans. A.I.M.E.* **221**, 975-982.
- [20] Dirac, P.A.M., K. Fuchs, R. Peierls and P. Preston. Applications to the Oblate Spheroid, Hemisphere and Oblate Hemi-spheroid. Declassified British Report MS-D-5, Part II, 1943.
- [21] Ehlers, P.F. *Particle Number Fluctuations and Their Relation to Geometrical Probability*. Ph.D. Thesis, U.B.C., 1972.
- [22] Ehlers, P.F. and E.G. Enns (1981). Random Secants of a Convex Body Generated by Surface Randomness. *J. Appl. Prob.* **18**, 157-166.
- [23] Enns, E.G. and P.F. Ehlers (1978). Random Paths Through a Convex Region. *J. Appl. Prob.* **15**, 144-152.
- [24] Enns, E.G. and P.F. Ehlers (1980). Random Paths Originating Within a Convex Region and Terminating On its Surface. *Austral. J. Statist.* **22**, 60-68.
- [25] Enns, E.G. and P.F. Ehlers (1988). Chords Through a Convex Body Generated From Within an Embedded Body. *J. Appl. Prob.* **25**, 700-707.
- [26] Enns, E.G., P.F. Ehlers and S. Stuhr (1981). Every Body Has Its Moments. *Statistical Distributions in Scientific Work* **5**, 387-396.
- [27] Exner, H.E. and H.L. Lukas (1971). The Experimental Verification of the Stationary Wagner-Lifshitz Distribution of Coarse Particles. *Metallography* **4**, 325-338.

- [28] Fullman, R.L. (1953). Measurement of Particle Sizes in Opaque Bodies. *Journal of Metals* **5**, 447-452.
- [29] Gasparyan, V.M. (1984). Pleijel Identity and Distribution of Chord Length for Planar Convex Domains. In Teubner Texte zur Mathematik – Band 65, pp. 91-94. [Stochastic Geometry, Geometric Statistics, Stereology. Proceedings of a Conference held at Oberwolfach, 1983. Rm. Ambartzumian and W. Weil, eds. B.C. Teubner Verlagsgesellschaft, Leipzig.]
- [30] Gille, H.W. (1987). The Intercept Length Distribution Density of a Cylinder of Revolution. *Experimentelle Technik der Physik* **35**, 93-98.
- [31] Gille, H.W. (1988). The Chord Length Distribution Density of Parallelepipeds with Their Limiting Cases. *Experimentelle Technik der Physik* **36**, 197-208.
- [32] Goldsmith, P.L. (1967). The calculation of true particle size distributions from the sizes observed in a thin slice. *Brit. J. Appl. Phys.* **18**, 813-830.
- [33] Goudsmit, S. (1945). Random Distribution of Lines in a Plane. *Reviews of Modern Physics* **17**, 321-322.
- [34] Gundersen, H.J.G. and E.B. Jensen (1983). Particle sizes and their distributions estimated from line- and point-sampled intercepts. Including graphical unfolding. *Journal of Microscopy* **131**, 291-310.
- [35] Gundersen, H.J.G., T.B. Jensen and R. Østerby (1978). Distribution of Membrane Thickness Determined By Lineal Analysis. *Journal of Microscopy* **113**, 27-43.
- [36] Gurland, J. (1963). The Fracture Strength of Sintered Tungsten Carbide-Cobalt Alloys in Relation to Composition and Particle Spacing. *Trans. A.I.M.E.* **227**, 1146-1150.
- [37] Hammersley, J.M. (1950). The Distribution of Distance in a Hypersphere. *Ann. Math. Stats.* **21**, 447-452.
- [38] Hanson, K.L. (1979). Determination of Grain Density in Space-Filling Geometries from Measurable Two-dimensional Parameters. *Acta Metallurgica* **27**, 515-521.
- [39] Hastie, T. and C. Loader (1993). Local Regression: Automatic Kernel Carpentry. *Statistical Science* **8** (No. 2), 120-143.

- [40] Heckbert, P.S. (1987). Ray Tracing JELL-O[®] Brand Gelatin. *Computer Graphics* **21**, 73-74.
- [41] Hilliard, J.E. (1962). The Counting and Sizing of Particles in Transmission Microscopy. *Trans. A.I.M.E.* **224**, 906-917.
- [42] Hilliard, J.E. (1968). Direct Determination of the Moments of the Size Distribution of Particles in an Opaque Sample. *Trans. A.I.M.E.* **242**, 1373-1380.
- [43] Horowitz, M. (1965). Probability of Random Paths Across Elementary Geometrical Shapes. *J. Appl. Prob.* **2**, 169-177.
- [44] Itoh, H. (1970). An Analytical Expression of the Intercept Length Distribution of Cubic Particles. *Metallography* **3**, 407-417.
- [45] Izenman, A.J. (1991). Recent Developments in Nonparametric Density Estimation. *JASA* **86**, 205-224.
- [46] Jensen, E.B. and Møller, J. (1986). Stereological Versions of Integral Geometric Formulae for n -dimensional Ellipsoids. *J. Appl. Prob.* **23**, 1031-1037.
- [47] Kellerer, A.M. (1971). Considerations on the Random Traversal of Convex Bodies and Solutions for General Cylinders. *Radiation Research* **47**, 359-376.
- [48] Kellerer, A.M. (1981). Proximity Functions for General Right Cylinders and Criteria for the Equivalence of Spherical and Cylindrical Proportional Counters in Microdosimetry. *Radiation Research* **86**, 264-286.
- [49] Kellerer, A.M. (1984). Chord-Length Distributions and Related Quantities for Spheroids. *Radiation Research* **98**, 425-437.
- [50] Kendall, M.G. and P.A.P. Moran. *Geometrical Probability*. Charles Griffin & Company Limited, London, 1963.
- [51] Kingman, J.F.C. (1965). Mean Free Paths In a Convex Reflecting Region. *J. Appl. Prob.* **2**, 162-188.
- [52] Kingman, J.F.C. (1969). Random Secants of a Convex Body. *J. Appl. Prob.* **6**, 660-672.
- [53] Kok, L.P. *100 Problems of my Wife and their Solution in Theoretical Stereology*. Coulomb Press Leyden, Leiden, 1990.
- [54] Kosten, C.W. (1960). The Mean Free Path in Room Acoustics. *Acustica* **10**, 245-250.

- [55] Lamport, L. *L^AT_EX: A Document Preparation System*. Addison-Wesley, Reading, 1986.
- [56] McLaren, A.S., P. Wadhams and R. Weintraub (1984). The Sea Ice Topography of M'Clure Strait in Winter and Summer of 1960 from Submarine Profiles. *Arctic* **37**, 110-120.
- [57] Melhuish, F.M. and A.R.G. Lang (1970). Lengths and Diameters of Plant Roots in Non-random Populations by Analysis of Plane Surfaces. *Biometrics* **26**, 421-431.
- [58] Melhuish, F.M. and A.R.G. Lang (1971). Quantitative Studies of Roots in Soil: 2. Analysis of Non-random Populations. *Soil Science* **112**, 161-166.
- [59] Langworthy, J. (1988). The Chord Distribution for a Right Circular Cylinder. *Naval Research Laboratory Memorandum Report 6220*.
- [60] Langworthy, J.B. (1989). A General Approach to Chord Length Distributions Applied to a Hemisphere. *Radiation Research* **118**, 21-36.
- [61] Langworthy, J.B. (1989). Depletion Region Geometry Analysis Applied to Single Event Sensitivity. *IEEE Transactions on Nuclear Science* **36**, 2427-2434 (corrected by Dr. Langworthy).
- [62] Langworthy, J.B. (1991). General Methods for Chord Distributions Applied to a Semicircle (unpublished — provided by Dr. Langworthy).
- [63] Langworthy, J.B. (1993). The Effects of Funneling on Space Upset Rate (preprint). Accepted for publication in February *Transactions on Nuclear Science of IEEE*.
- [64] Mäder, U. (1980). Chord Length Distribution for Circular Cylinders. *Radiation Research* **82**, 454-466.
- [65] Marcellus, R.W., and T.B. Morrison. *Ice Design Statistics for the Canadian Beaufort Sea*. Canada Marine Engineering Ltd. Report # 1015, prepared for the Environmental Impact Statement Partners, April, 1982.
- [66] Marsaglia, G. (1972). Choosing a Point From The Surface of a Sphere. *Ann. Math. Stats.* **43**, 645-646.
- [67] McIntyre, G.A. (1953). Estimation of Plant Density Using Line Transects. *J. Ecol.* **41**, 319-330.

- [68] Misi, T. *Random Bivariate Rays, Statistical Societies and Buffon's Pi*. Ph.D. Thesis, University of Calgary, 1992.
- [69] Møller, J. (1988). Stereological Analysis of Particles of Varying Ellipsoidal Shape. *J. Appl. Prob.* **25**, 322-335.
- [70] Morrison, T.B. *Development of Statistics Related to Ridge Spacing and Orientation in Multi-Year Ice Floes*. Proprietary report prepared for Gulf Canada Resources Limited, February 1989.
- [71] Naumovich, N.V., M.N. Bodyako and V.P. Kasichev (1980). Statistical Parameters of Some Polyhedrons. *Practical Metallography* **17**, 192-200.
- [72] Naumovich, N.V. and T.I. Kriskovets (1982). Influence of the Body Shape on the Profile of Chord Length Distribution. *Acta. Stereol.* **1**, 51-59.
- [73] Naumovich, N.V. and R. Warren (1978). Influence of Particle Shape and Spatial Size Distribution on Random Intercept Length Distributions. *Special Issue of Practical Metallography* **8**, 161-170.
- [74] Piefke, F. (1979). Chord Length Distribution of the Ellipse. *Lietuvos Matematikos Rinkinys* **19**, 45-54.
- [75] Preparata, F.P. and M.I. Shamos. *Computational Geometry: An Introduction*, 2nd and revised printing. Springer-Verlag, New York, 1985.
- [76] Press, W.H., B.P. Flannery, S.A. Teukolsky and W.T. Vetterling. *Numerical Recipes in C*. Cambridge University Press, Cambridge, 1988.
- [77] Primak, W. (1956). Gamma-Ray Dosage in Inhomogeneous Nuclear Reactors. *Journal of Applied Physics* **27**, 54-62.
- [78] Riss, J. and M.-C. Durand (1980). Stereological Properties of Polyhedra. *Mikroskopie* **37** (Suppl.), 387-389.
- [79] Riss, J., J. Grolier, M. Hucher and G. Sabatier (1982). Shape and Stereology of Two Ideal Pseudo Williams' Polyhedra. *Acta Stereol.* **1**, 37-43.
- [80] Rossi, H.H. (1967). Energy Distribution in the Absorption of Radiation. *Advances in Biological and Medical Physics* **11**, 27-85.
- [81] Rothrock, D.A. and A.S. Thorndike (1984). Measuring the Sea Ice Floe Size Distribution. *Journal of Geophysical Research* **89**, 6477-6486.
- [82] Russ, J.C. *Practical Stereology*. Plenum Press, New York, 1986.

- [83] Salkauskas, K. (1974). C^1 Splines for Interpolation of Rapidly Varying Data. *Rocky Mountain Journal of Statistics* **14**, 239-250.
- [84] Santaló, L.A. *On the Measure of Line Segments Entirely Contained in a Convex Body*, in Aspects of Mathematics and its Applications, J.A. Barroso, ed. North-Holland, 1986.
- [85] Schaer, J. and M.G. Stone. Face Traverses and a Volume Algorithm for Polyhedra. In Lecture Notes in Computer Science 555, H. Maurer (ed.). New Results and New Trends in Computer Science, Graz, Austria, June 1991 Proceedings. Springer Verlag, pp. 290-297.
- [86] Schneider, R. (1985). Inequalities for Random Flats Meeting a Convex Body. *J. Appl. Prob.* **22**, 710-716.
- [87] Schwartz, S.C. (1967). Estimation of Probability Density by an Orthogonal Series. *Ann. Math. Statist.* **38** 1361-1265.
- [88] Sepulveda, J.E., Miller, J.D. and C.L. Lin. *Generation of Irregularly Shaped Multiphase Particles for Liberation Analysis*. Proc. Fifteenth International Mineral Processing Conference, Cannes, 1985.
- [89] Sheng, T.K. (1985). The Distance Between Two Random Points in Plane Regions. *Adv. Appl. Prob.* **17**, 748-773.
- [90] Silverman, B.W. *Density Estimation*. Chapman and Hall, London, 1986.
- [91] Solomon, H. *Geometric Probability*. Society for Industrial and Applied Mathematics, Philadelphia, 1978.
- [92] Späth, H. *Spline Algorithms for Curves and Surfaces*. English translation by W.D. Hoskins and H.W. Sager, Utilitas Mathematica Publ., Inc., Winnipeg, 1974.
- [93] Stone, C.J. (1977). Consistent nonparametric regression (with discussion). *Ann. Statist.* **5**, 595-620.
- [94] Stone, M.G. (1986). A Mnemonic for Areas of Polygons. *American Math. Monthly* **93**, June-July, 479-480.
- [95] Stoyan, D., W.S. Kendall and J. Mecke. *Stochastic Geometry and Its Applications*. John Wiley, Chichester, 1987.
- [96] Strang, G. (1993). Polar Area is the Average of Strip Areas. *American Math. Monthly*, March, 250-254.

- [97] Wadhams, P., A.S. McLaren and R. Weintraub (1985). Ice Thickness Distribution in Davis Strait in February From Submarine Sonar Profiles. *Journal of Geophysical Research* **90**, 1069-1077.
- [98] Warren, R. (1971). An Experimental Study of the Stereology of Cubic Particles. *Metallography* **4**, 561-564.
- [99] Warren, R. (1987). Microstructural Modelling in Stereology. *Acta Stereol.* **6**, 157-173.
- [100] Warren, R. and M.-C. Durand (1983). Microstructural Modelling of Partially-Oriented, Elongated Particles in Opaque Samples. *Acta Stereol.* **2** (Suppl. I), 47-52.
- [101] Warren, R. and N. Naumovich (1977). Relative frequencies of random intercepts through convex bodies. *Journal of Microscopy* **110**, 113-120.
- [102] Wasén, J. and R. Warren. *A Catalogue of Stereological Characteristics of Selected Solid Bodies. Volume 1, Polyhedrons*. Department of Engineering Metals, Chalmers University of Technology, 1990.
- [103] Weibel, E.R. *Stereological Methods Volume 2 — Theoretical Foundations*. Academic Press, London, 1980.
- [104] Wichura, M.J. (1987) *The P_lCT_EX Manual*. T_EXUsers Group, Providence, Rhode Island.
- [105] Wicksell, S.D. (1925). The Corpuscle Problem. A Mathematical Study of a Biometric Problem. *Biometrika* **17**, 84-99.
- [106] Wicksel, S.E. (1925). The Corpuscle Problem. Second Memoir: Case of Ellipsoidal Corpuscles. *Biometrika* **18**, 151-172.
- [107] Wilson, W.S.J. and E.W. Emery (1968). Path Length Distributions Within Cylinders of Various Proportions. In *Proceedings of the Symposium on Microdosimetry, Ispra* (H.G. Ebert, ed.), pp. 79-92. Euratom, Brussels (1968).
- [108] You, Z. and A.K. Jain (1984). Performance Evaluation of Shape Matching via Chord Length Distribution. *Computer Vision, Graphics and Image Processing* **28**, 185-198.

Appendix A

Computer Code for Polygon Program

The computer algebra system MACSYMA (Release 417.125) was used when required to differentiate Ω (when Ω was known) to produce μ -, ν - and λ -random distributions and to integrate $\Omega(l)$ to produce expectations and variances for these same densities. MACSYMA was run on a 486-33 MHz computer with 16MB of RAM. Graphs were reproduced using P₁CT_EX macros provided in Wichura [104]. Random number generators were taken from Press *et al.* [76].

(polygon.c)

```

#include <stdio.h>
#include <stdlib.h>
#include <math.h>
#include "numrec.h" /* See Press et al. [76] */

#define MAXNUM 400
#define BIGNUM 40
#define PI 3.141596
#define TMP 60

float max(float c, float d)
{
    if (c >= d) return c;
    else return d;
}

float min(float a, float b)
{
    if (a <= b) return a;
    else return b;
}

void spline(x,y,n,yp1,ypr,y2)
float x[],y[],yp1,ypr,y2[];
int n;
{
    int i,k;
    float p,qn,sig,un,*u,*vector();
    void free_vector();

    u=vector(1,n-1);
    if (yp1 > 0.99e30)
        y2[1]=u[1]=0.0;
    else {
        y2[1] = -0.5;
        u[1]=(3.0/(x[2]-x[1]))*((y[2]-y[1])/(x[2]-x[1])-yp1);
    }
    for (i=2;i<=n-1;i++) {
        sig=(x[i]-x[i-1])/(x[i+1]-x[i-1]);
        p=sig*y2[i-1]+2.0;
        y2[i]=(sig-1.0)/p;
        u[i]=(y[i+1]-y[i])/(x[i+1]-x[i]) - (y[i]-y[i-1])/(x[i]-x[i-1]);
}

```

main(polygon.c)

```

    u[i]=(6.0*u[i]/(x[i+1]-x[i-1])-sig*u[i-1])/p;
}
if (ypn > 0.99e30)
    qn=un=0.0;
else {
    qn=0.5;
    un=(3.0/(x[n]-x[n-1]))*(ypn-(y[n]-y[n-1])/(x[n]-x[n-1]));
}
y2[n]=(un-qn*u[n-1])/(qn*y2[n-1]+1.0);
for (k=n-1;k>=1;k--)
    y2[k]=y2[k]*y2[k+1]+u[k];
free_vector(u,1,n-1);
}

void splint(xa,ya,y2a,n,x,y)
float xa[],ya[],y2a[],x,*y;
int n;
{
    int klo,khi,k;
    float h,b,a;
    void nrerror();

    klo=1;
    khi=n;
    while (khi-klo > 1) {
        k=(khi+klo) >> 1;
        if (xa[k] > x) khi=k;
        else klo=k;
    }
    h=xa[khi]-xa[klo];
    if (h == 0.0) nrerror("Bad XA input to routine SPLINT");
    a=(xa[khi]-x)/h;
    b=(x-xa[klo])/h;
    *y=((ya[khi]-ya[klo])/h)-((3.0*a*a-1.0)*h*y2a[klo]/6.0)+
        ((3.0*b*b-1.0)*h*y2a[khi]/6.0);
}

void
main()
{
    float p[56][2], q[56][2];
    float mx[TMP], my[TMP], *area, cl, maxcl, *overlap, vol, surf;
}

```

main(polygon.c)

```

float a, b, c, d, e, f, g, h, mpt, xpt, ypt, i1, i2, i3, i4, dist, sq;
float length, theta, ix, iy, ixt, iyt, *xint, *yint, t1, t2, t3, tol;
float yp1, ypn, y, *x, *y2, *der1;
float ttt, aaa, bbb;
float sid1, sid2, radii;
int j, i, ss, k, l, m, n, nopts, ind1, ind2, ind3, ind4, v, uu, z;          90
int cint, cvert;
    area    = vector(0, MAXNUM);
    xint    = vector(1, TMP);
    yint    = vector(1, TMP);
    overlap = vector(1, BIGNUM);
    y2      = vector(1, BIGNUM);
    x       = vector(1, BIGNUM);
    der1    = vector(1, BIGNUM);

/* ----- 100
 * Points, Tolerance and Interior Point Initializations.
 * -----
 * Arrange points in a counter-clockwise direction for convenience. This
 * algorithm then requires less sorting at the start. Indices for the
 * points should read [x][y], where x is the point number and y is 0
 * or 1 as the value is the x- or y-coordinate.
 * ----- */
    tol = 0.000001;
    nopts = 40;
    aaa = 2.0;
    bbb = 1.0;
    for (k = 0; k <= nopts-1; k++){
        ttt = 2.0*PI*((float) k)/((float) nopts);
        p[k][0] = aaa*cos(ttt);
        p[k][1] = bbb*sin(ttt);
    }

/* -----
 * -----
 * Maximum Chord Length.
 * ----- */20
    maxcl = 0.0;
    for (j = 1; j <= nopts - 1; j++){
        for (k = 0; k < j; k++){
            sq = (p[j][0]-p[k][0])*(p[j][0]-p[k][0]) +
                (p[j][1]-p[k][1])*(p[j][1]-p[k][1]);
            cl = (float) sqrt(sq);

```

main(polygon.c)

```

        if (cl >= maxcl) maxcl = cl;
    }
}
printf("Maximum Chord Length: %f\n", maxcl);
/* ----- 130
 * Volume of Polygon.
 * ----- */
vol = ((p[nopts-1][0]*p[0][1])-(p[0][0]*p[nopts-1][1]))/2.0;
for (k = 0; k <= nopts-2; k++){
    vol += ((p[k][0]*p[k+1][1])-(p[k+1][0]*p[k][1]))/2.0;
}
printf("Volume: %f\n", vol);
/* -----
 * Surface Area (Perimeter) of Polygon.
 * ----- */
surf = 0.0;
surf = sqrt((p[nopts-1][0]-p[0][0])*(p[nopts-1][0]-p[0][0]) +
            (p[nopts-1][1]-p[0][1])*(p[nopts-1][1]-p[0][1]));
for (k = 1; k <= nopts-1; k++){
    surf += sqrt((p[k][0]-p[k-1][0])*(p[k][0]-p[k-1][0]) +
                (p[k][1]-p[k-1][1])*(p[k][1]-p[k-1][1]));
}
printf("Surface Area: %f\n", surf);
/* ----- 140
 * -----
 * Actual program Loop.
 * ----- */
for(v = 1; v <= BIGNUM; v++) overlap[v] = 0.0;
for (v = 1; v <= BIGNUM; v++){
    length = v*maxcl/((float) BIGNUM);
    for (z = 0; z <= MAXNUM; z++){
        theta = (2.0 * PI * (float) z)/((float) MAXNUM);
        for (j = 0; j <= nopts - 1; j++){
            q[j][0] = p[j][0] + ((double) (length*cos(theta)));
            q[j][1] = p[j][1] + ((double) (length*sin(theta)));
        }
        ixt = ix+length*cos(theta);
        iyt = iy+length*sin(theta);
    }
}
/* -----
 * Intersection of original polygon with the translate.
 * ----- */

```

main(polygon.c)

```

ss = 1;
cint = 0;
for (j = 0; j <= nopts - 1; j++){
    if (j == nopts - 1){
        i1 = p[0][0];
        i2 = p[0][1];
    }
    else{
        i1 = p[j+1][0];
        i2 = p[j+1][1];
    }
    for (k = 0; k <= nopts - 1; k++){
        if (k == nopts - 1){
            i3 = q[0][0];
            i4 = q[0][1];
        }
        else{
            i3 = q[k+1][0];
            i4 = q[k+1][1];
        }
        a = i1-p[j][0];
        b = p[j][1]-i2;
        c = p[j][1]*a + p[j][0]*b;
        d = i3-q[k][0];
        e = q[k][1]-i4;
        f = q[k][1]*d + q[k][0]*e;
        mpt = (a*e)-(b*d); /* |A| */
        ypt = (c*e)-(b*f); /* |A_1| */
        xpt = (a*f)-(c*d); /* |A_2| */
        if ((mpt != 0.0) &&
            ((ypt/mpt) >= min(p[j][1],i2)-tol) &&
            ((ypt/mpt) >= min(q[k][1],i4)-tol) &&
            ((ypt/mpt) <= max(q[k][1],i4)+tol) &&
            ((xpt/mpt) >= min(q[k][0],i3)-tol) &&
            ((xpt/mpt) <= max(q[k][0],i3)+tol) &&
            ((ypt/mpt) <= max(p[j][1],i2)+tol) &&
            ((xpt/mpt) >= min(p[j][0],i1)-tol) &&
            ((xpt/mpt) <= max(p[j][0],i1)+tol)){
            xint[ss] = xpt/mpt;
            yint[ss] = ypt/mpt;
            ss++;
            cint++;

```


main(polygon.c)

```

        cvert++;
        ss++;
    }
}
}
/* ----- 300
 * Counterclockwise Sort of Points.
 * ----- */
    for (k = 0; k <= TMP - 1; k++){
        my[k] = 0.0;
        mx[k] = 0.0;
    }
    my[0] = yint[1];
    mx[0] = xint[1];
    for (j = 2; j <= ss - 1; j++){
        if ((yint[j] == my[0]) && (xint[j] < mx[0])){
            mx[0] = xint[j];
            my[0] = yint[j];
        }
        else if (yint[j] < my[0]){
            mx[0] = xint[j];
            my[0] = yint[j];
        }
    }
}
/* -----
 * NORTHEAST
 * ----- */
    uu = 10;
    ind2 = 1;
    for (k = ind2; k <= ss - 1; k++){
        dist = 10.0;
        uu = 0;
        for (j = 1; j <= ss - 1; j++){
            if ((xint[j] > mx[k-1]) &&
                (yint[j] - my[k-1] < dist)){
                dist = yint[j] - my[k-1];
                mx[k] = xint[j];
                my[k] = yint[j];
                uu++;
            }
        }
        if (uu != 0) ind2++;
    }
}

```

main(polygon.c)

```

        if (uu == 0) break;
    }
/* -----
 * NORTHWEST
 * ----- */
    uu = 10;
    for (k = ind2; k <= ss - 1; k++){
        dist = 10.0;
        uu = 0;
        for (j = 1; j <= ss - 1; j++){
            if ((yint[j] > my[k-1]) &&
                (mx[k-1] - xint[j] < dist)){
                dist = mx[k-1] - xint[j];
                mx[k] = xint[j];
                my[k] = yint[j];
                uu++;
            }
        }
        if (uu != 0) ind2++;
        if (uu == 0) break;
    }
/* -----
 * SOUTHWEST
 * ----- */
    uu = 10;
    for (k = ind2; k <= ss - 1; k++){
        dist = 10.0;
        uu = 0;
        for (j = 1; j <= ss - 1; j++){
            if ((xint[j] < mx[k-1]) &&
                (my[k-1] - yint[j] < dist)){
                dist = my[k-1] - yint[j];
                mx[k] = xint[j];
                my[k] = yint[j];
                uu++;
            }
        }
        if ((mx[ind2] == mx[ind2-1]) &&
            (my[ind2] == my[ind2-1])){
            uu = 0;
        }
    }
    if (uu != 0) ind2++;

```

main(polygon.c)

```

        if (uu == 0) break;
    }
}
/* ----- 380
 * SOUTHEAST
 * ----- */
    uu = 10;
    for (k = ind2; k <= ss - 1; k++){
        dist = 10.0;
        uu = 0;
        for (j = 1; j <= ss - 1; j++){
            if ((yint[j] < my[ind2-1]) &&
                (xint[j] - mx[ind2-1] < dist)){
                dist = xint[j] - mx[ind2-1];
                mx[ind2] = xint[j];
                my[ind2] = yint[j];
                uu++;
            }
            if ((mx[ind2] == mx[ind2-1]) &&
                (my[ind2] == my[ind2-1])){
                uu = 0;
            }
        }
    }
    if (uu != 0) ind2++;
    if (uu == 0) break;
}
/* ----- 400
 * Area (Stone's Formula).
 * ----- */
    area[z] = 0.0; /* Initialization */
    if ((cint == 0) || (cvert == 0)) area[z] = 0.0;
    else{
        area[z] = (mx[ind2-2]*my[0])-(mx[0]*my[ind2-2]);
        for (k = 0; k <= ind2-3; k++){
            area[z] += (mx[k]*my[k+1])-(mx[k+1]*my[k]);
        }
    }
    area[z] = 0.5*area[z];
}
ind3 = (ind4) = 0;
for (z = 0; z <= MAXNUM; z++) overlap[v] += area[z];
free_vector(area,1,MAXNUM);
overlap[v] = overlap[v]/((float) (MAXNUM) * vol);
/* ----- 420

```

main(polygon.c)

```

    printf("%f    %f\n", length, overlap[v]);
}
free_vector(xint,1,TMP);
free_vector(yint,1,TMP);
/* -----
* Segment Lambda Distribution.
* ----- */
for (v = 1; v <= BIGNUM; v++){
    length = v*maxcl/((float) BIGNUM);
    printf("%f %f\n", length, 2.0*PI*length*overlap[v]/vol); 430
}
/* -----
* Cubic Spline Fit to \Omega(l) with first and second derivatives.
* ----- */
printf("Cubic Spline Fit\n");
yp1 = 0.0;
ypn = 0.0;
for (v = 1; v <= BIGNUM; v++) x[v] = 0.0;
for (v = 1; v <= BIGNUM; v++){
    x[v] = v*maxcl/((float) BIGNUM); 440
}
spline(x,overlap,BIGNUM,yp1,ypn,y2);
printf("Second Derivatives\n");
for (v = 1; v <= BIGNUM; v++){
    printf("%f    %f\n", x[v], y2[v]);
}
for (v = 1; v <= BIGNUM; v++) der1[v] = 0.0;
printf("First Derivative\n");
for (v = 1; v <= BIGNUM; v++){
    splint(x,overlap,y2,BIGNUM,x[v],&y); 450
    der1[v] = y;
    printf("%f    %f\n", x[v], der1[v]);
}
/* -----
* Ray Alpha, Ray Lambda, Ray Nu Distributions.
* ----- */
printf("Segment Lambda Density\n");
for (v = 1; v <= BIGNUM; v++)
    printf("%f    %f\n", x[v], 2.0*PI*x[v]*overlap[v]/vol);
printf("Ray Nu Density\n"); 460
for (v = 1; v <= BIGNUM; v++)
    printf("%f    %f\n", x[v], -der1[v]);

```

main(polygon.c)

```

printf("Ray Lambda Density\n");
for (v = 1; v <= BIGNUM; v++)
    printf("%f    %f\n", x[v], -PI*x[v]*x[v]*der1[v]/vol);
/* -----
* Chord Lambda, Chord Nu, Chord Mu Distributions.
* ----- */
printf("Chord Nu Density\n");
for (v = 1; v <= BIGNUM; v++)
    printf("%f    %f\n", x[v], x[v]*y2[v]);
printf("Chord Lambda Density\n");
for (v = 1; v <= BIGNUM; v++)
    printf("%f    %f\n", x[v], PI*x[v]*x[v]*x[v]*y2[v]/(3.0*vol));
printf("Chord Mu Density\n");
for (v = 1; v <= BIGNUM; v++)
    printf("%f    %f\n", x[v], PI*vol*y2[v]/surf);
}

```

470